* Revised: February 21, 1979

MODEL OF ADVECTION, DIFFUSION AND CHEMISTRY OF AIR POLLUTION (MADCAP) EVALUATED AT SAN DIEGO AIR BASIN

Prepared By

SCIENCE APPLICATIONS, INC.
1200 PROSPECT STREET
POST OFFICE BOX 2351
LA JOLLA, CALIFORNIA 92038

Under ARB Contracts A6-210-30
and A5-041-80

LIBRARY
CALIFORNIA AIR RESOURCES BOA
P. O. Box 2815
Sacramento, CA 95812

May 1978

* (Note: Revision affects Cover Page and Abstract only)

LIBRARY
AIR RESOURCES BOARD
P. O. BOX 2815
SACRAMENTO, CA 95812

SCIENCE APPLICATIONS, INC.
LA JOLLA, CALIFORNIA

ENERGY AND ENVIRONMENTAL SCIENCES

- *P.O. Box 2351*
  1200 Prospect Street
  La Jolla, CA 92038
  (714) 459-0211
- *2760 29th Street*
  Suite 209
  Boulder, CO 80301
  (303) 449-7500
- *3730 Mt. Diablo Blvd.*
  Suite 235
  Lafayette, CA 94549
  (415) 283-5320
- *1651 Old Meadow Road*
  Suite 620
  McLean, VA 22101
  (703) 827-4713

ABSTRACT

This report presents the derivation and application of the regional photochemical model MADCAP and its data processors. The first chapter is an introduction to the MADCAP model. The second chapter includes derivation of the basic algorithms. Two validation runs with 37 x 51 x 5 grids on 10/3/75 and 10/16/75, for San Diego Air Basin are described in chapter 3. Input data for the validation runs are presented first, then it is followed by the comparisons between the MACDAP simulations and measured air quality data. Chapter 4 presents the results of three different sensitivity analyses; the inert pollutant analysis, the photochemistry analysis and the dispersion and photochemistry analysis of the San Diego baseline (20 x 10 x 5, 10/3/75) to variation of input data. Finally the conclusions and recommendations are stated in chapter 5. A complete user's manual for the MADCAP model as well as three data processors is given in the Appendix A.

The authors of this report would like to acknowledge the helpful discussion of Mr. A.J. Ranzieri of California Air Resource Board (CARB), and the valuable operation system supports of Messers. G. Knops and T. Woody of CARB. We also would like to acknowledge the computer time provided to us by California Air Resource Board.

"The statements and conclusions in this report are those of the contractor and not necessarily those of the California Air Resources Board. The mention of commercial products, their source or their use in connection with material reported herein is not to be construed as either an actual or implied endorsement of such products.

The ARB and its Research Screening Committee have concluded that MADCAP, in its present stage of development, is not acceptable for use in developing oxidant control strategies, air quality maintenance plans for oxidant or carrying out impact analyses for individual oxidant control measures. Because MADCAP is still an experimental model, it should not be used for these or similar purposes.

The fact that the ARB has not found the MADCAP model to be acceptable for these purposes, should not be construed as an adverse reflection upon the competency or the integrity of the contractor in performing the work described in this report."

CONTENTS

Section		Page
	ABSTRACT	i
	LIST OF ILLUSTRATIONS	iv
	LIST OF TABLES	vii
1	INTRODUCTION	1
2	DESCRIPTION OF THE MODEL	3
	2.1 Data Preparation/Pre-Processors	3
	2.1.1 PREBIC	5
	2.1.2 PREMET	6
	2.1.3 PRESOR	7
	2.2 Derivation of MADCAP Algorithms	10
	2.3 Limitations and Applicability of MADCAP	17
3	MADCAP EVALUATION AT SAN DIEGO	20
	3.1 Grid Parameters	20
	3.2 Baseline Input	22
	3.2.1 Initial and Boundary Conditions	22
	3.2.2 Meteorology	23
	3.2.2.1 Solar Intensity	26
	3.2.2.2 Water Vapor	26
	3.2.2.3 Diffusivities	26
	3.2.2.4 Wind Field	30
	3.2.2.5 Comparison Between 10/3/75 Baseline Wind Field and the Wind Field Predicted by WEST	34
	3.2.3 Sources	39
	3.3 Baseline 37 x 51 x 5 MADCAP Run on 10/3/75	45
	3.4 Baseline 20 x 10 x 5 MADCAP Run on 10/3/75	58
	3.5 Simulation 37 x 51 x 5 MADCAP Run on 10/16/75	64

CONTENTS (continued)

Section		Page
4	SENSITIVITY ANALYSIS ON MADCAP	68
	4.1 Sensitivity Parameters	71
	4.2 Inert Pollutants Analysis (Sensitivity Study Without Photochemistry)	74
	4.2.1 Sensitivity to Vertical Resolution	75
	4.2.2 Sensitivity to Horizontal Resolution	75
	4.2.3 Sensitivity to Time Step	78
	4.2.4 Sensitivity to Mixing Height	80
	4.2.5 Sensitivity to Diffusion	84
	4.2.6 Sensitivity to Diffusion Scheme	86
	4.3 Photochemical Analysis	89
	4.4 Dispersion and Photochemistry Analysis	92
	4.4.1 Sensitivity to NO_x Emission	92
	4.4.2 Sensitivity to Hydrocarbon Emissions	94
	4.4.3 Sensitivity to Hydrocarbon Split	96
	4.4.4 Sensitivity to Air Quality (Initial and Boundary Conditions)	96
5	CONCLUSIONS AND RECOMMENDATIONS	100
	REFERENCES	103
APPENDIX A:	MADCAP USER's MANUAL	A-1

ILLUSTRATIONS

Figure		Page
2.1	Schematic Diagram of MADCAP	18
3.1	San Diego Air Basin	21
3.2	CO Concentration at 0600 PST on 10/3/75	25
3.3	Solar Intensity Distributions on 10/3/75.	27
3.4	Water Concentration Distributions on 10/3/75. . .	28
3.5	Diffusivity Distributions on 10/3/75.	29
3.6	Wind Field at Ground Level, 0800 PST, 10/3/75 . .	31
3.7	Wind Field at Ground Level, 1600 PST, 10/3/75 . .	32
3.8	Variation of Highest Speed in the Small Grid. . .	33
3.9a	Wind Field Comparisons Between MADCAP and WEST, Ground Level, 0800 PST, 10/3/75	36
3.9b	Wind Field Comparisons Between MADCAP and WEST, Level 3, 0800 PST, 10/3/75.	37
3.10	Wind Field Comparisons Between MADCAP and WEST, Ground Level, 1600 PST, 10/3/75	38
3.11	CO Source Distributions on 10/3/75.	40
3.12	NO Source Distributions on 10/3/75.	41
3.13	HC1 Source Distributions on 10/3/75	42
3.14	HC2 Source Distributions on 10/3/75	43
3.15	HC3 Source Distributions on 10/3/75	44
3.16	CO Temporal Profiles, MADCAP 37 x 51 x 5, 10/3/75 Run	46
3.17	O_3 Temporal Profiles, MADCAP 37 x 51 x 5, 10/3/75 Run	48
3.18	NO Temporal Profiles, MADCAP 37 x 51 x 5 10/3/75 Run	49

ILLUSTRATIONS (continued)

Figure		Page
3.19	NO_2 Temporal Profiles, MADCAP 37 x 51 x 5, 10/3/75 Run	50
3.20	HC1 Temporal Profiles, MADCAP 37 x 51 x 5, 10/3/75 Run	52
3.21a	CO Spatial Pattern, MADCAP 37 x 51 x 5, 10/3/75 Run	53
3.21b	CO Spatial Pattern, MADCAP 37 x 51 x 5, 10/3/75 Run	54
3.22a	O_3 Spatial Pattern, MADCAP 37 x 51 x 5, 10/3/75 Run	55
3.22b	O_3 Spatial Pattern, MADCAP 37 x 51 x 5, 10/3/75 Run	56
3.23	CO Temporal Profiles, Comparison Between MADCAP 37 x 51 x 5 and MADCAP 20 x 10 x 5 Runs	59
3.24	O_3 Temporal Profiles, Comparison Between MADCAP 37 x 51 x 5 and MADCAP 20 x 10 x 5 Runs	61
3.25	O_3, NO, NO_2, Temporal Profiles, MADCAP 20 x 10 x 5, 10/3/75 Runs	62
3.26	HC1, HC2, HC3, Temporal Profiles, MADCAP 20 x 10 x 5, 10/3/75 Run	63
3.27	CO Temporal Profiles, MADCAP 37 x 51 x 5, 10/16/75 Run	65
3.28	O_3 Temporal Profiles, MADCAP 37 x 51 x 5, 10/15/75 Run	66
4.1	Sensitivity Region	69
4.2	The 20 x 10 Grid	70
4.3	Relationship of the NZ = 3 Grid to the Baseline NZ = 5 Grid	76
4.4	Dispersion Sensitivity to Vertical Resolution	77

ILLUSTRATIONS (continued)

Figure		Page
4.5	Dispersion Sensitivity to Horizontal Resolution	79
4.6	Dispersion Sensitivity to Number of Steps Per Hour	81
4.7	Relation of Sensitivity Diffusivities to Baseline Diffusivities	82
4.8	Variation of Inversion Base Height in San Diego County	83
4.9	Vertical Dispersion Sensitivity to Diffusion Scheme	87
4.10	Ground-Level Dispersion Sensitivity to Diffusion Scheme	88
4.11	MADCAP Sensitivity of Ozone to NO_x Emissions	93
4.12	MADCAP Sensitivity of Ozone to THC Emissions	95
4.13	MADCAP Sensitivity of Ozone to THC Splitting	97
4.14	Sensitivity of Ozone to Initial Boundary Conditions	98

TABLES

Table		Page
2.1	Hydrocarbon Splitting Factors	8 & 9
2.2	Photochemical Kinetics Mechanism.	15 & 16
3.1	Echo of Input to PREBIC	24
4.1	Sensitivity Parameters.	72
4.2	Photochemistry Sensitivity Analysis	91

MODEL OF ADVECTION, DIFFUSION AND CHEMISTRY OF AIR POLLUTION (MADCAP), EVALUATED AT SAN DIEGO AIR BASIN*

I. INTRODUCTION

MADCAP (an acronym for Model of Advection, Diffusion and Chemistry of Air Pollution) is a time-dependent regional air-pollution model for inert as well as reactive pollutants. It is a three-dimensional regional air quality model which can be easily and effectively used to determine oxidant control strategies. It is different from any of the other models, such as the 3-D Eulerian IMPACT model[1] or the one column Lagrangian DIFKIN model[2]. It is based on a horizontal Lagrangian and vertical Eulerian grid solution of the atmospheric diffusion equation.

It is the objective of this report to evaluate and test for validity of this model by using portions of the San Diego Air Basin and existing aerometric and emissions data bases. A sensitivity study on the model MADCAP with and without photochemistry was also performed to analyze the importance of the accuracy of the input data.

This report begins with a brief description of the model MADCAP and its data pre-processors. Some limitations of the model are discussed. Two representative ten-hour day simulations were made, and comparison between the predictions and measured air quality data are analyzed. These two validation runs were made on a large grid with a network of 37 x 50 x 5 zones. A smaller network of 20 x 10 x 5 zones was used to perform sensitivity studies on MADCAP. All sensitivity results are reported

---

* This final report includes all the findings under two separate contracts from CARB; Contracts # A6-210-30 and # A5-041-80.

in Chapter 4. Finally, conclusions and recommendations are made in Chapter 5. A complete user's manual of MADCAP and its pre-processors is included in the Appendix.

2. DESCRIPTION OF THE MODEL

MADCAP is a general time-dependent regional photochemical air pollution program that requires as inputs wind fields and emissions and meteorology profiles over the entire region of interest. Such raw data are available only at certain isolated measurement stations. Hence pre-processors that extrapolate the raw data over the entire domain of interest were developed. The programs PREBIC, PREMET AND PRESOR generate the initial and boundary conditions, the various meteorology profiles and the emissions profiles, respectively. In this chapter, the pre-processors will be briefly described (the detailed input, output and management of these pre-processors can be found in the user's manual), followed by the derivation and algorithms of the program MADCAP.

2.1 DATA PREPARATION/PRE-PROCESSORS

In the three separate pre-processors PREBIC, PREMET and PRESOR the data on any horizontal plane are extrapolated from the measured data at given stations (such as the meteorological stations) using an inverse square formula ($1/r^2$ extrapolation)

$$\phi_{ij} = \frac{\sum_{\ell} \phi_{\ell}/r_{\ell}^{2}}{\sum_{\ell} 1/r_{\ell}^{2}} ,$$

where ℓ is the index of the observation site, ϕ_{ij} is the extrapolated value at grid location (I,J) and ϕ_{ℓ} is the given value of the data at station ℓ. The distance from the ℓth station to the cell center of grid location (I,J) is designated by r_{ℓ}. For the vertical profiles, meteorological data and emissions data are handled differently and the methods of extrapolation in the z direction are described in the following sections.

All pre-processors are designed for simplicity in use and can be applied to any region with minimum alterations (some limitations on the pre-processors are discussed in user's

manual). For any given study region (such as the San Diego area), a basic 50 x 60 grid of cells is specified with constant grid size in both the x (E-W) and y (N-S) directions. All the data required by the MADCAP model for any sub-area within the basic grid can be easily processed by simply inputting the following four variables to the pre-processors (for more detail, see the user's manual):

MX - total number of cells in x direction of the sub-area

MY - total number of cells in y direction of the sub-area

MIX - number of cells to be shifted (relative to the 50 by 60 grid) in the east direction for the west-south corner of the sub-area

MIY - number of cells to be shifted (relative to the 50 by 60 grid) in the north direction for the west-south corner of the sub-area.

After specification of the time and date of the simulation, all the pre-processors check the validity of the data, such as the date, the time, the position of the data site and the measured data. If an invalid datum is encountered, for example a negative wind speed is found, the read-in data for that particular variable at the given site will be discarded and the next data card will be read in. However, if the date or time fail to match, a suitable diagnostic is printed and execution is suspended. This process will continue until all the data of a given type (such as the wind data, land use data, emissions data, etc.) are exhausted. After one type of data are read in, the pre-processors proceed to generate the data required for input to MADCAP within the specified sub-area.

Before writing the unformatted output onto a tape used as input to MADCAP, graphic display using the line printer (or CALCOMP plotter which can easily be incorporated) has been included in order to provide a rapid assessment of the input data. Also included is the capability of producing tabulated digital values of all the data, such as emissions fluxes, wind-flow fields, initial concentration profiles, etc. Finally, all the input data for MADCAP is stored on specific tapes and ready to be used in the simulation run of MADCAP.

2.1.1 PREBIC

PREBIC is designed to process the measured air quality data of the region into the proper form of initial and boundary conditions needed by MADCAP. The major species of the pollutants considered in MADCAP are CO, O_3, NO_2, NO, HC1, HC2 and HC3, where the hydrocarbon species are separated into three aggregated hydrocarbons according to the modified LIRAQ model by Gelinas and Skewes-Cox[3]. The three aggregated hydrocarbon species have the following properties:

HC1 is primarily composed of alkenes and some highly substituted aromatics. HC1 is assigned the reactive properties of propene, reacting with O, OH, and O3.

HC2 is primarily composed of alkanes, less reactive aromatics, partially halogenated paraffins and alcohols. HC2 is assigned the reactive properties of n-butane, reacting with O and OH.

HC3 is primarily composed of aldehydes and ketones, and is assigned the reactive properties of a 50-50 molar mixture of methanal and ethanal. HC3 undergoes photolysis as well as reacting with O, OH, peroxyl, and nitrate radicals.

PREBIC separates the emissions inventory data which are generally given in terms of either grams of total hydrocarbon (THC) or grams of non-methane hydrocarbons (NMHC) into the appropriate portion of the above-defined three hydrocarbon species. According to ref. 4, splitting factors can be defined for many different generic source types (table V in ref. 3) such as gasoline storage, gasoline exhaust, diesel exhaust, etc. The total emissions of HC1, HC2 and HC3 can be obtained by summing the product of the splitting factors and emissions of all the sources. In PREBIC, for the initial conditions, it is estimated that emissions of HC1 and HC2 (in ppm) can be approximated as 0.44 NMHC and 1.1 NMHC (measured in ppm) by using the splitting factors listed in Table 2.1 and actual hydrocarbon emission sources of a typical suburban area in Southern California.[10] Because of the reactive nature, the emission level of HC3 is very low in

comparison with HC1 and HC2, hence initial concentrations for HC3 are assumed to be zero for simplicity. After the measured air quality data are read in and validated, the initial conditions at the surface layer are determined by a $1/r^2$ extrapolation law horizontally over the entire level. Aloft air quality is assumed to be the same as that on the ground level. Boundary conditions for the air quality data are obtained similarly, except that these boundary data must be generated for each simulation hour.

2.1.2 PREMET

PREMET is a processing routine designed to manage the raw meteorological data into the required input form of MADCAP. There are two types of raw data, namely geological data which includes land usage data, fixed meteorological data such as surface roughness, and hourly meteorological data including surface temperature, relative humidity, wind data, cloud cover, ceiling height, pibal data, inversion data, solar irradiation and barometric pressure. Land use and surface roughness are to be input for every cell in the grid, and cloud cover, celing height, temperature, relative humidity inversion height and temperature are calculated by $1/r^2$ extrapolation conformal to the specified coastline. The ground level wind field, however, is generated by $1/r^2$ extrapolation not necessarily conformal to the coastline. The ground level stability class (SC) is found according to the method presented by Turner (ref. 5) as a function of the irradiation index and the wind speed on the surface layer. The radiation index depends on the angle of the sun above the southern horizon, the cloud cover, ceiling height and whether it is night or day. If there is an urban heat island (specified by the land use), the stability class is decreased by one (made more unstable).

The inversion data is adjusted to agree with the ground temperature, and the code tests for ground-based inversion and the case of no inversion. The inversion height at every grid point is then generated by $1/r^2$ extrapolation formular. The Monin-Obukhov length (MOL) is calculated from the surface roughness, the SC (calculated aloft again as a function of wind speed versus irradiation index; see ref. 5), and evaporative potential (as a function of land use) by fitting curves to the data presented by Myrup and Ranzieri (ref.6). If the surface roughness exceeds the limits of the curves in ref.6 , the MOL is set to the last acceptable value for the particular SC and evaporative potential. For neutral or near-neutral conditions, MOL is set to -100,000. With the MOL thus calculated, the vertical diffusivity is calculated according the Myrup-Ranzieri model. The code does not presently allow multiple inversions.

A power law extrapolation depending on SC as determined by inversion height extends the ground wind station data to all vertical levels, $S=S_o\ (Z/Z_o)^p$ where S is the speed at any height Z and p is given as a function of SC

SC	1	2	3	4	5	6	7
p	.15	.17	.2	.26	.39	.48	.54

The pibal data is extrapolated vertically using a $1/r^6$ extrapolation law, and the wind field is finally extrapolated horizontally over layers according to a $1/r^2$ extrapolation law.

2.1.3 PRESOR

PRESOR is designed to generate an emissions source scenario over the entire region based upon emissions fluxes at isolated points in the grid. The various source types, namely motor vehicle emissions, shipping emissions, rail data, area sources, ground level point sources (no stack), elevated point sources (stack) and aircraft emissions, are handled separately, and splitting factors of THC into HC1, HC2 and HC3 vary from one source type to another. The different splitting factors and inputs for different source types are described in Table 2.1.

Table 2.1 Hydrocarbon Splitting Factors

SOURCE TYPE	TOTAL INPUTS	HC SPLITS (HC1, HC2, HC3)	NO_2NO_x SPLITTING RATIO
Motor Vehicle	CO, NO_x		0.01
	THC: gasoline powered vehicle exhaust	(.0095, .017, 0.)	
	gasoline powered vehicle evaporation	(.0043, .018, 0.)	
	diesel powered vehicle exhaust	(.0032, .016, .0056)	
Shipping	CO, NO_x THC	(.0032, .016, .0056)	0.01
Railway	CO, NO_x, THC	(.0032, .016, .0056)	0.01
Area	CO, NO_x		0.02
	THC: gasoline marketing (underground storage	(.0068, .014, 0.)	
	gasoline marketing (auto tank filling)	(.0049, .018, 0.)	
	fuel combustion	(.0024, .0043, .0029)	
	waste burning and fires	(.008, .0073, .0024)	
	surface coating: heat treated	(.0004, .018, 0.)	
	surface coating: air dried industrial	(.0005, .021, .0004)	
	surface coating: air dried archit	(.0005, .021, .0004)	

Table 2.1 (continued)

SOURCE TYPE	TOTAL INPUTS	HC SPLITS (HC1, HC2, HC3)	NO_2/NO_x SPLITTIN RATIO
Area (continued)	THC: dry cleaning (petrol based)	(0., .03, 0.)	
	dry cleaning (synthetic)	(0., 0., 0.)	
	degreasing (halogenated)	(0., .02, 0 .)	
	degreasing (non-halogenated)	(0., .03, 0.)	
	industrial process source	(.0008, .017, .0008)	
	pesticites	(0., .03, 0.)	
Point Source (no stack)	*** (same as area sources)***		
Point Source (stack)	CO, NO_x		0.05
	THC	(.0032, .016, .0056)	
	stack height, stack diameter, exit velocity, temperature of plume, volume flow		
Aircraft	CO, NO_x		0.01
	THC: piston aircraft	(.0062, .015, 0.)	
	jet aircraft altitude	(.0065, .015, .0031)	

Beyond the splitting factors, the action of PRESOR is straightforward, with the plume rise calculated by any of the Briggs '69, Briggs '74 or TVA formalae. It should be mentioned that the stability class profile and the complete wind field as generated by PREMET are inputs to PRESOR for calculation of the plume rise, and so PREMET should be run prior to execution of PRESOR.

2.2 DERIVATION OF MADCAP ALGORITHMS

MADCAP is a time-dependent regional air pollution model for inert and reactive pollutants. It has been developed for optimization, ease of use and speed of solution. The optimization has been in utilization of a one hour Lagrangian formulation for each cell of a three-dimensional grid which permits chemical simulation one hour at a time. It is based on a horizontal Lagrangian and vertical Eulerian grid solution of atmospheric diffusion equation.

The atmospheric diffusion equation can be written as

$$\frac{\partial Ci}{\partial t} = -\bar{U}\cdot\bar{\nabla}C_i+\bar{\nabla}\cdot\bar{K}\cdot\bar{\nabla}C_i+S_i+\sum_{k,j} R_{ikj}C_kC_j,$$

where the time rate of change of the ith species concentration, $\frac{\partial C_i}{\partial t}$, is equal to the advection of the species, $-\bar{U}\cdot\bar{\nabla}C_i$, by wind velocity $\bar{U}$, plus diffusion of the species, $\bar{\nabla}\left(\bar{K}\cdot\bar{\nabla}C_i\right)$ with diffusity tensor $\bar{K}$; plus source emissions rate of the species, S_i, and plus the effect of chemical reactions forming or removing the species, $\sum_{k,j} R_{ikj}C_kC_j$.

The derivation of the MADCAP approximations stem from seven assumptions:

1. the atmospheric region of solution can be subdivided into cells,
2. concentrations are known only at cell centers and can be interpolated to other locations,

3. emissions, wind velocities and diffusivities are constant throughout each cell for each hour,
4. the time resolution required for regional modeling permits approximating an hour average by a single set of concentrations calculated with winds, diffusivities and sources constant throughout an hour,
5. the winds are horizontal (conformal to terrain),
6. diffusion in the vertical is the only important diffusion, and
7. even though the air is not restricted to move as a vertical column, the vertical diffusion can be approximated over a single hour as if it were (i.e., vertical wind shear is not great relative to horizontal cell dimensions).

The first assumption is common to all finite difference or grid models and with the second and third assumptions of variable centering specify the spatial resolution. It is worthwhile to note the assumptions do not require any specific type of grid, not even regular. In addition, the grids used for definition of each variable may be different. (However this has not been exploited presently in MADCAP.) The fourth assumption is key -- that one set of concentrations can be used for approximating hour averages. Strictly, this would require that the equation for hour averages (which could be developed by integrating the atmospheric diffusion equation over one hour) would be identical to the atmospheric diffusion equation with all terms averaged. The non-linear terms (advection, diffusion and chemical) prohibit this from being precisely true. The approximations used in deriving the split between advection and diffusion utilizes a time average so these terms are correct for one hour averages. However the chemical terms have many lumping assumptions built in; this provides just one more. Thus any chemical mechanism or reaction rates used must be validated against atmospheric data.

The last three assumptions specify the explicit approximations made in MADCAP to the atmospheric diffusion equation. By assumption 5:

$$-\overline{U}\cdot\overline{\nabla}C_i = -U\frac{\partial Ci}{\partial x} - V\frac{\partial Ci}{\partial y}$$

The vertical winds are necessary in an Eulerian grid to account for horizontal wind divergence. In MADCAP, Lagrangian cells do not produce concentration buildup (or depletion) due to a convergence (or divergence) in the winds. Each cell carries a single set of concentrations forward for an hour by changing its position, not by solving the above advection terms (see below). Assumption 6 reduces

$$\overline{\nabla}\cdot\overline{K}\cdot\ \overline{\nabla C}_i = \frac{\partial}{\partial z}\ K_z\ \frac{\partial C_i}{\partial z}$$

which operationally is calculated in MADCAP as

$$K_z(x,y,z)\ \frac{C_i(x,y,z-\Delta z) - 2\ C_i\ (x,y,z) + C_i(x,y,z+\Delta z)}{\Delta z^2}$$

only once per hour (at the beginning) by assumption 7.

The justification for these assumptions is the intended application of MADCAP only to regional air quality simulations. Regional air quality is envisioned not to have large horizontal gradients in concentrations so horizontal diffusion may be neglected. Vertical diffusion mixes pollutants in the vertical direction. No flux boundary conditions are assumed at both the top and bottom boundaries of the vertical column. In order to save computation time and permit all hour average calculation, the vertical diffusion computation is performed hourly. It is found that for San Diego County, the sensitivity runs (Section 4.2.6) indicate that 45 minutes of diffusion prior to source injection coupled with 15 minutes of diffusion after source injection would yield best agreement with measured concentrations. Hence, the post diffusion (for 15 minutes) scheme is used in this report.

With these assumptions, the algorithms used in MADCAP can be derived as follows. Horizontal advection, transport by the horizontal winds, is simulated by tracking the one hour trajectory separately for each cell center on every vertical level. This is done backwards from the cell center at the end of the hour. That is, N steps are taken over sub-hour intervals, Δt, using

$$x = x - u(x,y,z)\ \Delta t$$

$$y = y - v(x,y,z)\ \Delta t$$

successively from a cell center position until $N\,\Delta t = 1$ hour. One hour was chosen only for consistency with the ambient air quality standards. The number of steps taken, N, has been arbitrarily set at 10. This number can be envisioned as the number of straight line segments used to approximate the one hour trajectory.

Since the one hour trajectory is approximated by these N steps, it is convenient to store the source emissions at the end points of these same steps. Finally, the x, y position, calculated to be the starting point for the one hour trajectory ending at the cell center, is used to acquire an initial concentration. This initial concentration is interpolated from the known cell center concentrations of this previous hour. The interpolation algorithm adopted in MADCAP is simply using the closest value if the trajectory traverses over three cells, or using an area-weighted average of the closest four cells on the given level. If the trajectory passes outside of the grid boundaries, the initial concentrations are those specified as boundary conditions. The effects of vertical diffusion are calculated at this starting point for 45 minutes to be used as a rate as specified by assumption 7. These diffusion rates are used as sources or removal terms. The approximate equation to be solved is

$$\frac{\partial C_i}{\partial t} = D_i + S_i + \sum_{k,j} R_{ikj} C_k C_j$$

for diffusion rate D_i of the i species. This equation can be solved by any of the methods used by the many chemical modules used for chemical reaction simulation.

The photochemical kinetic mechanism adopted in the MADCAP is the modified version of the LIRAQ-2 photochemical model by Gelinas and Skewes-Cox. This model employs three hydrocarbon species and a preliminary sulfer dioxide reaction set in a 58 step lamped parameter kinetic mechanism. Table 2.2 shows the basic mechanism and the approximate rate data. It should be noted that this extended mechanism is to be viewed as experimental rather than firm. In fact, photochemical kinetic mechanism are themselves a very active research field. Though the modified LIRAQ-2 kinetics scheme is presently incorporated into MADCAP, either of the simplified five species, 15 reaction, model developed by GRC[7], or the 15-species, 39 reaction, chemical model[8] can be successfully adopted into the MADCAP model. It is also the purpose of this study to compare the measured air quality data with the predictions from MADCAP to verify the validity of this updated version of the LIRAQ-2 photochemical model.

The chemical module encoded in MADCAP uses the approximate equation of the form

$$\frac{\partial C_i}{\partial t} = A_i - B_i C_i$$

where A_i includes all terms producing species C_i (chemical formation, source emissions and vertical diffusion into the cell) and $B_i C_i$ the removal of species C_i by chemical reactions and diffusion out of the cell. The source emissions are interpolated from the values stored during the backwards trajactory tracing. In this form, the equation is solved by a predictor-corrector of the analytic form.

$$C_i(t+\Delta t) = {}^{A}i/B_i + (C_i(t) - {}^{A}i/B_i)e^{-B_i \Delta t}$$

Table 2.2 Photochemical Kinetics Mechanism

		A	C
1	NO2+ hν = NO+O	1.2E-2	
2	HNO2+hν = HO+NO	7.2E-4	
3	H2O2+hν = HO+HO	5.5E-6	
4	NO3+hν = NO2+O	2.8E-3	
5	O3+hν = O2+O2	5.1E-4	
6	O3+hν+H2O = 2HO+O	2.2E-5	
7	RNO2+hν = RO+NO	1.9E-3	
8	HC3+hν = HO2+HO2+CO	2.7E-5	
9	HC3+hν = RO2+HO2	2.7E-5	
10	O+O+2M=O3+2M	1.0E-34	-510.
11	O3+NO = NO2+O2	9.0E-13	1200.
12	O+NO+ZM=NO2+ZM	4.0E-33	940.
13	O+NO2 = NO+O2	9.1E-12	
14	O+NO2+ZM = NO3+ZM	3.5E-32	-300.
15	O3+NO2 = NO3+O2	1.1E-13	2450.
16	NO2+NO3 = N2O5	3.8E-12	
17	N2O5 - NO2+NO3	5.7E-14	10600.
18	NO3+NO = NO2+NO2	8.7E-12	
19	N2O5+H2O - HNO3+HNO3	3.0E-16	3300.
20	HO+NO2 = HNO3	7.0E-12	
21	HO+NO = HNO2	7.0E-12	
22	HO2+NO = HO+NO2	2.0E-13	
23	HO2+NO2 = HNO2+O2	3.0E-14	
24	HO+HNO3 = H2O+NO3	1.3E-13	
25	HO2+HO2 = H2O2+O2	3.0E-12	
26	HO2+HO = H2O+O2	2.0E-11	
27	HO+CO = HO2+CO2	1.4E-13	
28	HC1+O = RO2+.5RCO3+.5HO2	1.0E-11	360.
29	HC1+O3 = HO2+RO+HC3	7.0E-15	1900.
30	HC1+O3 = Ozonide	7.0E-15	1900.
31	HC1+HO = RO2+HC3	5.0E-11	350.
32	HC1+HO = RO2+H2O	3.0E-11	350.
33	HC2+O = RO2+HO	4.1E-11	2000.
34	HC2+HO = RO2+H2O	4.0E-11	900.
35	HC3+O = HO+HO2+CO	4.0E-12	900.
36	HC3+HO = RCO3+H2O	3.0E-11	350.
37	HC3+HO2 = H2O2+RCO3	8.0E-13	3700.
38	HC3+NO3 = HNO3+RCO3	3.0E-15	900.
39	HC3+HO = CO+HO2+H2O	3.0E-11	350.
40	HC3+NO3 = CO+HNO3+HO2	3.0E-15	650.
41	HC3+RO2 = RHO2+RCO3	8.0E-13	3750.
42	RO2+NO = RNO3	0.0E-00	
43	RO2+NO = RO+NO2	5.0E-12	300.
44	RCO3+NO = RO2+NO2+CO2	6.5E-12	600.
45	RCO3+NO2 = PAN	3.04E-14	
46	RO+NO2 = RNO3	5.0E-14	
47	RO+NO = RNO2	5.0E-14	
48	RO+O2 = HO2+HC3	1.6E-13	3300.
49	RO2+RO2 = RO+RO+O2	6.7E-14	

Table 2.2 (Continued)

		A	C
50	R02+H02 = R0+H0+02	6.7E-14	
51	S02+R02 = R0+S04	2.0E-15	
52	S02+R0 = H02+S04	4.0E-13	
53	S02+H02 - H0+S04	9.0E-16	
54	S02+H0+ZM = H02+S04+ZM	2.4E-32	
55	S02+0+ZM = S04+ZM	3.4E-32	1130.
56	S02+RC03 = R02+S04	1.03-15	
57	HN03+hν = H0+N02	4.9E-7	
58	N205+hν = N02+N02+0	2.9E-5	

Rate Constant of the Form: K=Aexp (-C/T) in units of $m^{-3}sec^{-1}$

Dynamic Species: N02, N0, 03, HC1, HC2, HC3, N205, HN03, HN02, H02, RN02, H202, C0, S02, S04

Non-Accumulating Species: RO_2, RC03

Quasi-Equilibrium: 0, HO, N03, R0

HC1 - aliphatic olefins

HC2 - alkanes, cycloparaffins, less reactive aromatics and oxygenates

HC3 - aldehydes and keytones

This completes the description of the algorithms used in MADCAP. To summarize, MADCAP approximates the solution of the atmospheric diffusion equation on a horizontal Lagrangain and vertical Eulerian grid. Advection is treated as only horizontal and solved by the Lagrangian cell movement. Diffusion is treated only in the vertical, calculated at the beginning of each hour and end of each hour and entered as an additional source or removal term. The chemical reactions can be calculated based on any approximate chemical mechanism and solved by predictor-corrector method.

Figure 2.1, shows the basic structure of the MADCAP model Each box represents a major modular component of the model, and appropriate comments have been included to demonstrate the function of each module.

2.3 LIMITATIONS AND APPLICABILITY OF MADCAP

MADCAP is formulated for regional air pollution and strictly can be applied only to problems satisfying the seven assumptions. MADCAP has all of the usual limitations of grid models in resolution and point source simulation. In addition, some operational constraints are placed on the code. Since the diffusion rate is calculated at the beginning and end of each hour and used within the hour, it can neither dominate the cell concentration nor completely empty a cell in one hour for the MADCAP solution to be appropriate. Thus MADCAP is encoded with a maximum cutoff in case of its incorrect application to problems with large gradients.

It is envisioned that typical MADCAP horizontal resolution would be 1-10 KM. Thus, the 3 cell per hour cutoff for using an area weighted interpolation of the initial concentration corresponds to the wind speed range 1-11 m/sec. At the lower end of this range, the large dispersion caused by the interpolation is very reasonable due to the lack of precision in low wind speed measurements and the variability of slow winds, but at the high end this may be undesirable.

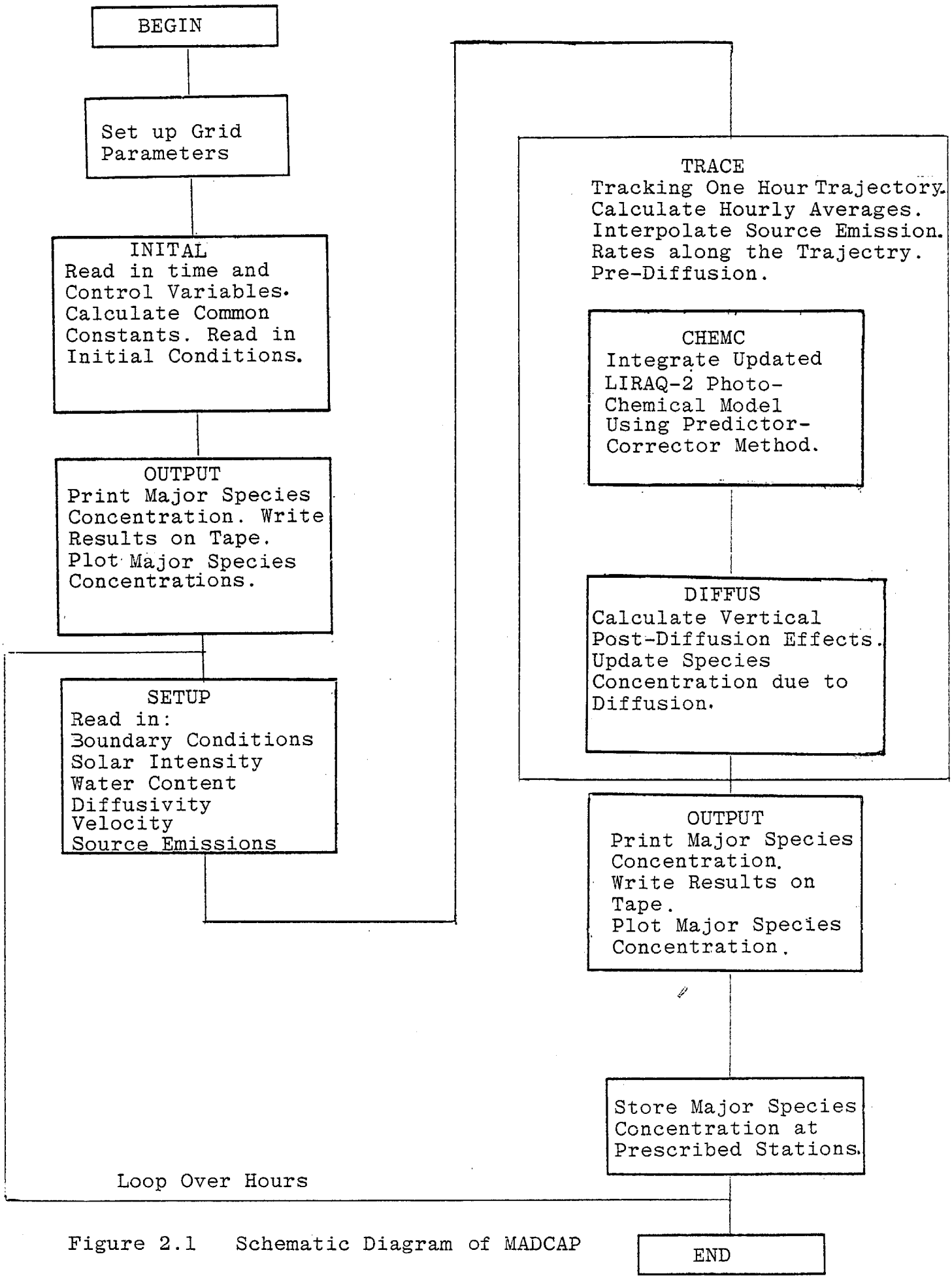

Figure 2.1 Schematic Diagram of MADCAP

MADCAP is applicable to regional air quality simulation. Its advantages in this application include: no time step limitation, solution of non-equilibrium chemistry only once per hour for each cell, and a simple and efficient formulation.

Application of MADCAP to San Diego County with its relative uniformity of sources and 2 Km grid appears to be well within the range of applicability discussed above.

MADCAP can also be applied to any other regional air quality simulations. With the present form, it can be applied to the coastal region as well as inland region (see user's manual). When it is employed to simulate air quality predictions in coastal areas, the coast line has to be on the left hand side of the grid (west coast region). However, with minimum modifications, MADCAP can be applied to any region of interest.

3. MADCAP EVALUATION AT SAN DIEGO

One of the objectives of this study is to evaluate and validate the air quality model MADCAP. The San Diego Air Basin was selected to be the region of this study. Using the air quality and meteorological data gathered in San Diego in 1975 and provided by California Air Resource Board as the input data, MADCAP was run for the two dates, October 3, 1975 and October 16, 1975. In this chapter, comparisons of the simulated results and the measured air pollutant concentrations are discussed.

3.1 GRID PARAMETERS

The original 50 x 60 master grid selected for San Diego is shown in Figure 3.1. A uniform grid size of 2 Km is chosen in both of the horizontal directions, whereas a variable zoning is employed in the vertical direction. For application to San Diego County, five vertical layers conformal to terrain are chosen to be of height 50 m, 75 m, 125 m, 250 m, and 500 m. This results in the top of the grid being 1000 meters above local ground level with cell centers at 25 m, 87.5 m, 187.5 m, 375 m and 750 m.

For the two validation runs (10/3/75 and 10/16/75), a region covering 37 x 51 grid cells is used (Figure 3.1). Within this region, there are a total of 39 recording stations which include both air quality and meteorological stations. However, there are only nine stations providing complete air quality data for the two chosen days. These stations are Oceanside, San Marcos, Escondido, Poway, Kearny Mesa, El Cajon, San Diego, Chula Vista and Imperial Beach (Figure 3.1).

For the sensitivity study (Chapter 4), a much smaller region is choosen (20 x 10 grid cells, Figure 3.1) encompassing only five stations - San Diego, El Cajon, Kearny Mesa, Chollas and Santee, where only the last two stations had ozone measurements on the two selected days.

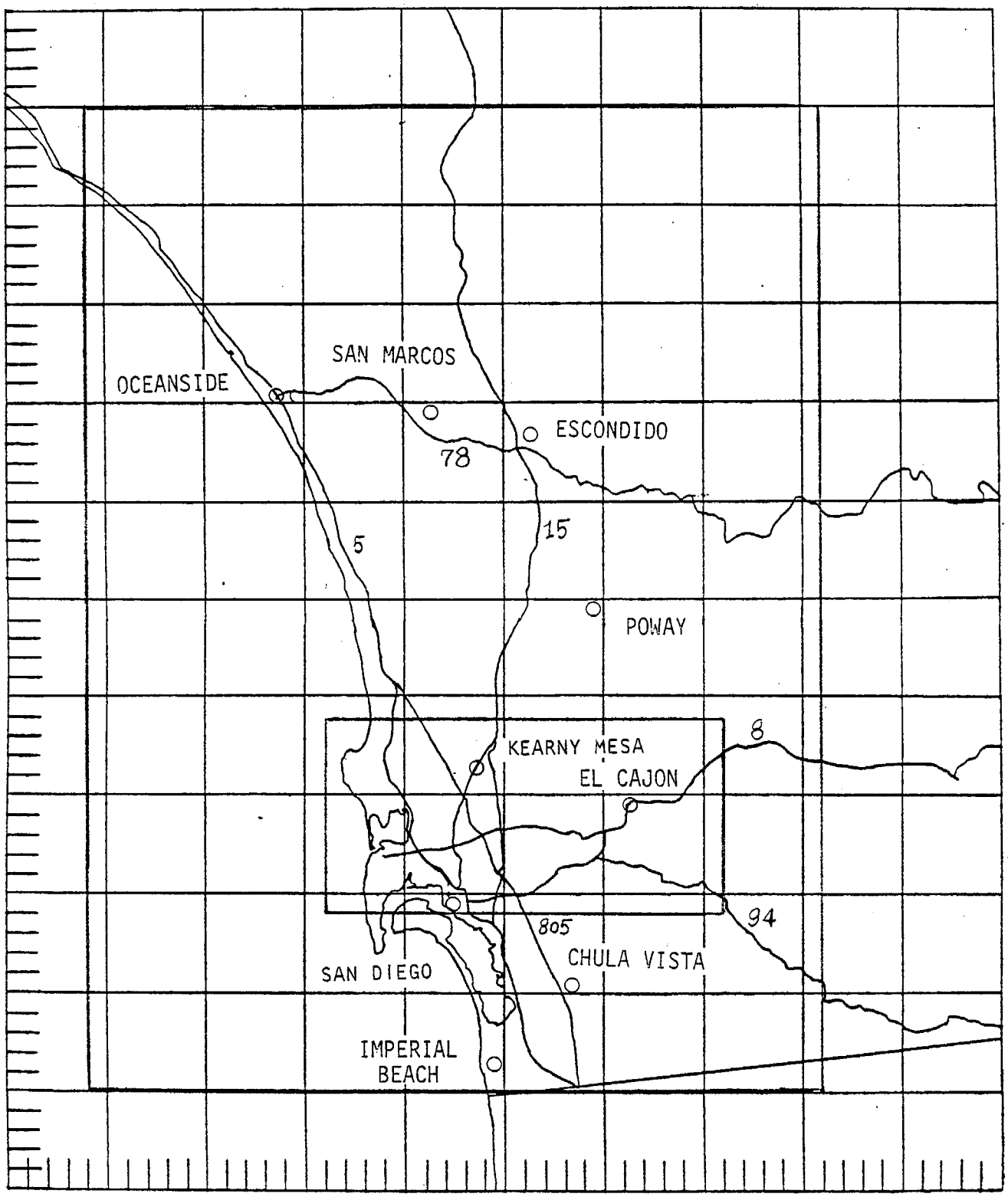

Figure 3.1 San Diego Air Basin

3.2 BASELINE INPUT DATA

Eleven consecutive hours on both October 3, 1975 and October 16, 1975 were selected to form the baseline input data. Both these time periods start at six o'clock (PST in the morning and terminate at four o'clock (PST) in the afternoon (0600 to 1600 PST). The timing convention used in MADCAP is that all data from hour T, which generally represents an hour average, is used to predict concentrations at time (T + 1) hour.

To generate the required MADCAP input, raw data was processed by the three codes; PREBIC, PREMET AND PRESOR. While the output from the pre-processors is relative to the sub-grid chosen (e.g. 37 x 51), it should be noted that all raw input is used, and the sub-grid output is merely a subset of the processing. For example, the wind field on the 37 x 51 grid accurately reflects all wind sites - not only those within the sub-grid.

Presentation of the input data and results of a three-dimensional, eleven hour run involves several problems, especially in light of the fact the computer output is several thousand pages. Therefore in this report, only the salient effects are reported and discussed. Except where vertical effects are important, only the ground level results are presented. As for the baseline input data, only the run of 10/3/75 is reported here.

3.2.1 Initial and Boundary Conditions

PREBIC is the submodule which interpolates raw air quality concentration measurements throughout the study region. The first hour (0600) is used to initialize concentrations in MADCAP. For subsequent hours, concentrations along the upper and lower grid perimeters are utilized as the north and south boundary value input to MADCAP. As for the east and west boundary value inputs, the concentrations within the mountain boundary grids and coast boundary grids are used.

Table 3.1 is an example of the raw data input for hour 0600 PST, while Figure 3.2 displays the carbon monoxide output for the same hour which is used as an initial condition. Similar initial and boundary condition output are generated for ozone, nitrogen dioxide, nitrogen monoxide and three classes of reactive hydrocarbons. In these printer plot figures, the actual parameter value is obtained by consulting the correspondence maximum and minimum values immediately below the plot. For example in Figure 3.2 the region covered by 6's corresponds to a concentration of 3.67 ppm. Blanks have a value intermediate between two adjacent numbers so that in Figure 3.2 the blanks between the 6's and the 5's correspond to values in the range 3.22 ppm to 3.67 ppm.

It is interesting to note that the early morning, and in particular the initial condition hour of 0600 PST, is generally the highest CO concentration found during the 11-hour period. Perhaps this was the result of CO accumulation during overnight stagnant conditions.

3.2.2 Meteorology

For each hour, meteorological conditions within the grid must be defined for every cell. Thus for each cell MADCAP requires values for solar insolation, water vapor, diffusivity and wind speed and direction. These values are created by the submodule PREMET. The raw data input to PREMET consists of surface roughness and land use, which remain constant in time and hourly values at various recording sites of ground temperature, relative humidity, wind speed, wind direction, cloud cover, ceiling height, ultra-violet radiation and inversion height. The following subsections present the output of PREMET which represents the baseline meteorological input data to MADCAP.

Table 3.1 Echo of Input to PREBIC

CARD NO.	TYPE	I	J	YR	MO	DA	HR	CONCENTRATION BY SPECIES CO	NOX	NO2	NO	SO2	PART	CH4	NMHC	THC	O3
1	31	27	38	75	10	3	6	4.00	-6.00	0.05	0.14	-6.00	-6.	2.20	1.50	-6.00	0.0
2	31	22	39	75	10	3	6	3.00	-6.00	0.11	0.07	-6.00	-6.	1.94	0.35	-6.00	-6.00
3	31	23	15	75	10	3	6	3.00	-6.00	0.10	0.11	-6.00	-6.	2.00	0.80	-6.00	0.01
4	31	25	22	75	10	3	6	3.00	-6.00	0.06	0.15	0.0	-6.	1.80	0.50	-6.00	0.0
5	31	28	11	75	10	3	6	2.00	-6.00	0.05	0.03	0.0	-6.	1.80	0.50	-6.00	0.01
6	31	25	7	75	10	3	6	1.00	-6.00	0.06	0.01	0.0	-6.	2.00	0.20	-6.00	0.0
7	31	14	41	75	10	3	6	1.00	-6.00	0.04	0.02	0.0	-6.	2.00	0.40	-6.00	0.01
8	31	19	31	75	10	3	6	-6.00	-6.00	-6.00	-6.00	-6.00	-6.	-6.00	-6.00	-6.00	0.01
9	31	4	56	75	10	3	6	-6.00	-6.00	-6.00	-6.00	-6.00	-6.	-6.00	-6.00	-6.00	0.0
10	31	24	56	75	10	3	6	-6.00	-6.00	-6.00	-6.00	-6.00	-6.	-6.00	-6.00	-6.00	0.0
11	31	28	16	75	10	3	6	-6.00	-6.00	-6.00	-6.00	-6.00	-6.	-6.00	-6.00	-6.00	0.0
12	31	29	29	75	10	3	6	-6.00	-6.00	0.04	0.03	-6.00	-6.	1.99	0.22	-6.00	0.02
13	31	32	22	75	10	3	6	-6.00	-6.00	0.08	0.0	-6.00	-6.	-6.00	-6.00	-6.00	-6.00
14	31	41	22	75	10	3	6	-6.00	-6.00	-6.00	-6.00	-6.00	-6.	-6.00	-6.00	-6.00	0.0

TOTAL NUMBER OF AQ SITES FOR THIS HOUR IS: 14

DATE=10/ 3/75 HR= 600 PST

```
10/ 3/75      PLOT OF CE(I,J,1) FROM PREBIC        CO (PPM)
*3333333333            444444444                        55555*
333333333333           444444444                     555555555
3333333333333333       44444444                   555555555555
333333333333333333      4444444              5555555555555555
333333333333333333      4444444            555555555555555555
333            3333333  444444           55555555555555555555
                33333    44444         5555555555555555555555
                  3333   4444        555555555555555555555555
     2222222222     333  444       55555555555555555555555555
   22222222222222   33   444     5555555555555555555555555555
  222222         222  33   44    5555555                555555555
 22222     1111   22  3  444   55555                       55555
2222    11111 1111 22 3  44   5555                            55
2222   111        11 2 3  44  5555    666666
222    11   00000 1 2 3 44   555   66666666666
2222  111  000000   2 3 4   555  666    66666666
2222   11   00000 1 23 4    555 66        6666666
 222    11        1 2 3 4   555 6 77777    666666
  2222   11111111 2 3 44   5555 6 777777    666666
   22222          2  3 44   555 66 777777    666666
     22222222222  33  4   5555 66  777      6666666
3                 33  44   555   66         66666666
3333            3333  444   5555   6666666666666666
333333333333333     444    5555    666666666666666666
33333333333       4444    55555      66666666666666666
                 44444    55555         666666666666666
                444444    555555        6666666666666666666
            44444444      55555555      66666666666666666666
         444444444        55555555     666666666666666666666
    4444444444444         555555555    6666           6666666
444444444444444           5555555555  666               66666
444444444444444           5555555555  66  77777777 77     666
4444444444444             55555555555 6  7        777    666
444444444444              55555555555 6 7 888 888   77     66
4444444444444              5555555555 6 7 8 999  88  777   66
444444444444               555555555 6  8 9   99 88  77   66
44444444444444               555555  6  89    99 88 777   66
444444444444444               55555  6 78 99999 88  77   666
4444444444444444                555  6 7 88  88  777   6666
44444444444444444                 555 66 77   7777   6666
444444444444444444                    55 666     666666
4444444444444444444444          4444444  55
44444444444444444444444444     44   3   44   5555555555555
44444444              444444444   33   333  44    555555555
                            333        333  444
                      333333    222222    333   4444
                  333333   222     2222    333    44444
               3333333   22  11   11 222    333    4444444
             3333333   222  1  000  1  22    333     444444
*           3333333    22  11 00000 11  22   3333     44444*
```

MINIMUM VALUE = 1.000E+00 MAXIMUM VALUE = 5.000E+00

Figure 3.2 CO Concentration at 0600 PST on 10/3/75

3.2.2.1 10/3/75 Baseline Solar Intensity

A value for each cell of solar intensity (in watts/m^2) is created from measurements of ultra-violet radiation at one or two sites within the large 50 x 60 grid. Cloud cover obviously affects the ground measurements and this is taken into account both at the measurement site and at each cell for which a value is synthesized. Thus, the resulting solar intensity pattern strongly reflects the cloud cover pattern if present. This can be clearly seen from Figure 3.3 where solar intensity follows the coastal cloud pattern for 0700 PST and sunny coastal region at 1200 PST. At 0600 PST, the solar intensity was essentially zero.

3.2.2.2 10/3/75 Baseline Water Vapor

MADCAP requires the definition of water vapor in absolute units of ppm (not relative humidity) for each cell, every hour. PREMET creates this from primary measurements at a few sites of relative humidity and of ground temperature. The known, and tabulated temperature dependent density of saturated air is used for this conversion. Figure 3.4 presents the water vapor inputs to MADCAP at 0600 PST and 1200 PST respectively. Again, notice that the humidity contours are conformal to the coast lines.

3.2.2.3 10/3/75 Baseline Diffusivities

PREMET generates a three-dimensional array of vertical diffusion values each hour using the Myrup-Ranzieri scheme which is based on a calculation of the Monin-Obukhov length. As with most diffusivity algorithms the basic input consists of local wind speed, atmospheric stability and height above ground, but in addition, account is taken of surface roughness and land use. Characteristically, the diffusivities so generated show a wide range of values (a factor of 500) within each layer (accentuated for the lower levels) and moderate interlevel variation of about a factor of 10. The absolute range of diffusivities is seen to be 0 to 1000 m^2/sec. Figures 3.5 presents the baseline diffusivities for the ground layer at 0600 and 1200 PST. These figures clearly indicate a very

OUTPUT FROM PREMET VERSION= 0/ 1

10/ 3/75 PLOT OF SOLAR INTENSITY AS INFERRED FROM CLOUD COVER (WATTS/M**2)

10/ 3/75 HR= 700 PST

```
*   124  6   4  4  678 999  88 777  6666       55555555555   *
    124 7    4  4  678 999  88  77   666       55555555555
    124 7    4  4  678 999  88  77   666       55555555555
   0124 7    4  4  678 999  88  77   666       55555555555
   0124 7    4  4  678 999  88  77   666       55555555555
     1 46     4  4   78 9999 88  77   666       55555555555
          67  4  445   89999  88 77   6666       55555555555
        2   7654  4 5678 9999  8  77   6666       5555555555
       0 124677     4    8 9999 88  77   666       555555555
            35    4   45    9999  88 77   6666       5555555
          00  46  6  3 4  67899 99  8  77   6666       555555
           00   67 65     5678 9 99  8  77   6666       55555
             0012  876  3 4    899 99 88  77   666       5555
             00 1  6 8   33 45678 9  9  8  77   6666       555
              00013 7 7  33 45    9  99 88 777  6666       55
                00   688   33  567899  9  8  77   6666
                 0613 8975 33 45 78 9  99 88 777  6666
                 000 2 79 64333      9   9  8  77   6666
                   00013  975333 4  78 9  99 88  77  6666
                    00  5 9  33 34     9   9  8  77   666
                    00 25 9  3  3      9   9  8  77   666
                    000 1      3 3 456789   99 88 77   66666
0000000000000000000000000  6  7    3456789   99 88 77   66666
0000000000000000000000000  6  7    3456789   99 88 777  66666
0000000000000000000000000   7 863  3  5   9   99 8  77   666
0000000000000000000000000   7 863 23 45   9   99 8  77   666
0000000000000000000000000  47 86322  456  9   99 8  77   666
0000000000000000000000000   89  22 3    8     9  8  77  66
0000000000000000000000000   8   22 3    89    9  8  77  66
0000000000000000000000000   8 7 2223    89    9  8  77  66
0000000000000000000000002 8 7  223      89    9  8  77  66
0000000000000000000000002   74  23      89    9  8  77  66
0000000000000000000000025   74  23      89    9  8  77  66
0000000000000000000000 36 86   23456789    9 88 777  66
0000000000000000000000 4   52   345       99 8  77   666
0000000000000000000000 3       23456789    9 88 777  666
0000000000000000000000 0025     112     89    9  8  77  66
0000000000000000000000 0025      12     89    9  8  77  66
0000000000000000000000 00 5      12     89    9  8  77  66
0000000000000000000000 00     63 1      89    9  8  77  66
0000000000000000000000 0      63 1      89    9  8  77  66
0000000000000000000000 0      6301      8     9  8  77  66
0000000000000000000000000000000135 420 35  4   7 88     88 777
0000000000000000000000000000000 0 2  763          9   9  88
0000000000000000000000000000000  0 4 9630    4        9  8
0000000000000000000000000000000000 01   7  112    6789   99
0000000000000000000000000000000000   0 5    012    789   999
0000000000000000000000000000000000   0 5    012    789   999
0000000000000000000000000000000000   0 5874 012    789   999
*0000000000000000000000000000000000   0 5874 012    789   99*
```

MINIMUM VALUE = 2.656E-01 MAXIMUM VALUE = 7.500E+00

DATE=10/ 3/75 HR=1200 PST

```
* 5 4433 34566  7  8 99 999   8888     777777777777        *
6 5 4433 34566  7  8 99 999   8888     777777777777
6 5 4 3  3456   7  8 99 999   8888     777777777777
6 5 4 3  3456   7  8 9   99   8888     777777777777
6 5 4 3  3456   7 8  9   999  8888     777777777777
 6 5 4 3  3456  77 8  9   999  8888     777777777777
  66 5 4 3      6  77 8 99  999  8888     777777777777
    665  43   456  77  8 9   999   888     777777777777
      6 5 4 3  3456  77 8 99   999  8888     777777777777
        6 5 4       777 8 9    99   8888     777777777777
           5 4 3   4 6  77 8 99   999   888     777777777777
           655  3 2  56  77  8 9    99   888     777777777777
              5 4  2234   777 8 99   999  8888     777777777777
777777777777655 432 2 56 777  8 9    99   888     777777777
7777777777   5 43 223 6 7777 8 9    999  8888     777777777
7777777777 7777 655  32 2 5 7777 8 99    99   888     777777
7777777777 77777  5 43   35 77777 8 9    999  8888     777777
7777777777 777777765 4  2  46 7777 8 9    99   888     7777
7777777777 77777777  5  32  35 7777  8 9    999  8888     777
                 7 5 43  1   77777 8 9    99  8888     777
                 765 43  1   77777 8 9    99  8888     777
                     54  212  77777 8 9    99   888
                     5   21 3 7 777   9    999  8888
                     5   2    7 777   9    999  8888
888888888888888888888    43  024   777 8 9    99   888
888888888888888888888    43  024   77 8 9    99   888
888888888888888888888    43  024   77 8 9    99   888
888888888888888888888 65   2  3    77  8 9    99  8888
888888888888888888888 65 3 2  3    77  8 9    99  8888
                      6543 2  3 88  7  8 9    99  8888
                      6543 2  3 88  7  8 9    99  8888
                     8 543 2  3 88    8 9    99  8888
                     8 543 2  36 8    8 9    99  8888
9999999999999999999999   65432 1 4  8    8 9    99  8888
9999999999999999999999 7    210 58 8    8 9    99   888
9999999999999999999999  5  2  2 788    8 9    99  8888
9999999999999999999999   4322 1  9 8    8 9    99  8888
9999999999999999999999 7 4 2211  9 8    8 9    99  8888
                      7 4 22114 9 8    8 9    99  8888
                      7 4 22114 9 8    8 9    99  8888
                      7 4 221 479 8    8 9    99  8888
                      7 4 221 47  6    8 9    99  8888
                     98765   3  7 65678   999999999   8888
                           43 2  47 98    8 9    99
                          9  43 2   7 98    8 9    999
                           75 3 223 8  8    8 9    999
                           75   2 3 8  8    8 9    99
                           75   2 3 8  8    8 9    99
                           75   2 3 8  8    8 9    99
*                          75   2 36   8    8 9    9*
```

MINIMUM VALUE = 1.401E+01 MAXIMUM VALUE = 3.100E+01

Figure 3.3 Solar Intensity Distributions on 10/3/75

```
OUTPUT FROM PREMET     VERSION= 0/ 1

10/ 3/75       PLOT OF WATER CONCENTRATION  (PPM)      HR= 600PST

43  3333  33333333 2  11  111  2  3332101 23   78 999 8 7 6*
33   333  33333333 2  1   111  2  3332101 234  78 999 8 7 66
33   333  33333333 2  1   111  2  3 32101 234  78 999 8 7 66
33   333  33333333 2  1   111  2  3 32101 234 6789999 8 7 66
33   333  33333333 2  1   111  2 33 3 1 1 234 6789 99 8 7 66
333   33   33333333 2  1   111  2 33 32 11  345678999 8 7
3333    33    33333333 2 11   111 22 3  321 12  45   9 99 8
333333   333   3333333 22 11   11  2  3  3211 23    899 9 88
33333333    33    3333333 2  1    11  2 3      11  3456789  99
333333333     33   33333333 2 11   111 22 3      1 2        9
3333333333 2 33    3333  3 2  11   11  2 3 44 2 1  34 67 9
33333333333   33    3333  3  2 11   11  2 3  4   1  34  7899
3333333333333    33    3333  3 2  11   11  2 3 44  1 2  456
3333333333333 2 33    3333   3 2 11   11  2 3 4443   234  77
33333333333333  2 33    333   3 2 111  111 22 3444    23
3333333333333333 2233    3333   3 2 111  11  2 3 4 4 2 2 344
333333333333333 2233     333   3 2  11  111 22  4  42  23 4
3333333333333333  2 33    333   3 2  11   11  2 3 4   222 3
33333333333333333333 22 3     333   3 2  11  111 22  4   3222
3333333333333333333 2  3     333   3 2  11   11  2  4 55 222
33333333333333333333 22 3     333   3 2  11   11  2  4 5   22
3333333333333333333  2 33    3333   3 2  11  11  2 3  55 3
33333333333333333333 2 3      333   3 2  11  111 2 3  5 533
33333333333333333333 22 3     333   3 2   1  111 2 3  5   3
3333333333333333333333 223     333  4 32   1   11  2 34  66
3333333333333333333333 223     3333 4 322  1   11  2 34
3333333333333333333333 2 3     3333 4 322      11  2 34
                       32        333   3 2   1   11 22   55
                       3  3      333   3 2   1   11 22   55
                       3  3      333   3 2   1   11 22   5
                        333     3333   3 2   1   11 22   5
                        4 34 3  3333   3 2  21   11 22   5
                        4  443  3333   3 2  210  11 22   5
                       444 4    3333   3 2   10   1  2 34
                      44 44    33333   322 2 00 11   2  45677
                      44 44    33333   3 2 2      1  2 34   7
                       4444443    3333  3 2  210  11 2 3
                       4444443  4 3333  3 2  210  11 2 3
4444444444444444444444444443  4 3333  3 2  210  11 2 3
444444444444444444444444443  4  333  3 2  210  11 2 3
44444444444444444444444444443  4  333  3 2   10  11 2 3
4444444444444444444444444444433 43 333  3 2   10  11 2 3
44444444444444444444444444443  4 333   3  22  1111    2  44
444444444444444444444444444444444  3  33 33 33 2       111
4444444444444444444444444444444444433  3  33  3 2   10  11
44444444444444444444444444444444444444 33  33333 33 2  1    1
444444444444444444444444444444444  44  3  3 333 33 2    0
444444444444444444444444444444444  44  3  3 333 33 2    0
44444444444444444444444444444444  443 3  3 333333 2    0
*44444444444444444444444444444444  443 3    33333  2      *

MINIMUM VALUE = 1.178E+04     MAXIMUM VALUE = 2.707E+04
```

```
OUTPUT FROM PREMET     VERSION= 0/ 1

10/ 3/75       PLOT OF WATER CONCENTRATION  (PPM)      HR=1200PST

*    55      6 7 876543 22 3 4   55        6666          6666*
     55      6 7 876543 22 3 4   55        6666          66666
     55      6 7 876543 22 3 4   55        6666          66666
     55      6 7 876543 2  3 4   55        6666          66666
     55      6 7 876543 2  3 4   55        6666          66666
    4 55      6 7  765 3 22 3 4   55       66666           6666
44   4 555     66          222   4  555      6666           66
4444   4555      6 7 8  543 2223 44  555       6666
44444     555      6 78876  322223 44  55       66666
4444444      55     667 867    222   4  555       6666
44444444 33 555      6  8   5  22 23 44  55       66666
44444444   34555      6 7888 543 2223 44  555       66666
444444444  33 555      6  88 6   222 3 44  55       6666
4444444444443  555     6678 8 543222 3 44  555  6   66666
444444444444  3 555      678  7 43 22 3  4   55   6   6666
4444444444444 3 4 55      6 78 8 5 322 33 44  555  66  66666
444444444444443 4 55      678  7 4322 33  4   55  66  66666
4444444444444444  35 55 6   6   9 6   22333 44  55   66 6666
44444444444444444 32  55  6   678 97 4322  33 4   55  666 66
4444444444444444444  3 555 6   6 8 9 6 322  33 44  55  666666
4444444444444444444  3 555 6   6 8   64322  33 44  55  666666
444444444444444444444 14 55 6 5 6 7 9 75  223 3  4  555 66666
44444444444444444444   555 665  6789 7   2  33  4  555  6666
                       555 665  67 997   2  333 4  555  6666
                     4   555   5 6     8  3222333 44  55  666
                     41  5 5   5 6     8   222 33 44  55  666
                     4  45 5   5 6     8   222 33  4  55  666
                       30  5 56655 6789   432 2 33 44  55  6
5555555555 5555555555555    5 56655 6789   432 2  3 44  55  6
5555555555 5555555555555  3   56655 67899  432 22 3 44  55  6
5555555555 555555555555554    566 5 67899  432 22 3 44  55  6
5555555555 5555555555555      566 5 67899  432  2 3 44  55  6
                     544      566 5667899  4 2  2 3 44  55  6
                     5        566 56 78  75  2  2 3 4  555 66
                        65  5  6     8  322  23  4  55  6
                     5  5 5 655 6 789875  2  2 3 4  555 666
6666666666 666666666666     6   6 56678 97 4 2     3 44  55  6
6666666666 666666666666     6 4 6556678 97 4 2     3 44  55  6
6666666666 666666666666   4 6 4 65566    7 4 2     3 44  55  6
6666666666 666666666666   4 6 4 65 66    7 4 2     3 44  55  6
6666666666 666666666666   4 6  565 66    7 432     3 44  55  6
6666666666 666666666666   4 6  565 66    7 432     3 44  55  6
                     65556  55  6 67     444 33333  44 555
                            5 5 5 55  6 7 887 4322 2 3 44
                            6     3  5     8 7 432     3
                            6  55   5 66 7 8  54 2  2 33
                               56435 56  7 8  5  2  2
                               56435 56  7 8  5  2  2
                               5 435 56  7 8  5  2  2
*                                 43  6     8  5  2  2 *

MINIMUM VALUE = 1.075E+04     MAXIMUM VALUE = 2.431E+04
```

Figure 3.4 Water Concentration Distributions on 10/3/75

DATE=10/ 3/75 HR= 600 PST

DIFFUSIVITIES (M**2/SEC) FOR THE LAYER

MINIMUM VALUE = 2.121E-05 MAXIMUM VALUE = 1.076E+01

DATE=10/ 3/75 HR=1200 PST

K= 1

DIFFUSIVITIES (M**2/SEC) FOR THE LAYER

MINIMUM VALUE = 1.062E-01 MAXIMUM VALUE = 2.594E+01

Figure 3.5 Diffusivity Distributions on 10/3/75

complex pattern of calculated diffusivities--undoubtedly reflecting the influence of the numerous inputs and calculations required to generate them. Upper levels also have the same characteristics consistent with previous comments regarding magnitude.

3.2.2.4 10/3/75 Baseline Wind Field

The baseline wind field consists of a wind speed and direction value for every cell in the 3-D grid for each of the eleven hours. The calculated field has no vertical components. PREMET creates these values by simple interpolation of measured data. Figures 3.6 through 3.7 display the baseline wind fields for the ground layer at 0800 and 1600 PST. Since no pibals were used in this baseline, the upper levels have wind fields identical in direction to the ground level but speeded up by the appropriate stability-controlled power law. These figures are computer-generated plots using vector component output values generated by PREMET. The relative length of the arrow assigned to each cell indicates the magnitude of the wind speed.

An examination of these plots and the wind data for all hours reveals that on October 3, 1975 the day started with mixed winds characteristic of the meeting of ocean and drainage flows but soon settled down to onshore flow which gradually rotated from about 320° at 0900 PST to 225° at 1600 PST for the San Diego metropolitan area. In the North County, the prevailing wind is 90° at 0900 PST at shoreline and gradually changes to the northwest direction in the afternoon. Due to the drainage flow, two stagnate regions are observed in the morning, i.e., the El Cajon region and the Poway region. As the westerly wind prevails in the afternoon, these stagnate regions disappear with time. The highest winds occurred in early afternoon and were mostly due east. Figure 3.8 summarizes the variation of maximum wind speed found in the small grid which encompasses the San Diego metropolitan area during the

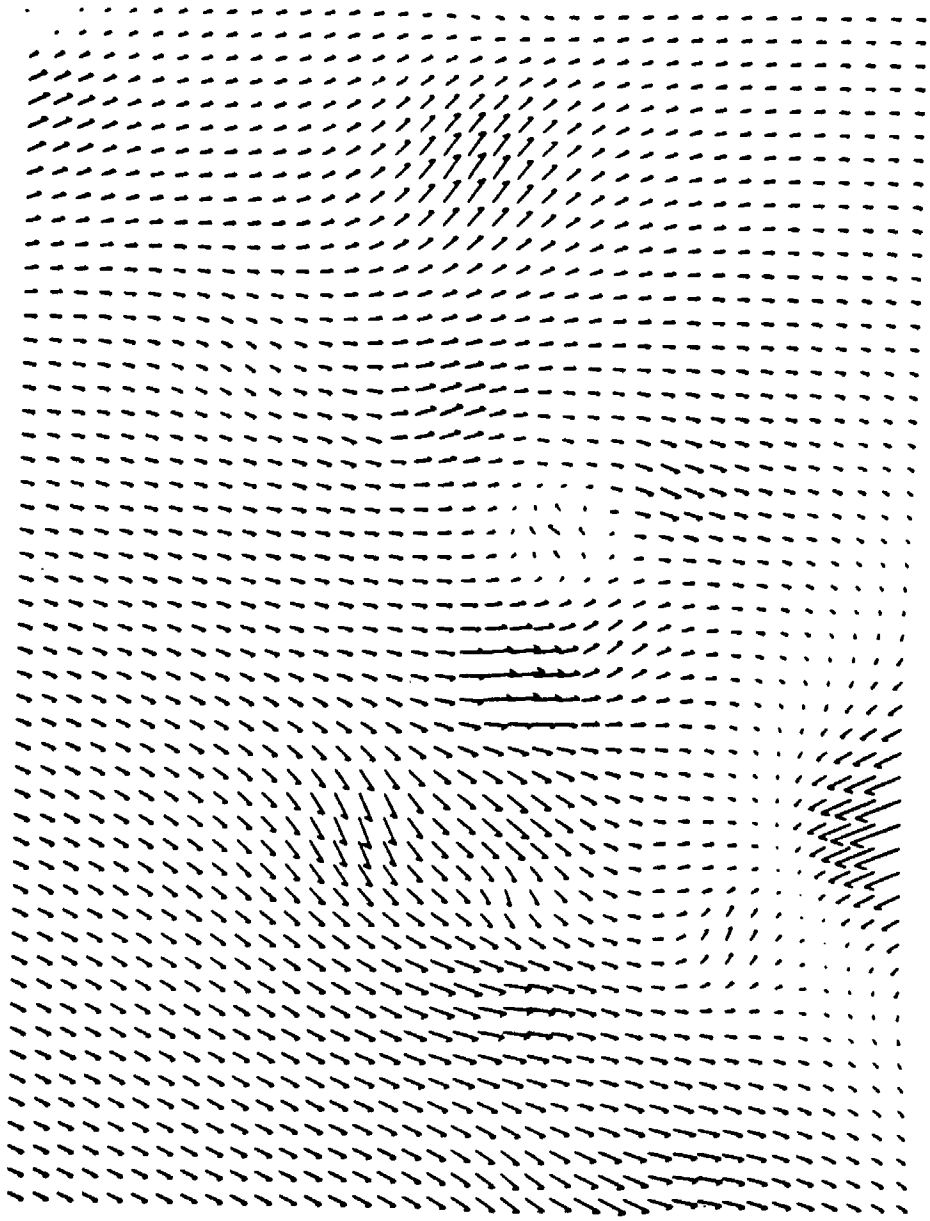

Figure 3.6 Wind Field at Ground Level, 0800 PST, 10/3/75

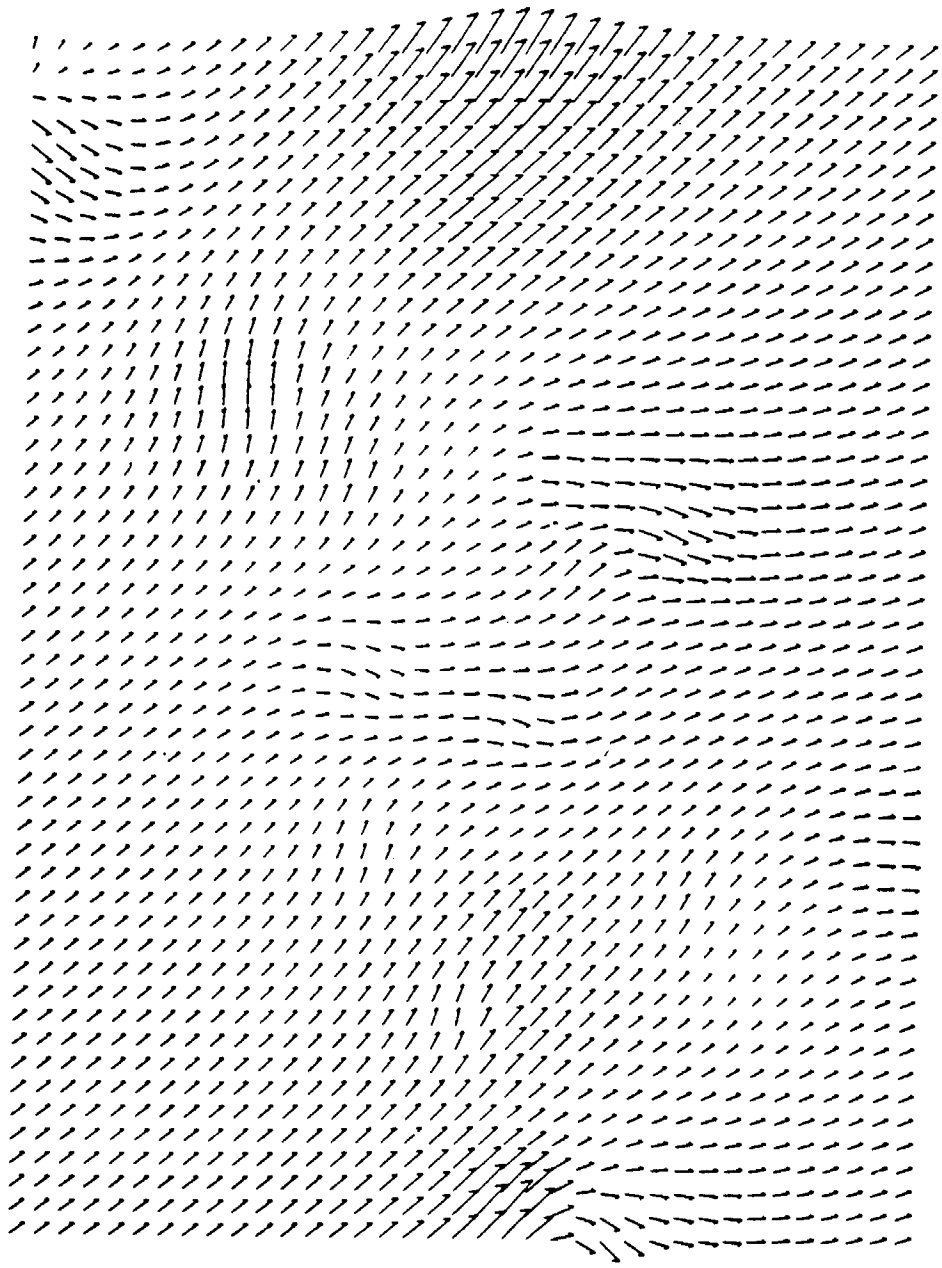

MADCAP K= 1 10/ 3/75/16

Figure 3.7 Wind Field at Ground Level, 1600 PST, 10/3/75

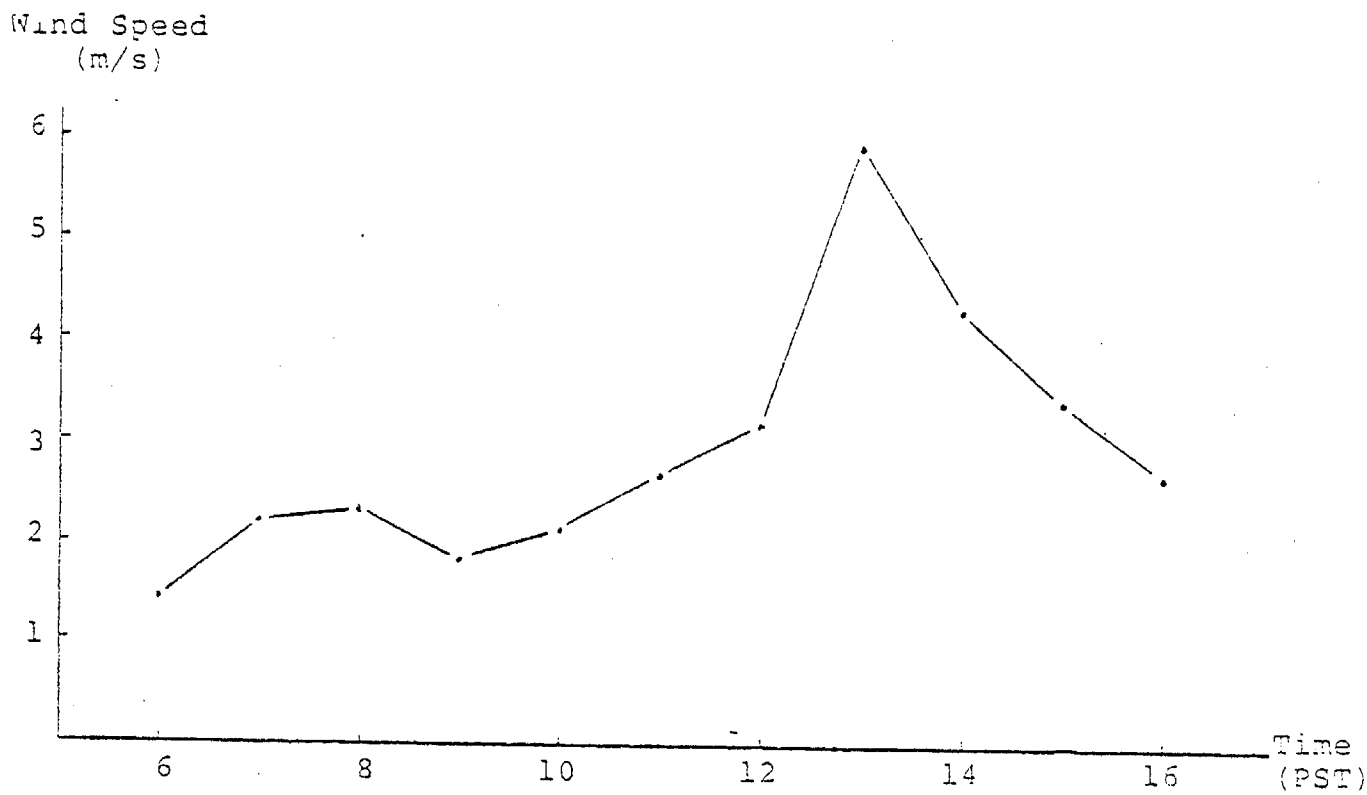

October 3, 1975

Figure 3.8 Variation of Highest Speed in the Small Grid

course of these eleven hours and clearly shows the wind pick-up in the early afternoon. With the possible exception of hours 0900 and 1000 which show southerly winds in the eastern part of the grid, the hourly wind field varies uniformly from cell to cell and appears physically consistent.

3.2.2.5 Comparison Between 10/3/75 Baseline Wind Field And The Wind Field Predicted By WEST

In MADCAP, a simple $1/r^2$ interpolation of measured wind data is used to generate the wind field in a three-dimensional grid space. For a realistic and accurate regional model simulation, it is essential to establish the validity of the wind field used in the model. In here the resultant wind field from $1/r^2$ interpolation is compared with the divergence-free wind field generated by WEST.

The WEST module was first used in the DEPICT[9] code and later used in IMPACT[1]. The detailed theory can be found in Reference 1. A brief description is given below. WEST uses an iterative procedure to adjust the calculated wind field such that the wind field satisfies the incompressible mass conservation equation, or $\nabla.\overline{V} = 0$. The initial wind field is calculated by employing the same $1/r^2$ interpolation method on the measured wind data. The adjusted non-divergent velocity component $\overline{V}$ is defined as

$$\overline{V} = \overline{V}_o + \overline{V}' = \overline{V}_o + \overline{\tau} \cdot \nabla\phi$$

where $\overline{V}_o$ is the initial wind field and $\overline{V}'$ is a perturbation wind field which can be expressed as a product of the three dimensional transmission function $\overline{\tau}$ and a velocity potential ϕ. After substituting the above equation into the incompressible continuity equation, a Poisson equation governing the velocity potential is formed. The perturbation velocity $\overline{V}'$ can be obtained by solving the resultant Poisson equation for ϕ. Combining the perturbation velocity and the initial velocity field gives a new velocity field which is used as the initial wind field for the subsequent iteration. This process can be continued until the residual velocity (or perturbation

velocity) approaches zero (or a certain convergence criterion is satisfied).

Also in WEST, a weighting factor is used in the calculation. A weighting factor of unity forces the velocity vector components at observation stations to remain unchanged, while a factor of non-unity allows the vector to change as a result of the adjustment procedure.

In this report, the same input data are used for both the MADCAP wind field generator and the WEST routine. The inversion heights and stability distribution from PREMET and measured wind speed are used as the input to the WEST module.

Figures 3.9 and 3.10 show the comparisons between the wind field generated by the method used in the MADCAP and the wind field calculated by the WEST routine. In general, the wind fields agree with each other very well except along the northern boundary at 1600 PST. Since the WEST routine generates a divergence-free wind field, the flux across the boundary has to be adjusted to conserve total mass. Therefore, noticeable changes occur at the boundaries. The wind speed predicted by MADCAP and WEST agree with each other to within five percent except at a few boundary points. The wind field patterns of MADCAP and WEST are similar. For most of the region the wind direction in a grid agrees well within a few degrees. Along the boundaries the wind direction predicted by MADCAP differ by as much as 20% from the predictions of the WEST calculation. At some points, e.g. the northwest corner at 1600 PST on 10/3/75, the wind direction predictions differ by more than 90 degrees. However, this is only a local effect where WEST has to adjust the wind field on the boundaries to satisfy the divergence free condition. In general, the agreement is remarkable.

It should also be noted that in this comparison, the vertical levels are assumed to be conformal with the ground level. The same assumption is used to run the WEST routine in order to make a fair comparison with the wind field generated in a Lagragian cell.

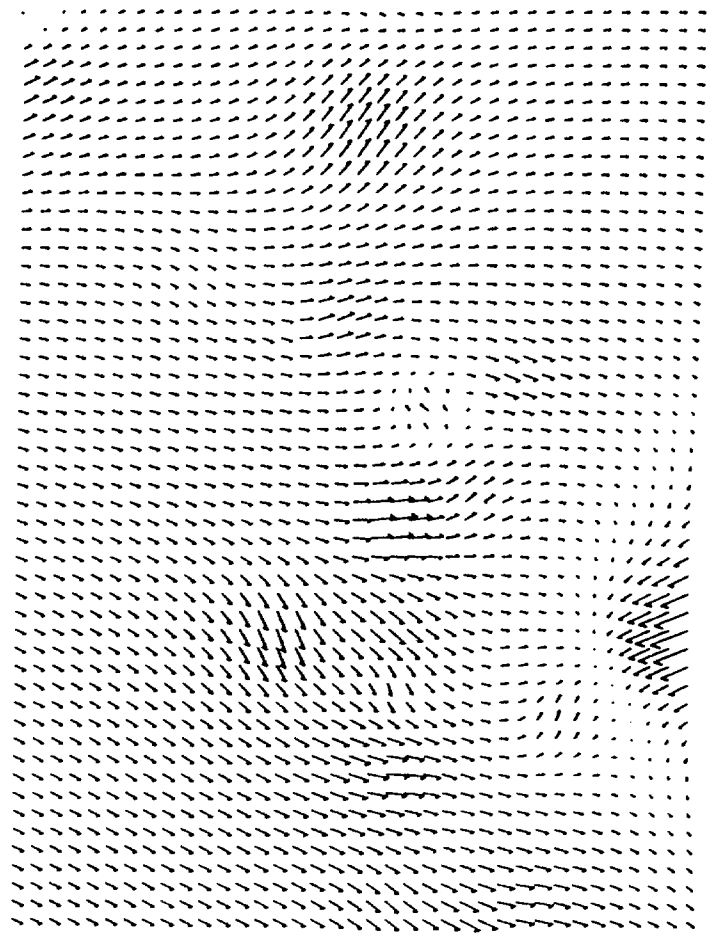

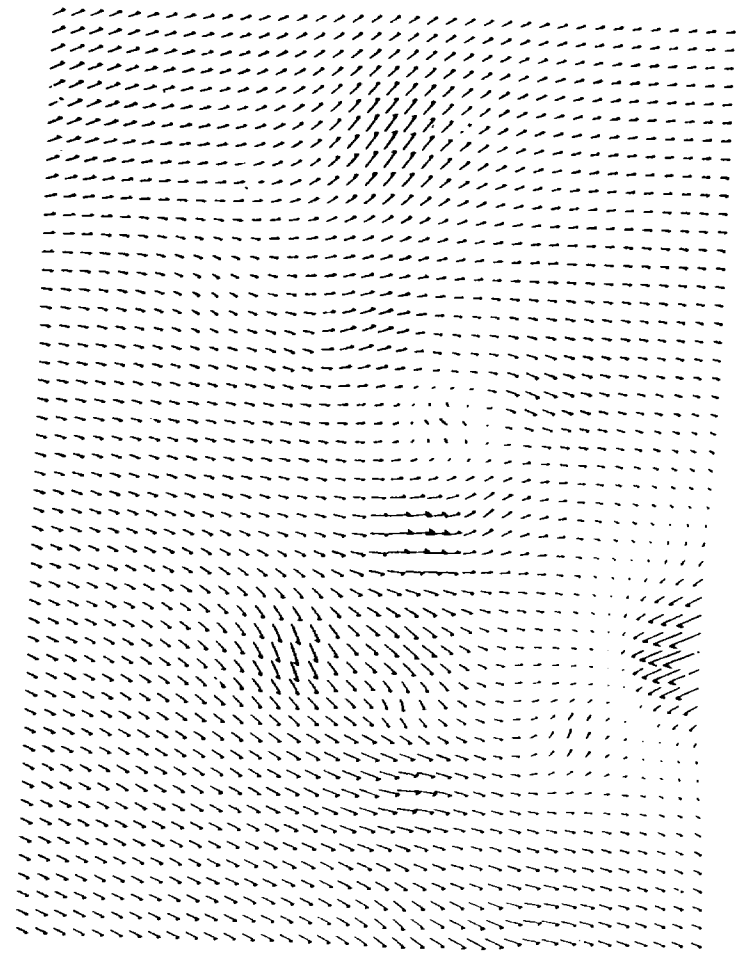

Figure 3.9a Wind Fields Comparisons Between MADCAP and WEST, Ground Level, 0800 PST, 10/3/75

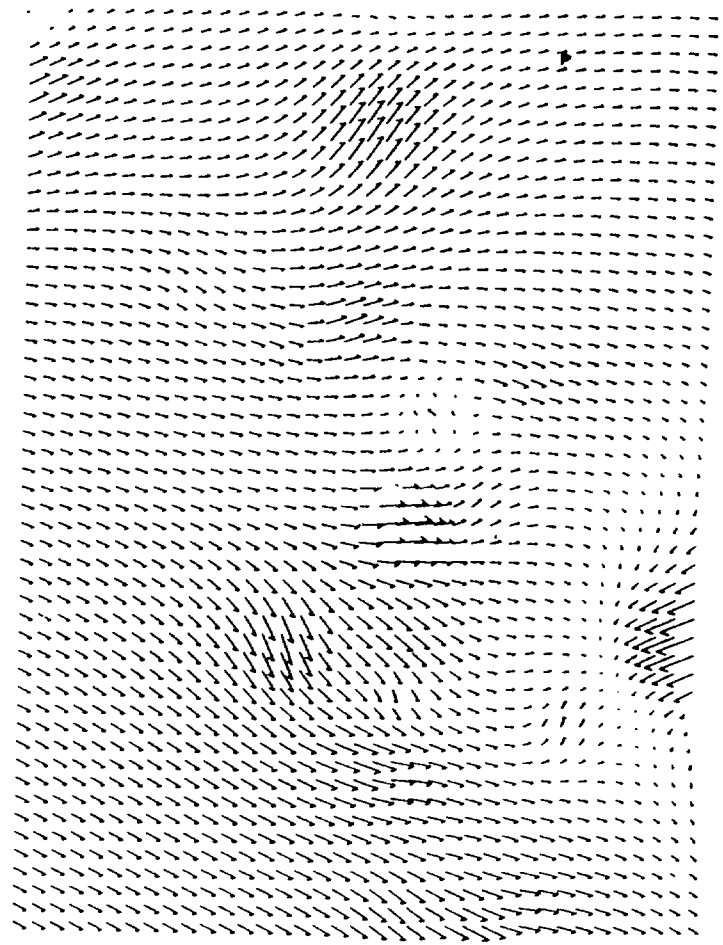

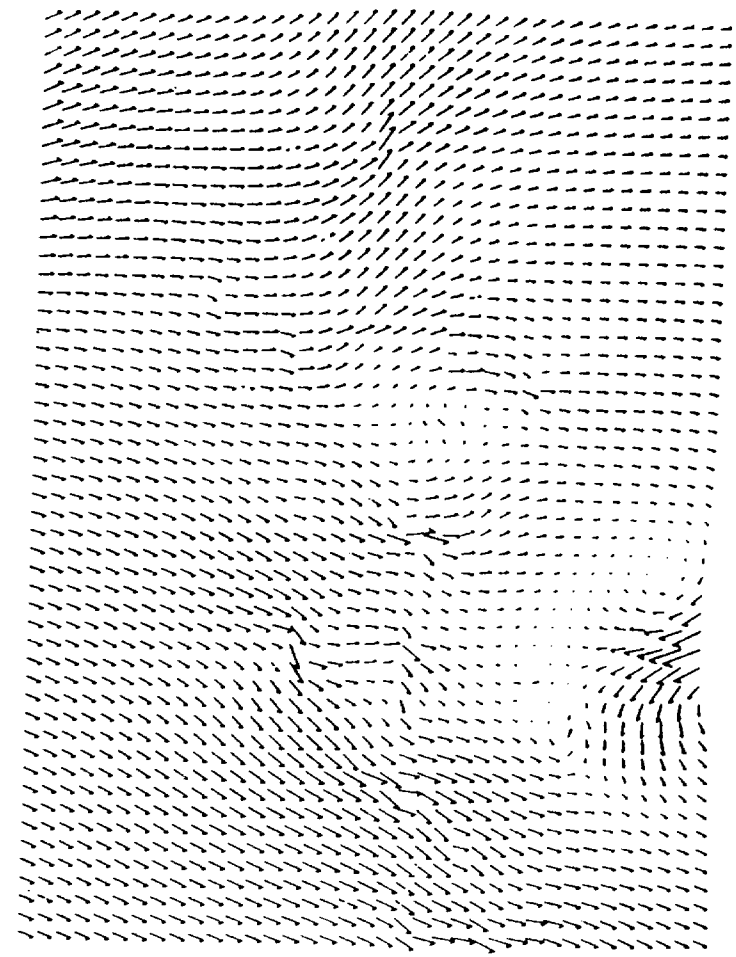

Figure 3.9b Wind Field Comparisons Between MADCAP and WEST, Level 3, 0800 PST, 10/3/75

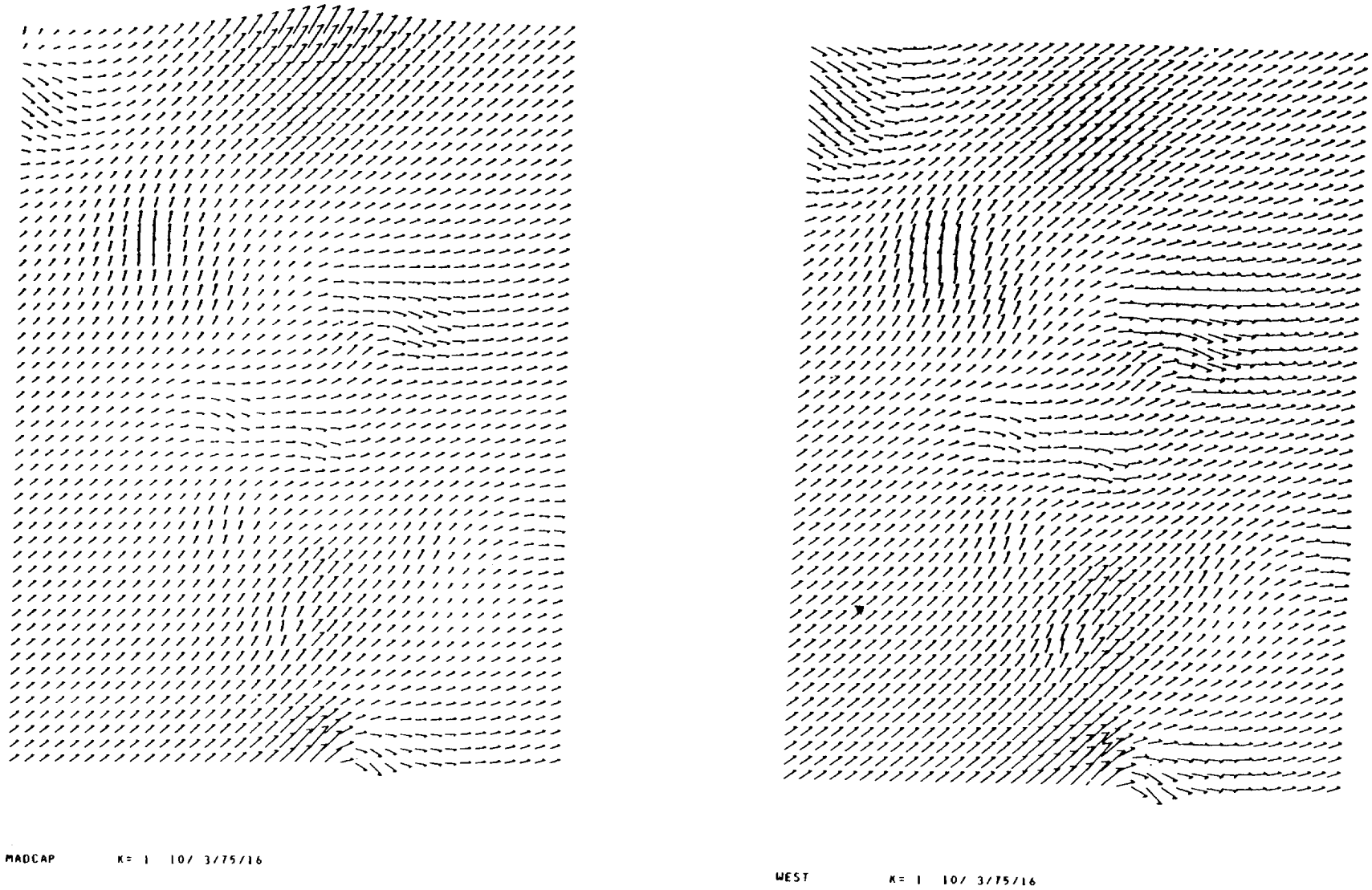

Figure 3.10 Wind Field Comparisons Between MADCAP and WEST, Ground Level, 1600 PST, 10/3/75

3.2.3 Sources

To predict air pollutant concentrations, MADCAP utilizes the LIRAQ photochemical system and requires as input the emission source rates for all species for each cell for each hour. Since source rates for most of the esoteric species of the LIRAQ mechanism are unknown and the source strength for ozone is taken as zero relative to ambient levels, this requirement reduces to the demand for input source rates for CO, NO_2, NO, and LIRAQ reactive hydrocarbons 1, 2 and 3. These values are created by PRESOR from raw input in the form of CO, NOX and THC assigned to each ground cell. PRESOR processes data from motor vehicles, shipping emissions, railway emissions, area emissions, stack emissions (including all relevant stack parameters) and lastly aircraft emissions. Using this information PRESOR splits NOX into NO and NO_2 and also splits THC into HC1, HC2 and HC3. Additionally, PRESOR computes plume rise for stack emissions and finally converts all emissions rates from kg/sec into ppm/min by using the known volume of the emission cell. The final emission rate for each cell is accumulated from all the specific sources present in that cell. The hourly result from PRESOR is a three-dimensional array of source strengths in ppm/min for each cell and each species, i.e., CO, NO_2, NO, HC1, HC2 and HC3. The ground level emissions for all sources are shown in Figure 3.11 through Figure 3.15. CO is a major pollutant emitted from mobile sources (traffic). Figure 3.11 shows the early morning emission at 0600 PST where the emission pattern is along major freeways (Figure 3.1) during rush hour. Oxides of nitrogen (NO_2 and NO) are emitted by both the stationary and mobile sources. Hence, the emission pattern not only reflects the rush hour period but also indicates high emissions throughout the daytime (Figure 3.12). The split between NO_2 and NO is 1 to 20 or less, depending upon the source type. The emission pattern of NO_2 is similar to the NO emission pattern and is not shown here. The

** ALL SOURCES LEVEL 1 CO (PPM/MIN)

DATE=10/ 3/75 HR= 600 PST

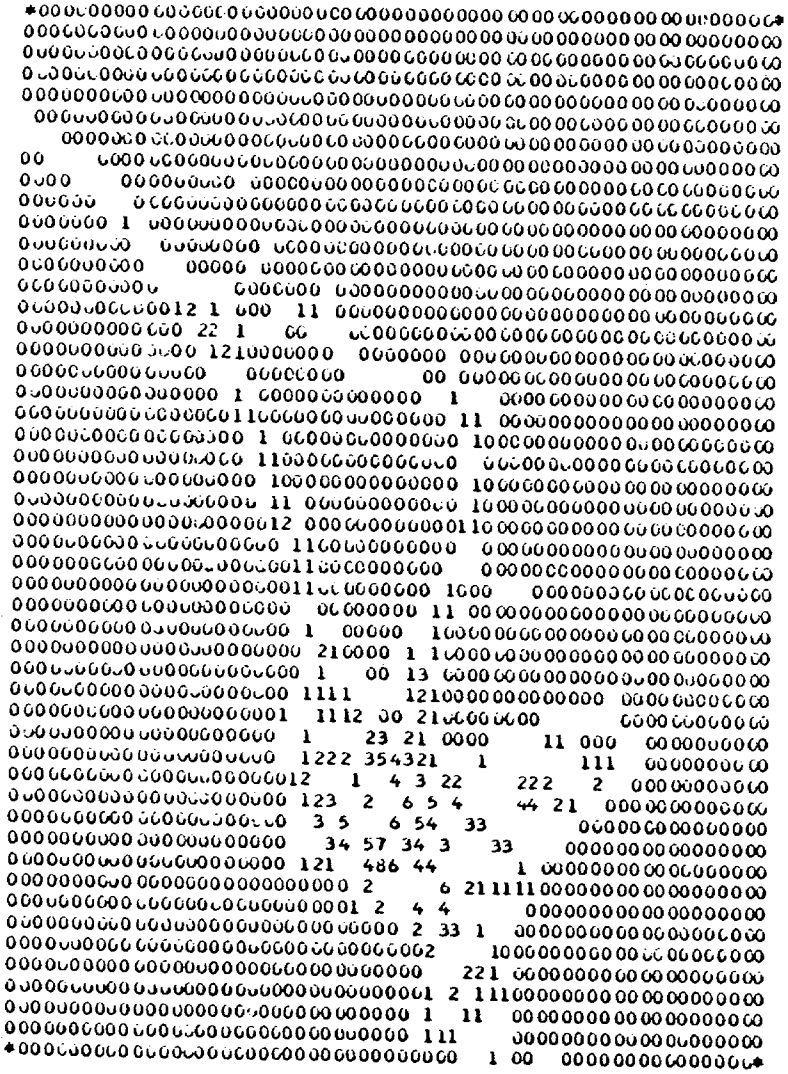

MINIMUM VALUE = 0.0 MAXIMUM VALUE = 5.051E-02

DATE=10/ 3/75 HR=1200 PST

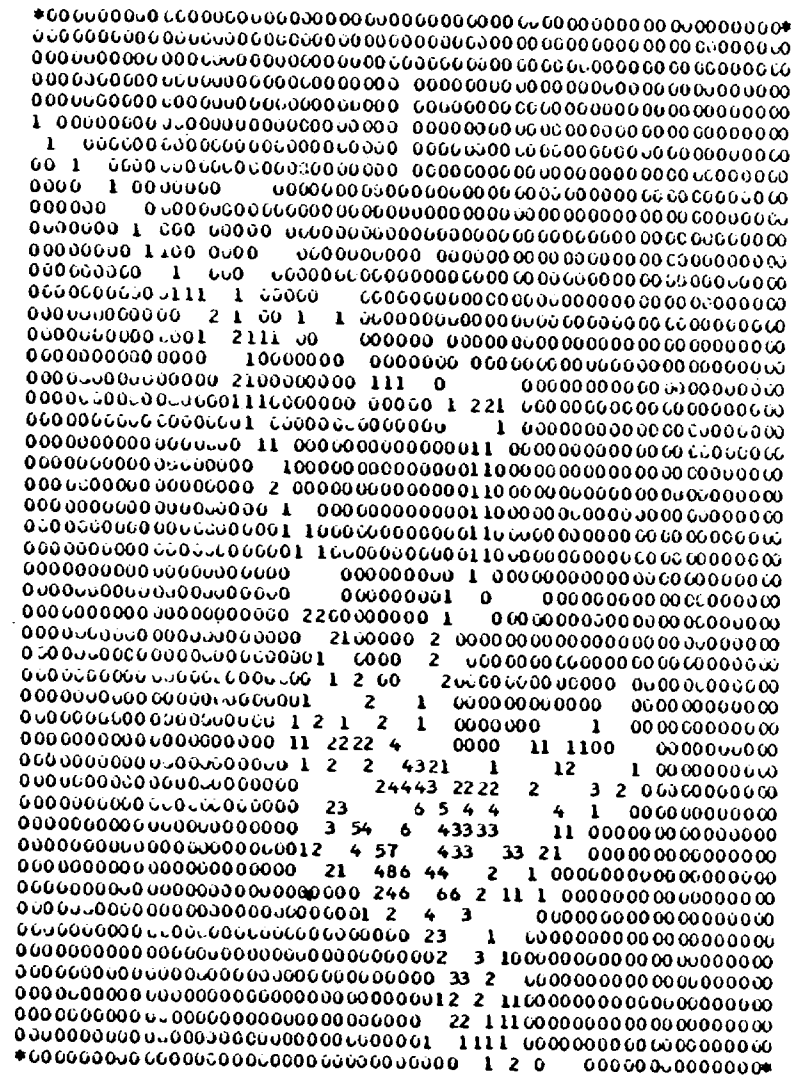

MINIMUM VALUE = 0.0 MAXIMUM VALUE = 4.480E-02

Figure 3.11 CO Source Distributions on 10/3/75

** ALL SOURCES LEVEL 1 NO (PPM/MIN)

DATE=10/ 3/75 HR= 600 PST

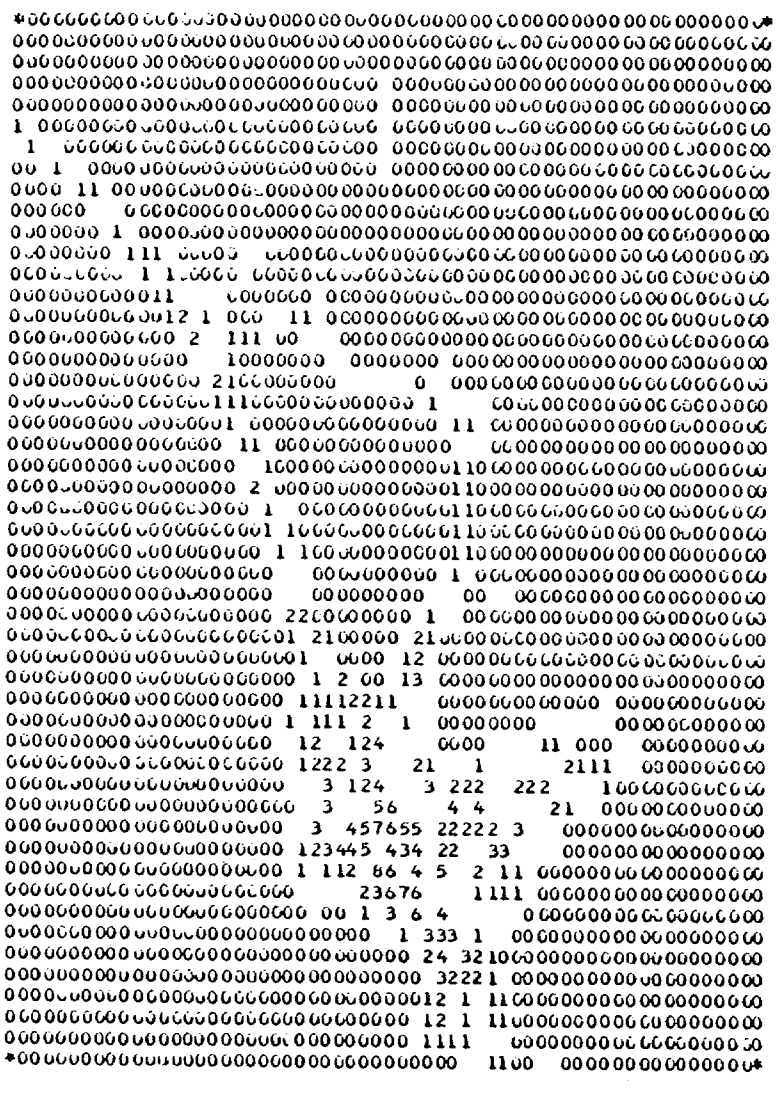

MINIMUM VALUE = 0.0 MAXIMUM VALUE = 4.327E-03

DATE=10/ 3/75 HR=1200 PST

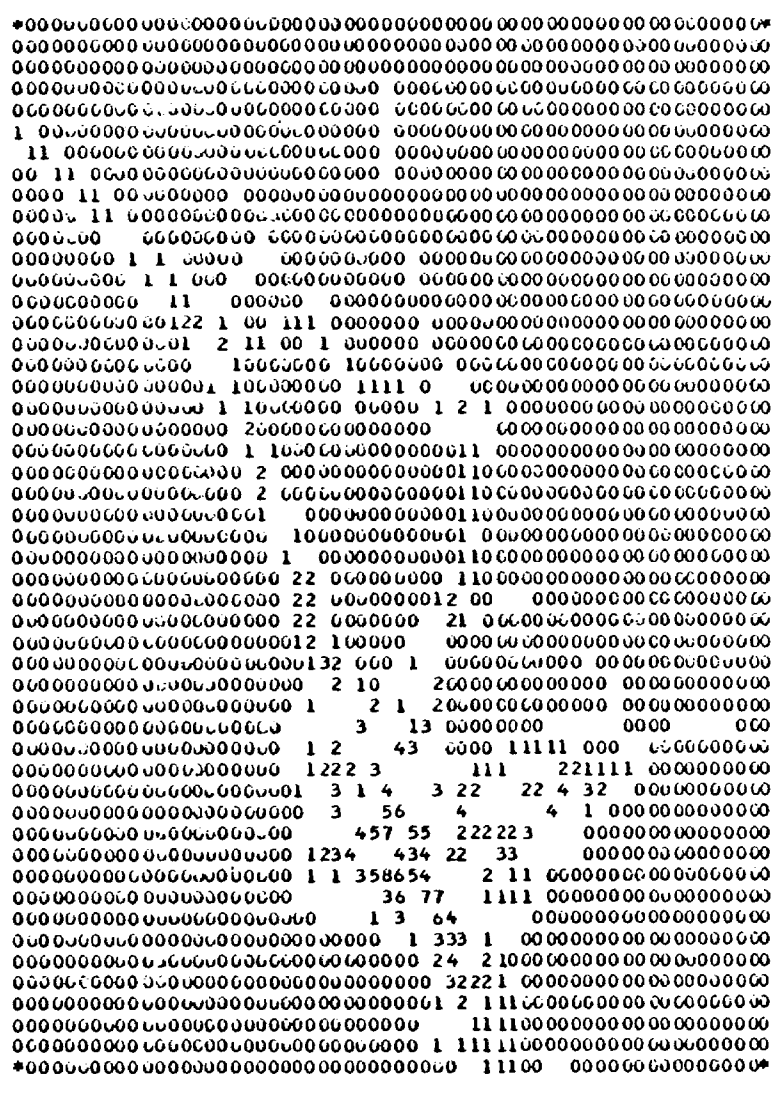

MINIMUM VALUE = 0.0 MAXIMUM VALUE = 4.552E-03

Figure 3.12 NO Source Distributions on 10/3/75

** ALL SOURCES LEVEL 1 HCl(PPM/MIN)

DATE=10/ 3/75 HR= 600 PST

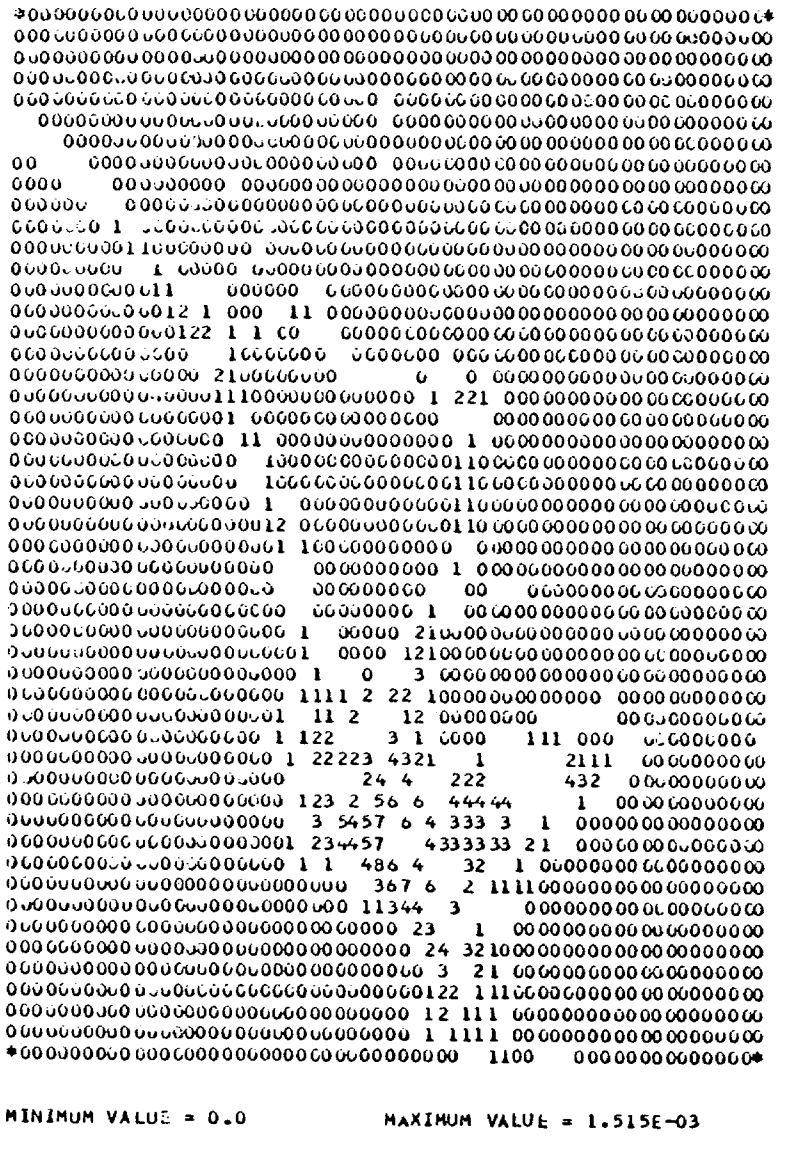

MINIMUM VALUE = 0.0 MAXIMUM VALUE = 1.515E-03

DATE=10/ 3/75 HR=1200 PST

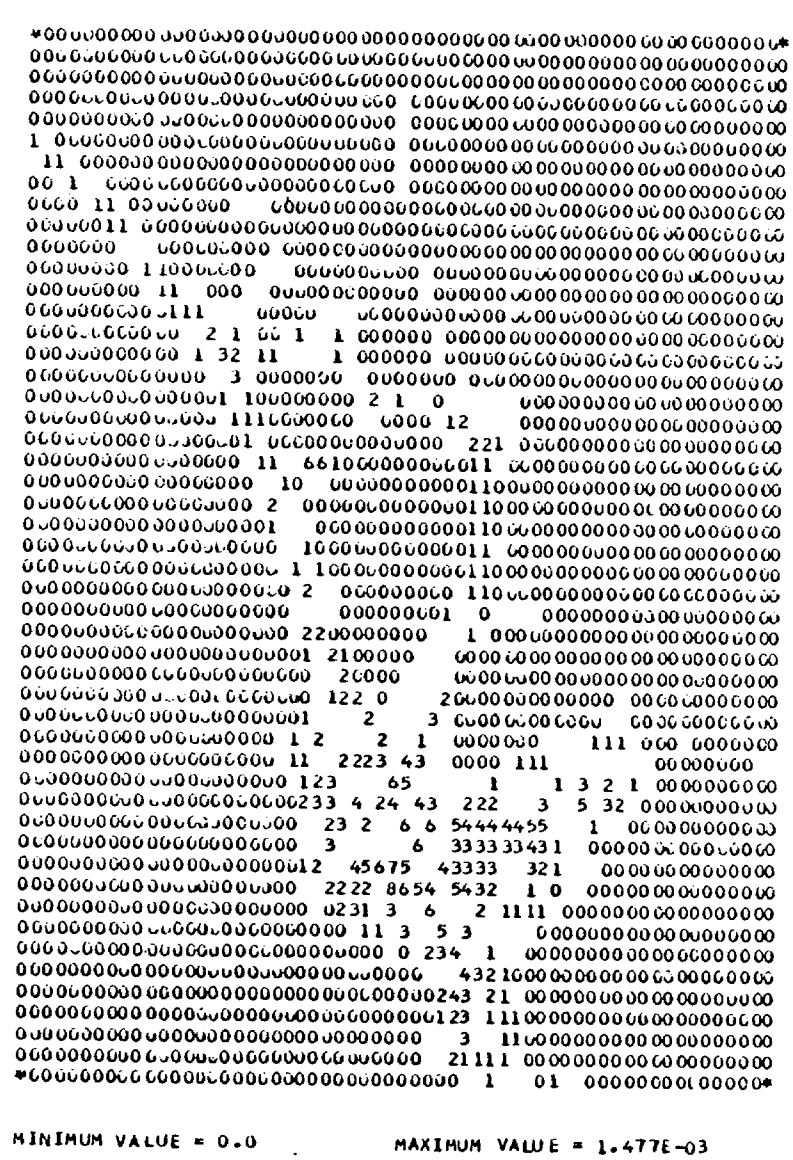

MINIMUM VALUE = 0.0 MAXIMUM VALUE = 1.477E-03

Figure 3.13 HCl Source Distributions on 10/3/75

** ALL SOURCES LEVEL 1 HC2(PPM/MIN)

DATE=10/ 3/75 HR= 600 PST

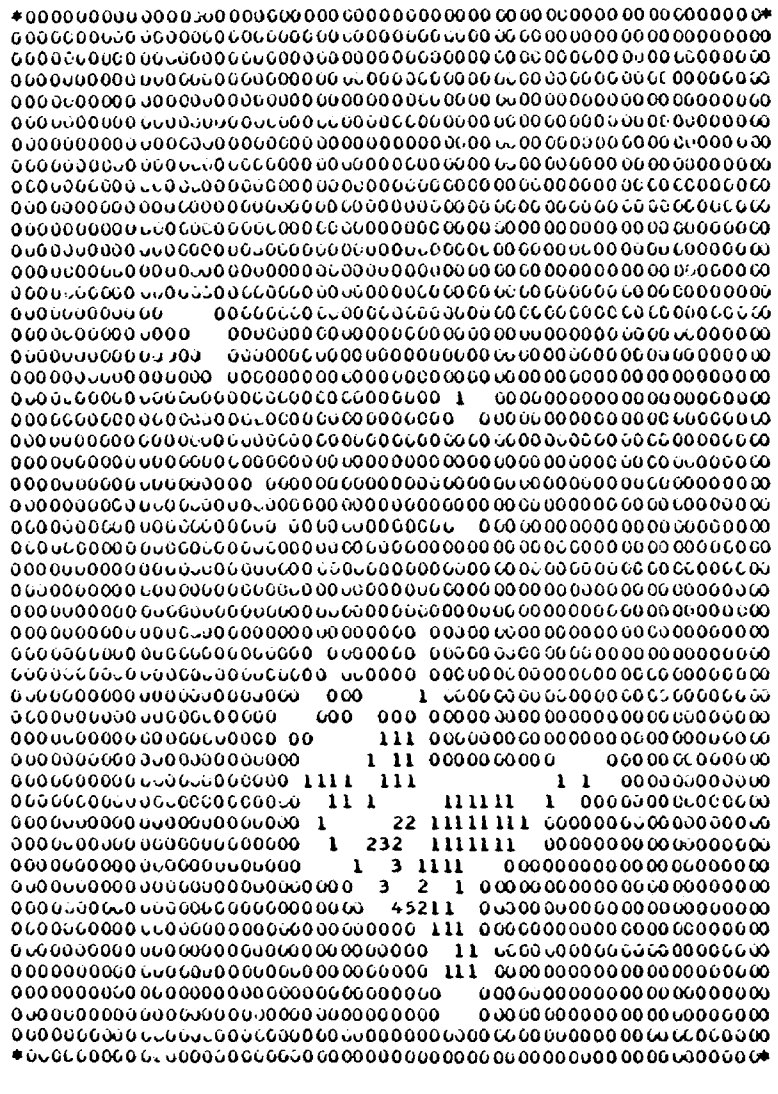

MINIMUM VALUE = 0.0 MAXIMUM VALUE = 1.871E-02

DATE=10/ 3/75 HR=1200 PST

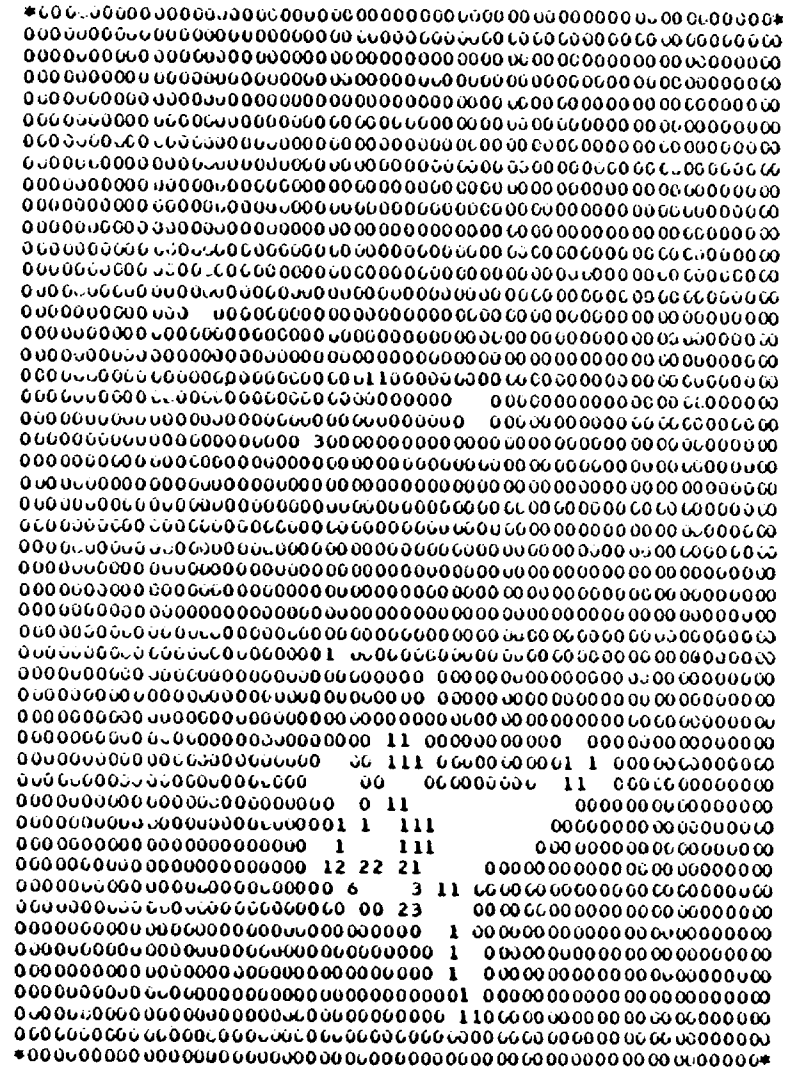

MINIMUM VALUE = 0.0 MAXIMUM VALUE = 3.843E-02

Figure 3.14 HC2 Source Distributions on 10/3/75

** ALL SOURCES LEVEL 1 HC3(PPM/MIN)

DATE=10/ 3/75 HR= 600 PST

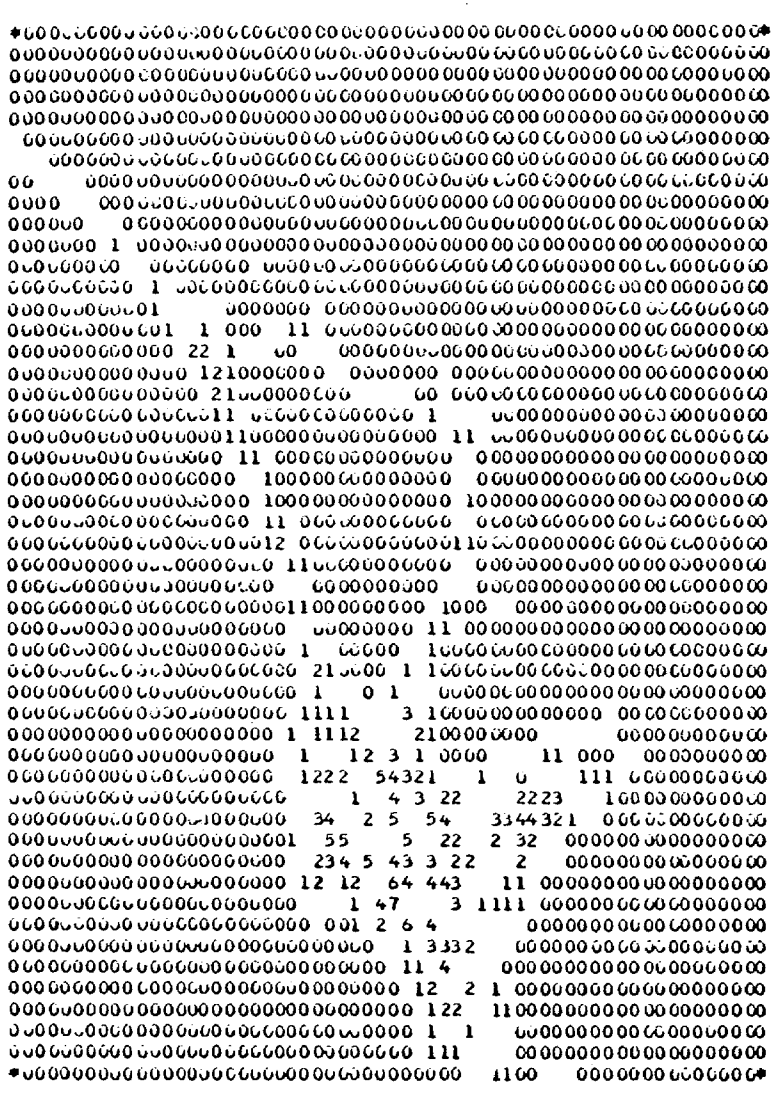

MINIMUM VALUE = 0.0 MAXIMUM VALUE = 4.759E-04

DATE=10/ 3/75 HR=1200 PST

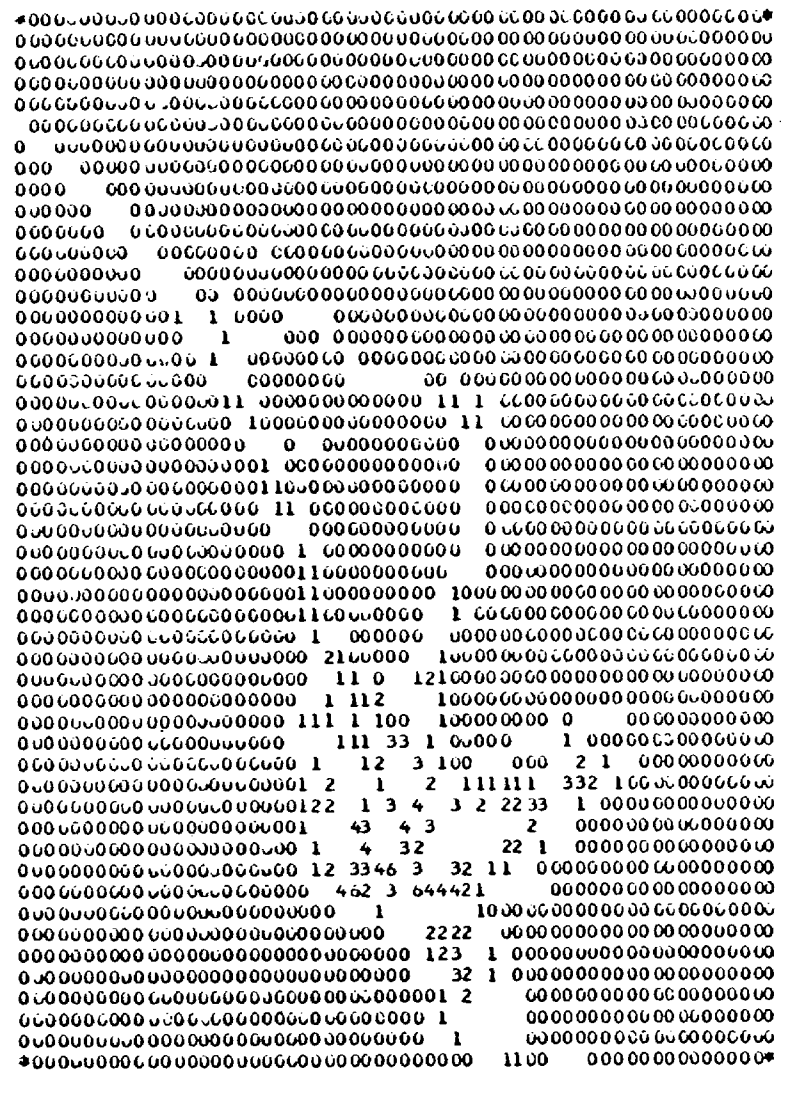

MINIMUM VALUE = 0.0 MAXIMUM VALUE = 6.587E-04

Figure 3.15 HC3 Source Distributions on 10/3/75

three reactive hydrocarbon species are the major pollutants from industrial sources. It is evident from Figure 3.13 to Figure 3.15 that the hydrocarbon emissions are concentrated along the coast and within the central part of the San Diego region. Temporally, the emission rates of the hydrocarbons increase in the morning and decrease towards the end of the day.

3.3 BASELINE 37 x 51 x 5 MADCAP RUN ON 10/3/75

In this section, the MADCAP predictions on 10/3/75 are analysed and verified in comparison with the measured data provided by CARB. Carbon monoxide (CO) is generally considered to be representative of transport (or dispersion) phenomena in the atmosphere due to its non-reactive nature. Figure 3.16 shows the time history of CO at nine air quality stations within the larger 37 x 51 x 5 grid. In general, the simulation shows a remarkable agreement with the measurement for most of the stations on 10/3/75, considering the one-hour time shift allowable in the solution method. The general trend shows high CO concentration in the morning, low in the afternoon and gradually increasing toward the evening rush hour. There are a few discrepancies between the simulated and measured data. At Oceanside, an early morning peak in CO is predicted whereas the measured data does not show any change at all. At San Marcos, a peak of CO appears at about 1000 PST in the simulation, while the measured data show a peak at 1300 PST in the afternoon. At Kearny Mesa, the prediction shows a CO concentration of 3 ppm which is much higher than the measured concentration of 1 ppm. These discrepancies also appear in the simulation run of 10/16/75 (See Section 3.5). The discrepancy between simulated and measured data might be due to the assumptions used in the model. An hourly average of the pollutants within a 2 Km x 2 Km square grid is simulated, while the actual measured data depends on the location of the air quality station and sometimes can not be considered representative of the average

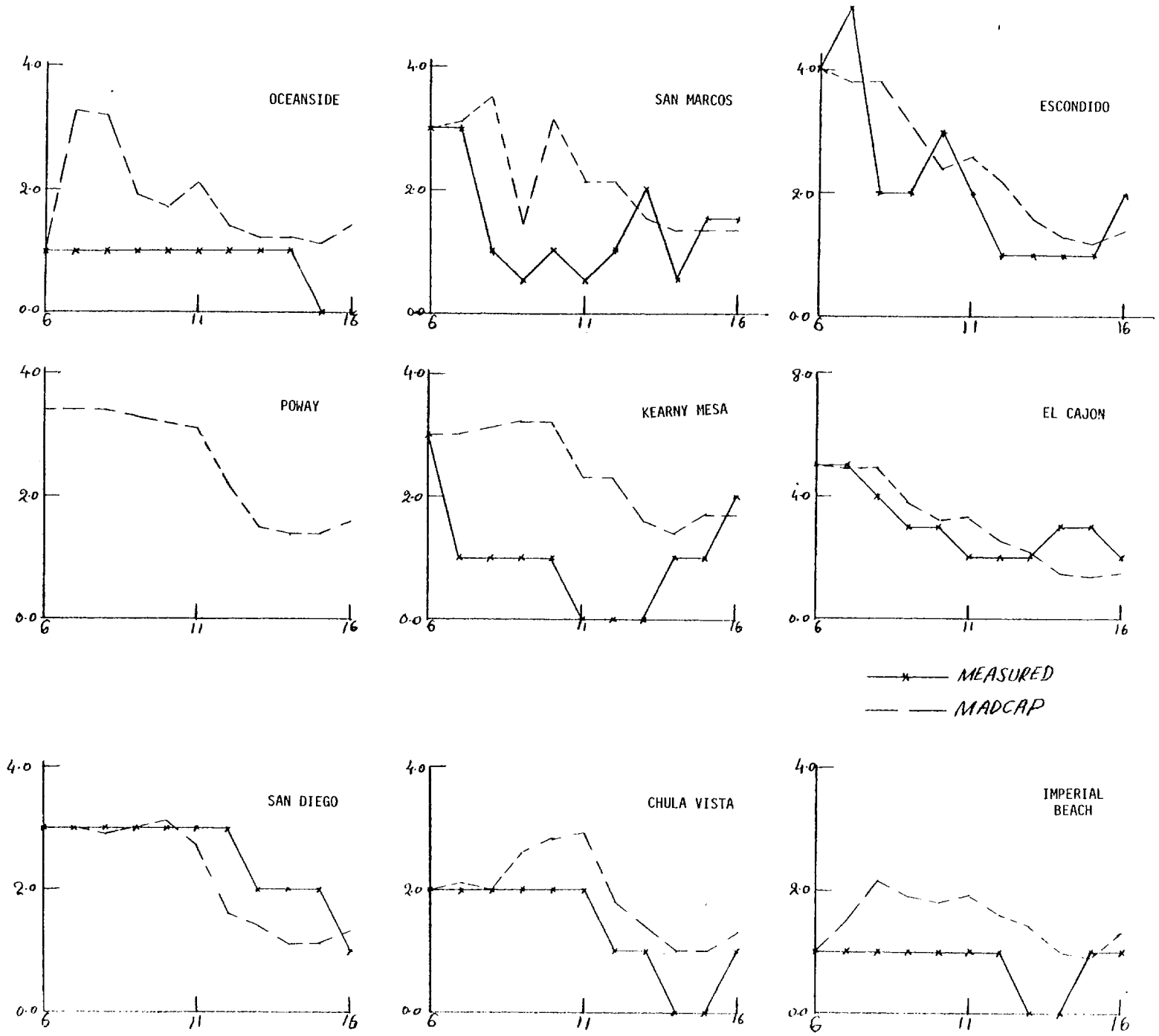

PPM of CO vs Hours PST

Figure 3.16 CO Temporal Profiles, MADCAP 37 x 51 x 5, 10/3/75 Run

pollutant concentration within the square grid over an hour. At Kearny Mesa, the early norming south-south-westerly wind transports much of the CO emissions from the nearby freeway into this cell. At the same time due to the relatively high wind speed (in the order of 5 m/sec) within this cell (in comparison with the neighboring cells), a more stable condition is predicted in the vertical direction than in the adjacent cells. Hence a smaller vertical diffusivity (on the order of 2 m^2/sec) is calculated. Since no explicit horizontal diffusion is allowed in this model, all these effects result in a high concentration of CO in the Kearny Mesa cell.

Figure 3.17 shows the temporal ozone variations at different stations. Again, the simulation predicts the correct ozone tendency and peaks to within the one-hour allowable time shift. Because of lack of insolation and high emissions of NO in the morning, the early hour ozone concentration is very low and almost depleted by the NO and O_3 reaction. By 1000 PST, the insolation is sufficient to photochemically generate high ozone concentrations. In general, the ozone concentration peaks around 1200 and 1300 PST. The simulated data indicate an enhanced transport for Poway and Kearny Mesa after 1200 PST as compared to the measured data. This could be a consequence of the diffusion treatment and the fact that there were clouds in the general vicinity of Poway and Kearny Mesa in the afternoon on 10/3/75. El Cajon also shows a discrepancy between the simulation and measured data. This may be due to the measurement difficulties at the El Cajon station. It has been shown that there is a discrepancy between the CARB supplied data and the official SDAPCD record. The triangle in the El Cajon plot shows the data collected at SDAPCD. With this data point, the simulation predicts the correct trend at El Cajon also.

Figures 3.18 and 3.19 display the simulation of NO and NO_2 at different stations located within the San Diego Air Basin,

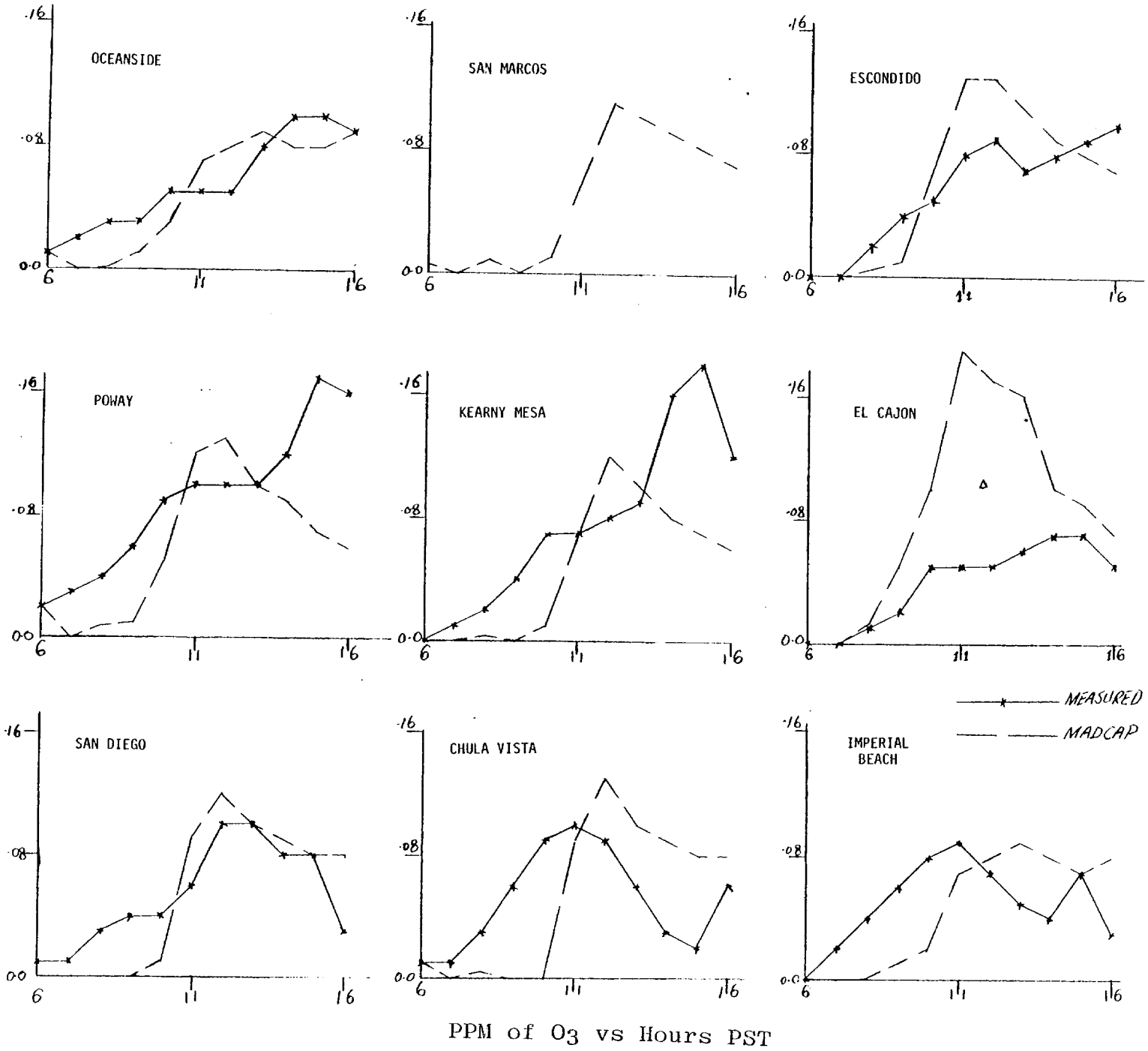

Figure 3.17 O_3 Temporal Profiles, MADCAP 37 x 51 x 5, 10/3/75 Run

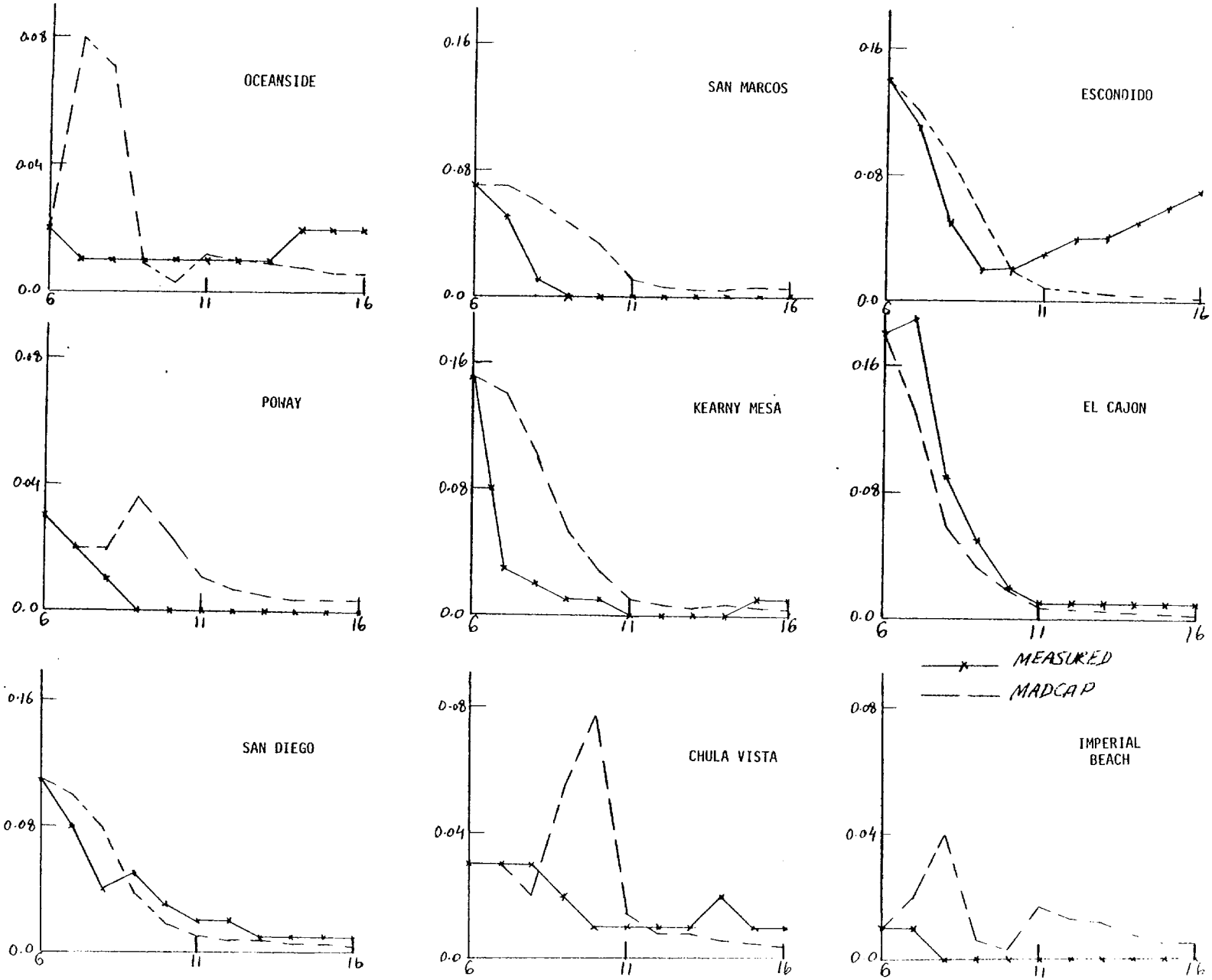

PPM of NO vs Hours PST

Figure 3.18 NO Temporal Profiles, MADCAP 37 x 51 x 5, 10/3/75 Run

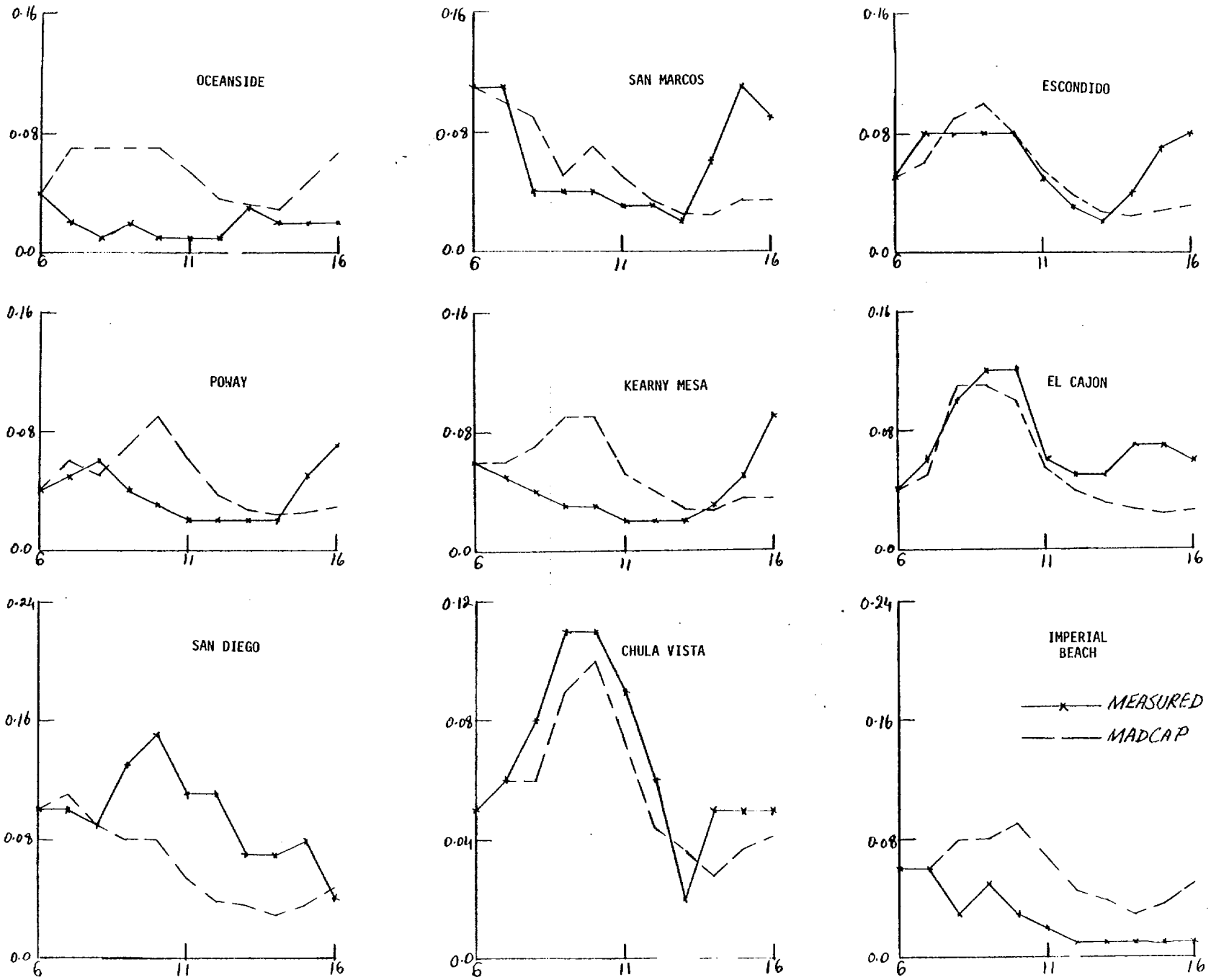

PPM of NO_2 vs Hours PST

Figure 3.19 NO_2 Temporal Profiles, MADCAP 37 x 51 x 5, 10/3/75 Run

respectively. Early morning NO peaks from the rush hour emissions account for the correspondingly low ozone concentration prediction. Whenever the simulation calculates NO concentration exceeding the measured NO, it is generally true that the predicted O_3 level is also less than the measured ozone. At the same time, the simulation and measurement NO_2 trends follow the corresponding ozone trends. Again, exceptions are at the Poway and Kearny Mesa stations possibly due to the incorrect transport phenomena. El Cajon shows excellent agreement between prediction and measurement of both NO and NO_2, and this fact tends to suggest that the ozone measurements at El Cajon were anomalous and erroneous.

Temporal variation of the hydrocarbon species HC1 is shown in Figure 3.20. Again, the trends of the simulation show a good agreement with the observed values except at a few stations such as Oceanside and Escondido. In this comparison, since no measured HC1, HC2 and HC3 data are available, the predicted HC1 data were compared with 0.44 times the measured hydrocarbon data to establish the trend. The observed Escondido hydrocarbons are very much higher than the predicted at about 1000 hours. This may be caused by local or additional sources located close to the measuring station or by the enhanced transport predicted in the Escondido area. The hydrocarbon species HC2 shows the same trend as HC1 and the same discrepancy at Escondido. We have not included the HC2 plots in this report.

Spatial variation of the MADCAP simulation for the inert pollutant CO is shown in Figure 3.21a and 3.21b, whereas the ozone distribution is shown in Figure 3.22a and 3.22b. In the early hours at 0700 PST, just one hour into the simulation, the CO distribution closely resembles the initial conditions (Figure 3.2) where a high concentration of CO exists in the El Cajon valley area. By 0900 PST, the CO pattern follows the coastline with higher concentrations in the inland and southeast regions. This pattern reflects the rush hour freeway emission and the early

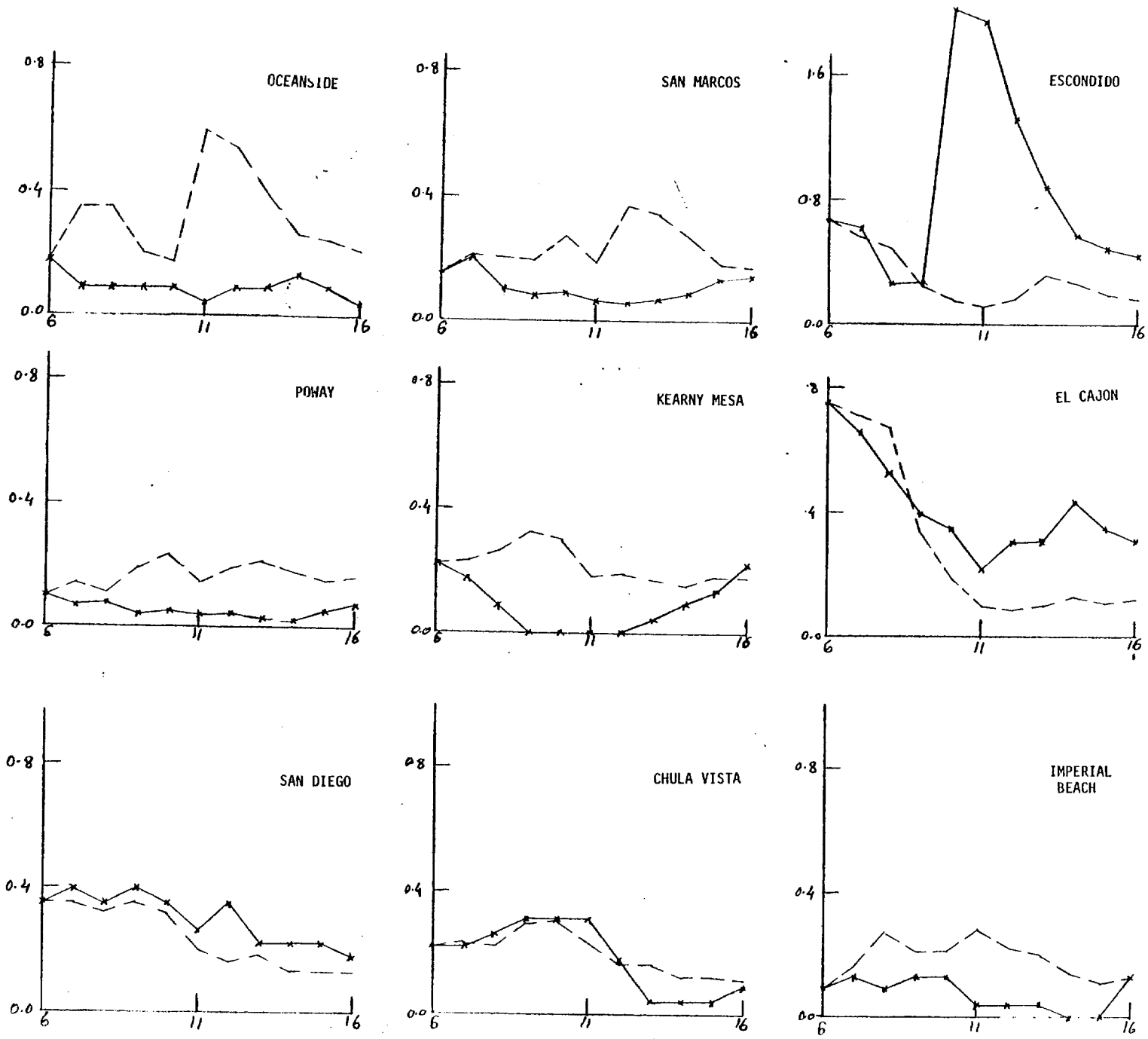

PPM of HCl vs Hours PST

Figure 3.20 HCl Temporal Profiles, MADCAP 37 x 51 x 5, 10/3/75 Run

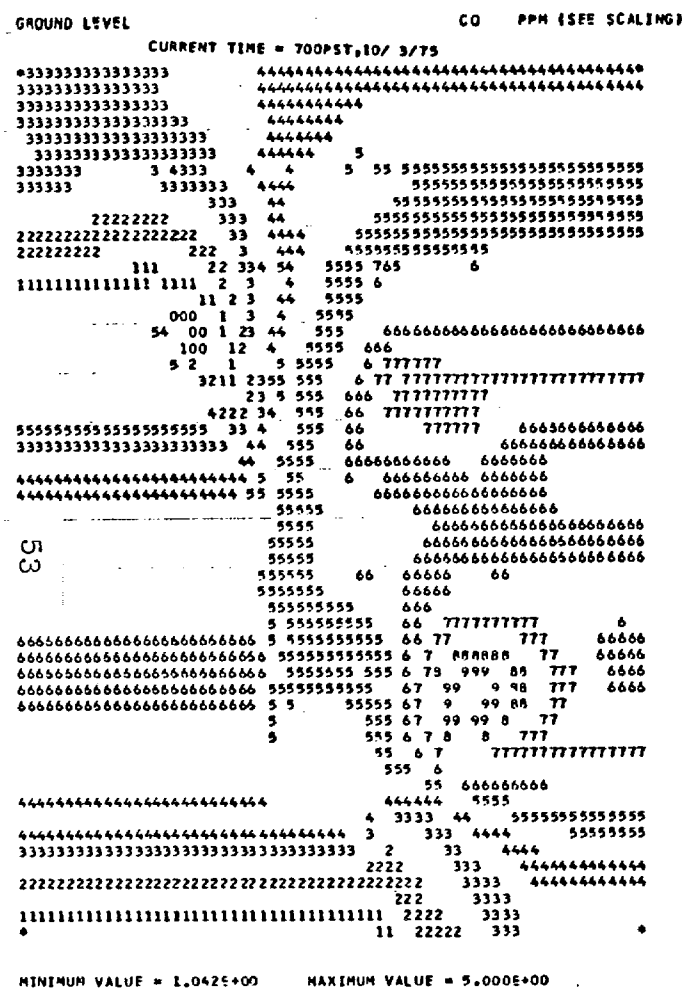

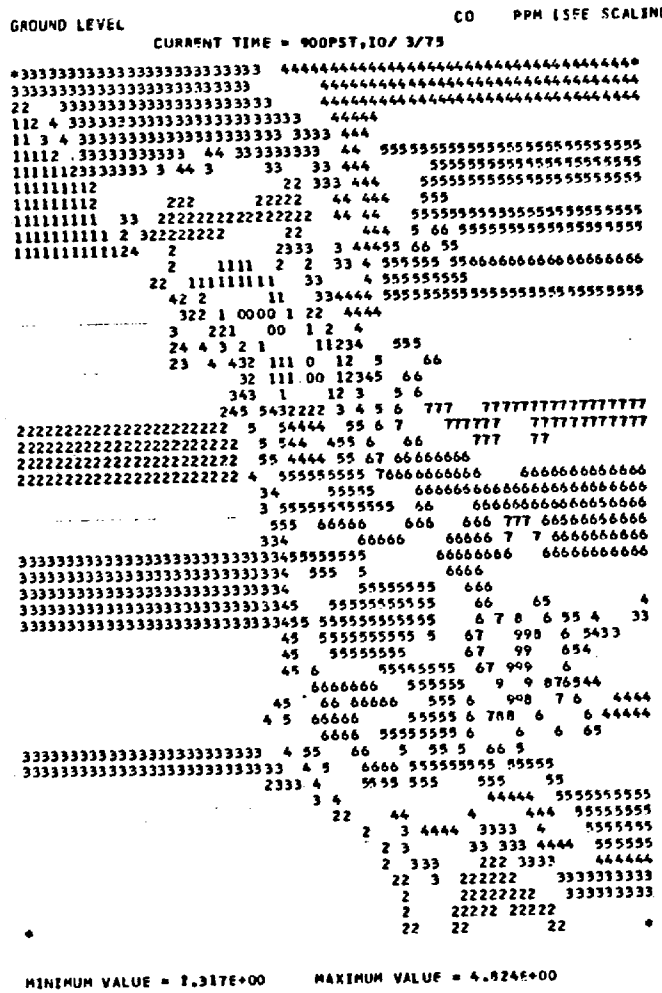

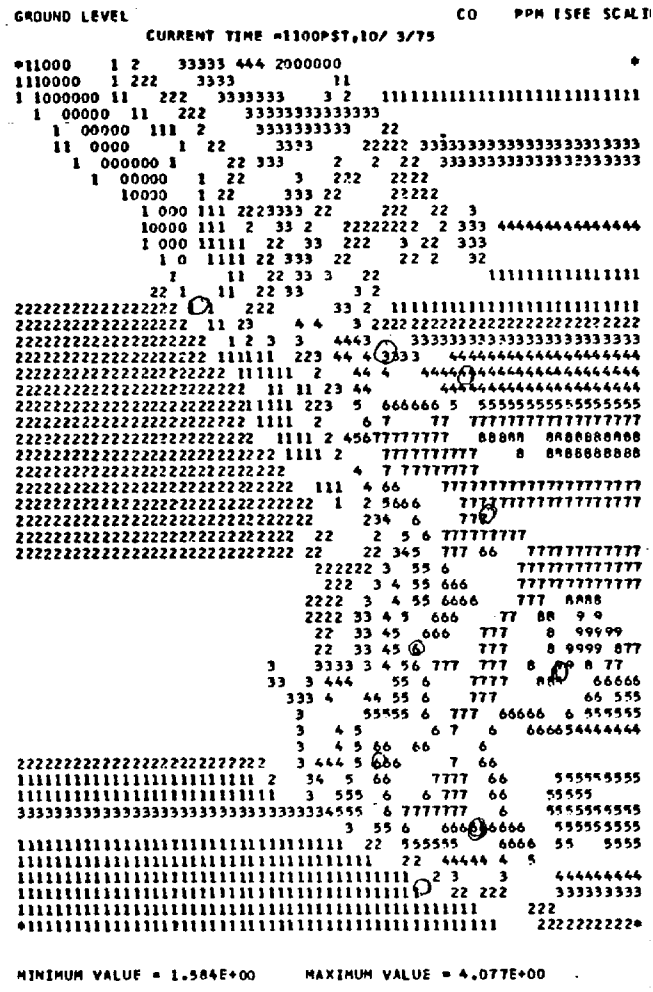

Figure 3.21a CO Spatial Pattern, MADCAP 37 x 51 x 5, 10/3/75 Run

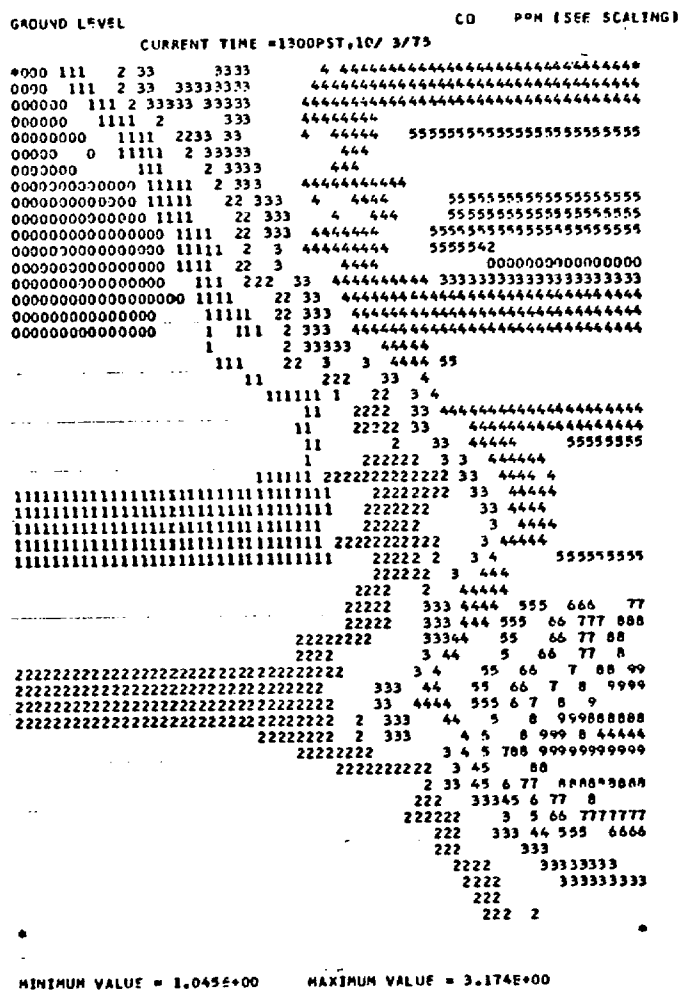

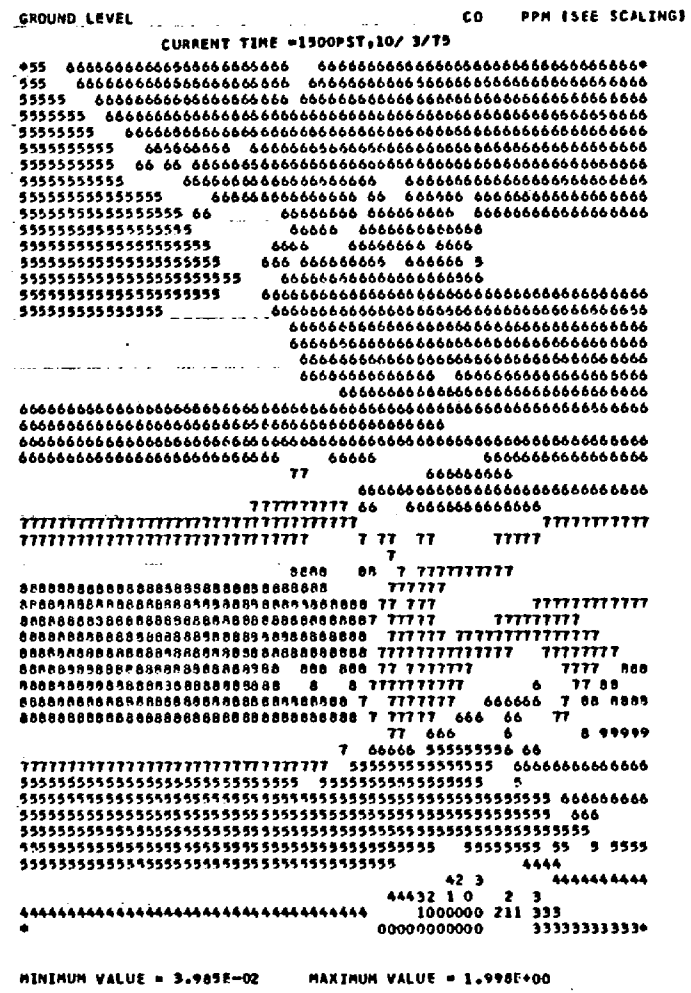

Figure 3.21b CO Spatial Pattern, MADCAP 37 x 51 x 5, 10/3/75 Run

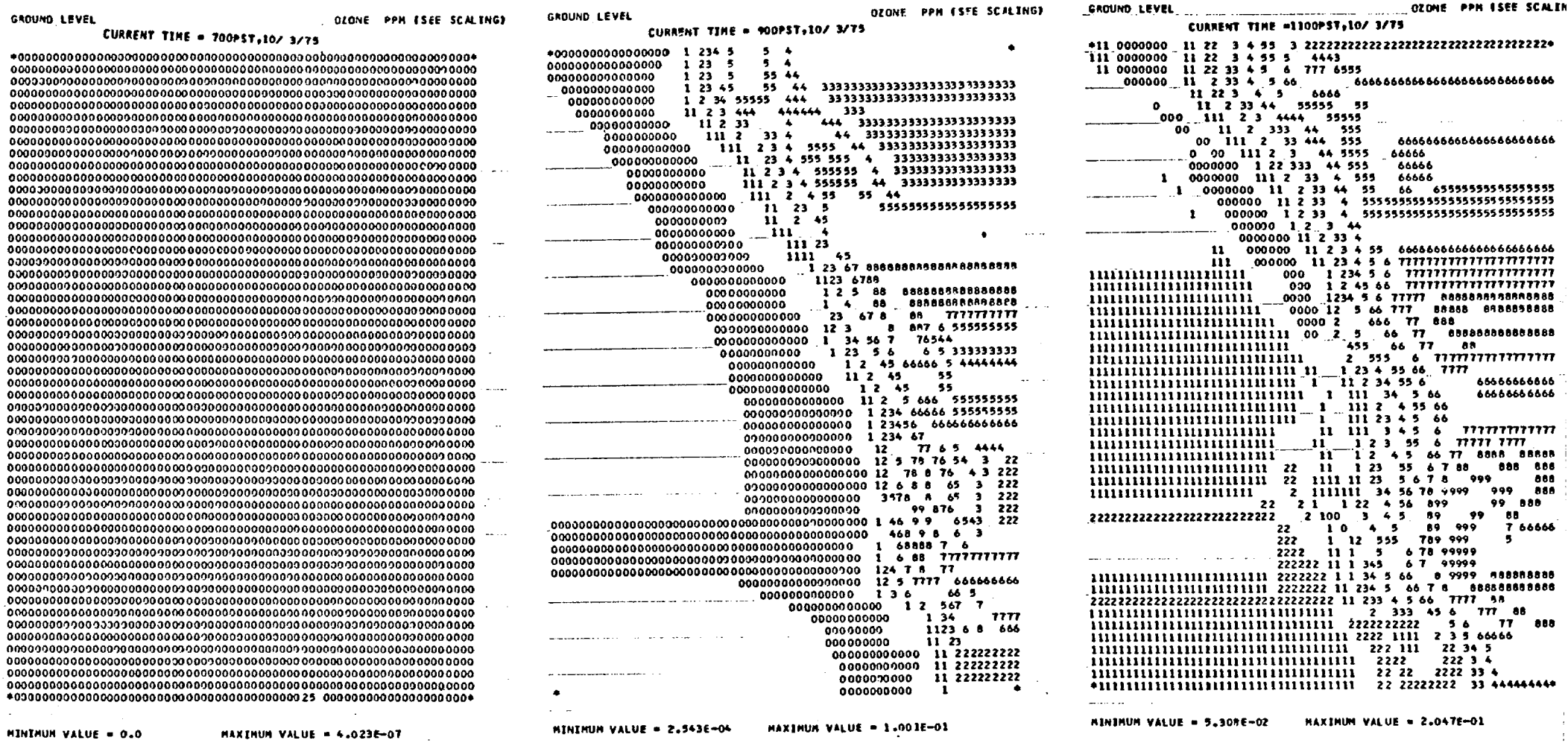

Figure 3.22a O_3 Spatial Pattern, MADCAP 37 x 51 x 5, 10/3/75 Run

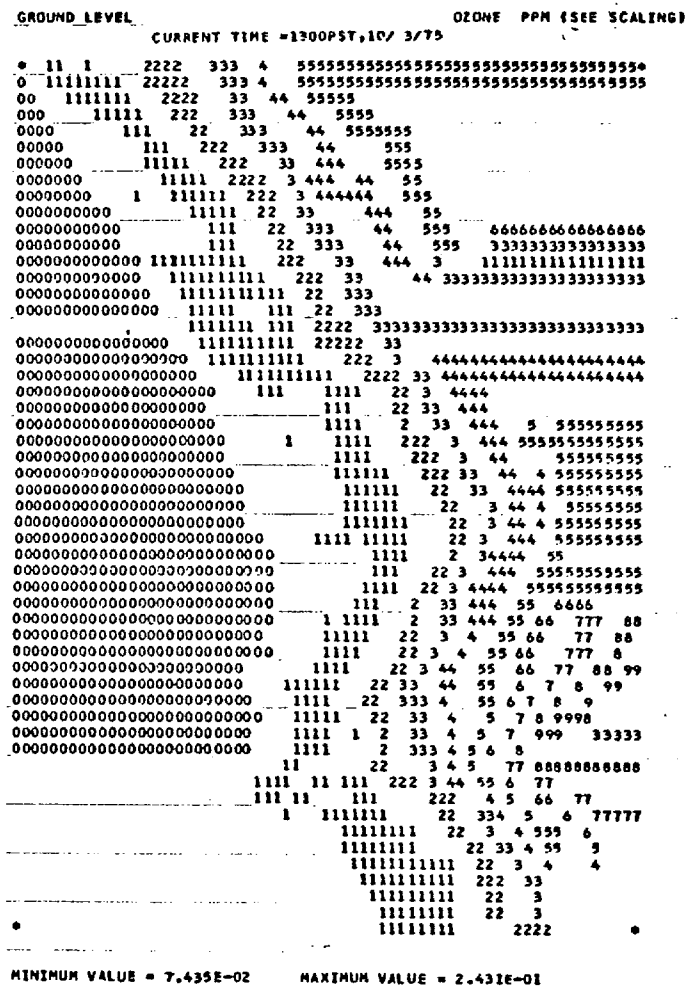

Figure 3.22b O_3 Spatial Pattern, MADCAP 37 x 51 x 5, 10/3/75 Run

morning south south-westerly wind direction. This pattern persists with a gradually decreasing level until about 1300. In the afternoon when the westerly wind prevails, most of the CO is transported out of the grid and hence a much lower CO concentration level (maximum of 2 ppm at 1500 PST vs 5 ppm at about 0900 PST) is observed uniformly across the San Diego Air Basin, except at the south center part of San Diego (Figure 3.21a at 1500 PST) where the prevailing wind is in the northwest direction.

Early in the morning, with minimum insolation and a high NO emission rate, ozone is almost depleted by the recombination of NO and O_3. However, by 0900 PST, the insolation is sufficiently high to generate ozone in the atmosphere, but due to the cloudiness along the coastline the ozone pattern follows the coast closely and increases towards the inland area. The coastline pattern breaks at about 1000 PST at which point most of the San Diego area was sunny on 10/3/75. The maximum level of ozone attained at about 1300 PST at El Cajon resulted from both the high solar intensity and a stagnate condition in that area. At 1500 PST, the transport by advection and diffusion and the decreasing insolation reduce the ozone level throughout the whole region and a uniform pattern is seen in San Diego, except the region east of El Cajon.

The NO pattern follows the initial overnight pattern in the morning. The initial high concentration of NO decreases to a low level after about 0700 PST due to the depletion reaction with ozone. In the daytime it generally follows the coastline pattern with increasing levels to the east. NO_2 closely follows the ozone pattern as described previously. All hydrocarbons reflect the industrial pattern in the daytime with a slight increase of HC3 as afternoon approaches. Again the spatial pattern shows a strong tendency of low concentration close to the coastline and the pollutants increase towards the east with an afternoon stagnate condition close to the El Cajon area.

In summary, for the date 10/3/75, the MADCAP simulation generally shows a good agreement with the measured data except for a few anomalies observed at some isolated stations. Ozone is depleted in the early morning and built up toward 1300 PST and then gradually decreases. It is also observed that the ozone spatial pattern closely follows the coastline and builds up toward the East County of San Diego.

3.4 BASELINE 20 x 10 x 5 MADCAP RUN ON 10/3/75

In order to save computation time, a smaller grid (20 x 10 x 5) including five air quality stations (San Diego, Kearny Mesa, El Cajon, Santee and Chollas, See Chapter 4) is used to study the sensitivity of the MADCAP model (Figure 3.1). For this small regional study, the input data are exactly the same as the larger regional simulation (37 x 51 x 5). Qualitative trends of pollutants in this small regional simulation are similar to the trends described for the large regional simulation. However, due to the shift of the boundaries in the small regional simulation, some of the results are slightly different.

Figure 3.23 shows a comparison between the 37 x 51 x 5 simulation and the 20 x 10 x 5 simulation. The general trends are similar. However, due to the fact that the Kearny Mesa station is adjacent to the north boundary of the small regional simulation, the boundary conditions are strongly influenced by the measurement at Kearny Mesa. Hence, the CO concentrations predicted in the small regional simulations agree better than the concentrations in the large regional simulation. It should also be pointed out that due to the morning wind direction (south south-westerly) in the large regional simulation, a large amount of the CO emissions from the nearby freeway have been transported into the Kearny Mesa cell. However, for the smaller grid, only the CO concentration on the north boundary (which is low since it is strongly dependent upon measured data at Kearny Mesa) can be transported into the

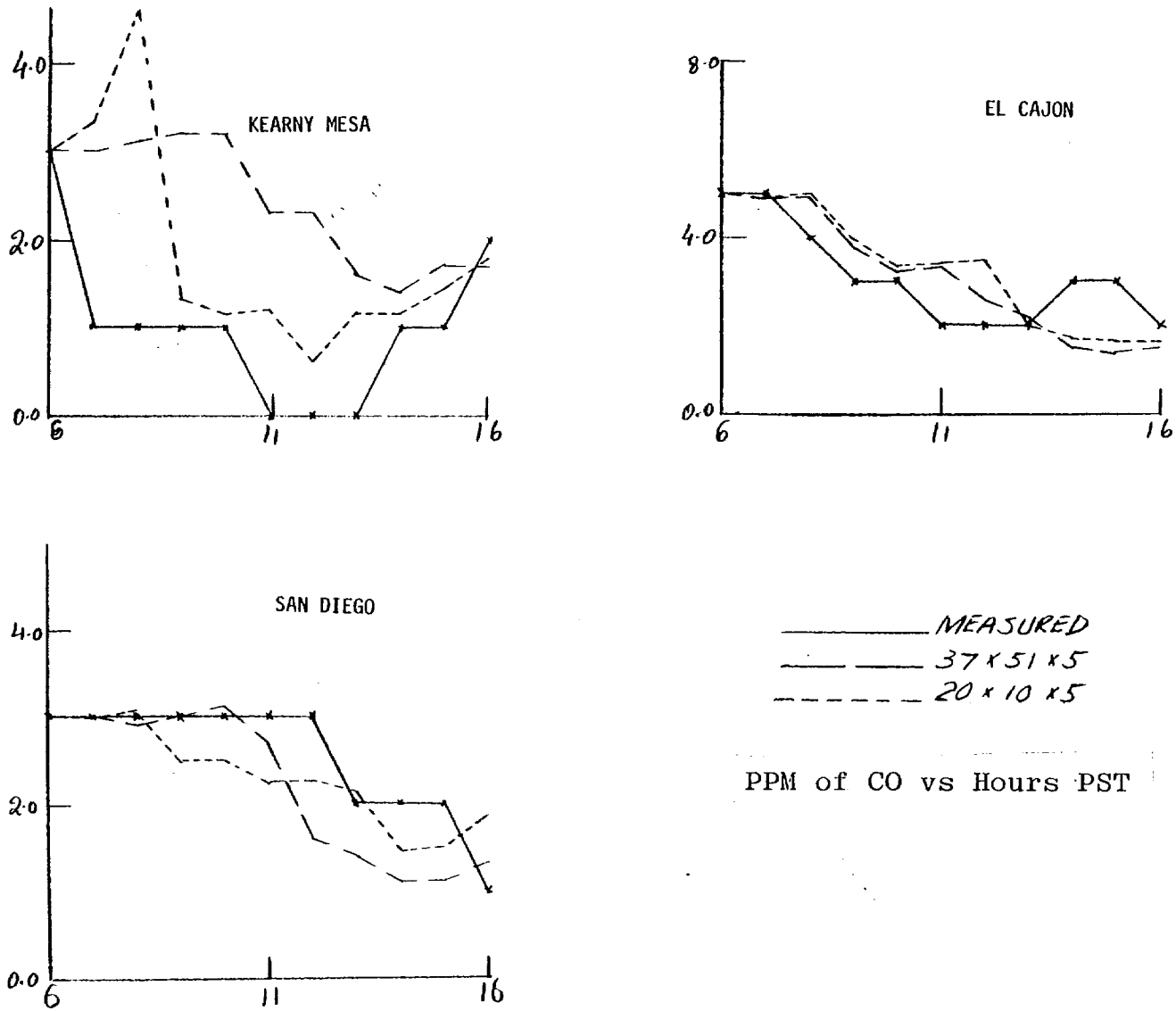

Figure 3.23 CO Temporal Profiles, Comparison Between MADCAP 37 x 51 x 5 and MADCAP 20 x 10 x 5, 10/3/75 Runs

Kearny Mesa cell. Except for the discrepancy at Kearny Mesa, the small regional simulation agrees well with the large regional simulation results. Figure 3.24 shows the comparison of ozone concentrations at different stations. Again the agreement between the small and large regional simulations is remarkable. The only discrepancy appears at El Cajon where an ozone depression is predicted by the small regional simulation at 1200 PST. This could be the result of different boundary conditions imposed in the different simulations.

Figure 3.25 shows the predicted NO, NO_2, and O_3 temporal variations at five stations from the small regional simulation, which generally agree with the trends predicted by the large regional simulation. Early in the morning, high emissions of NO nearly deplete the ozone. As insolation increases, ozone is generated and peaks around noon then gradually decreases in the afternoon. It is noticed that NO_2 is effective as an ozone precursor, as the NO_2 photodissociates into NO and O atoms and then the O atoms combine with O_2 to produce the ozone. Figure 3.26 shows the relationships between the three hydrocarbon species. It is observed that in the ambient atmosphere, oxygenate (HC3) has a very low level of concentration (in the morning) and is generated through the chemical reaction of olefins (HC1) and available ozone. At every station, the trends are similar. HC1 and HC2 have high level concentrations in the morning and show a minimum around noon, increase slightly at about 1300 PST, and then maintain a fairly constant level throughout the afternoon.

In general, the small regional simulation also shows good agreement between the predictions and observed measurements with similar buildup, maximum and decay of ozone. However, the results are highly influenced by the imposed boundary conditions.

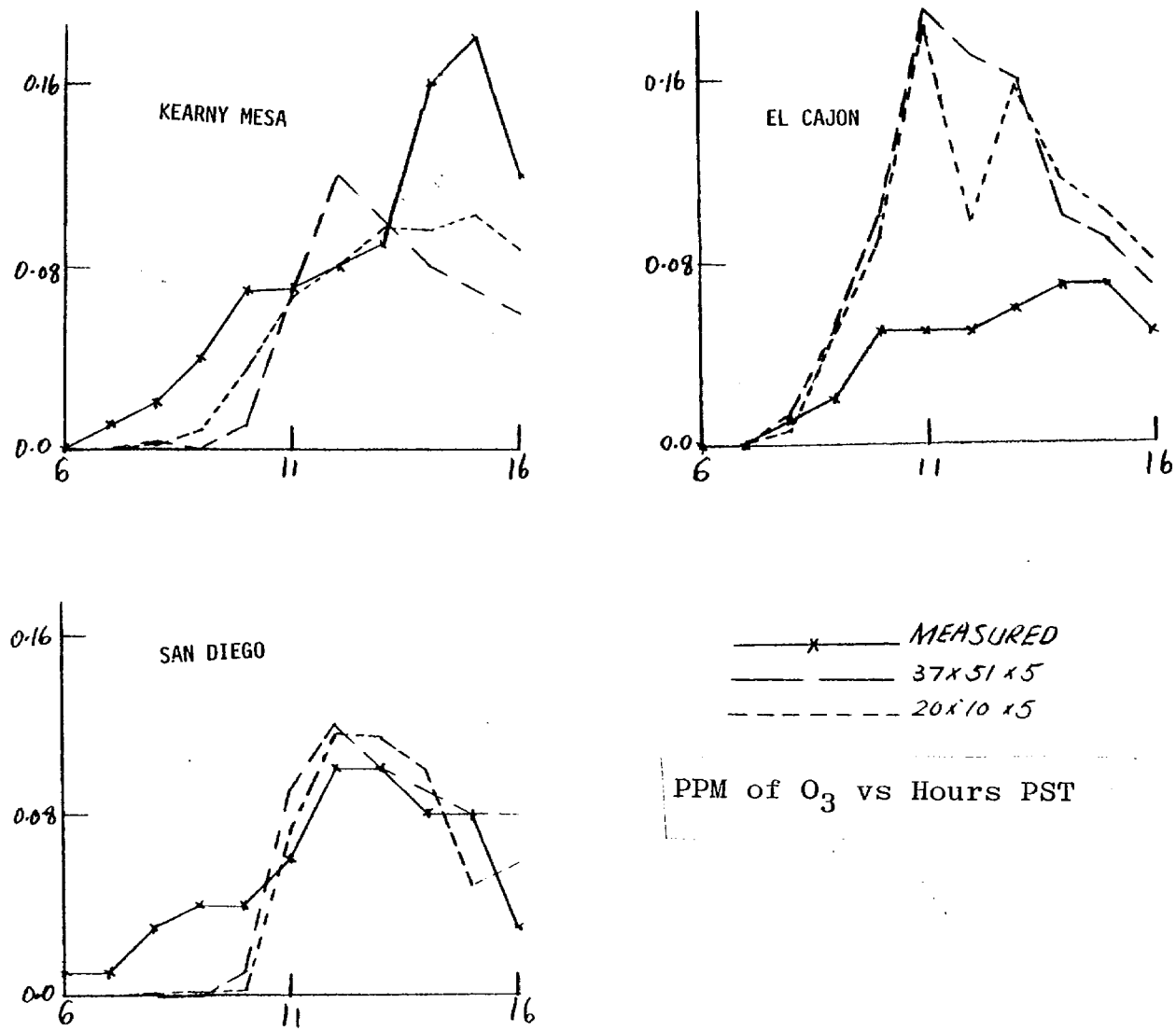

Figure 3.24 O_3 Temporal Profiles, Comparison Between MADCAP 37 x 51 x 5 and MADCAP 20 x 10 x 5, 10/3/75 Runs

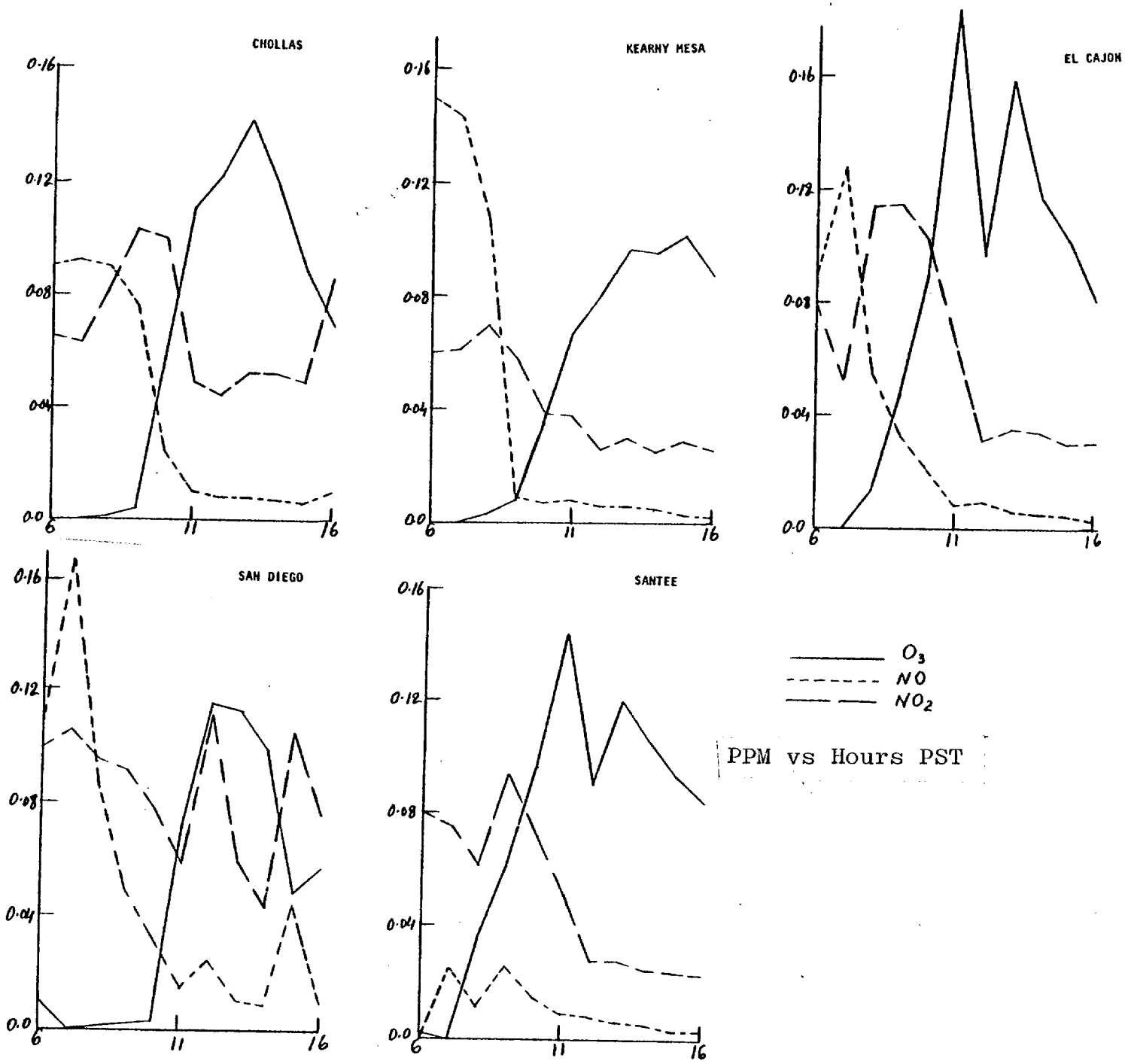

Figure 3.25 O_3, NO, NO_2, Temporal Profiles, MADCAP 20 x 10 x 5, 10/3/75 Run

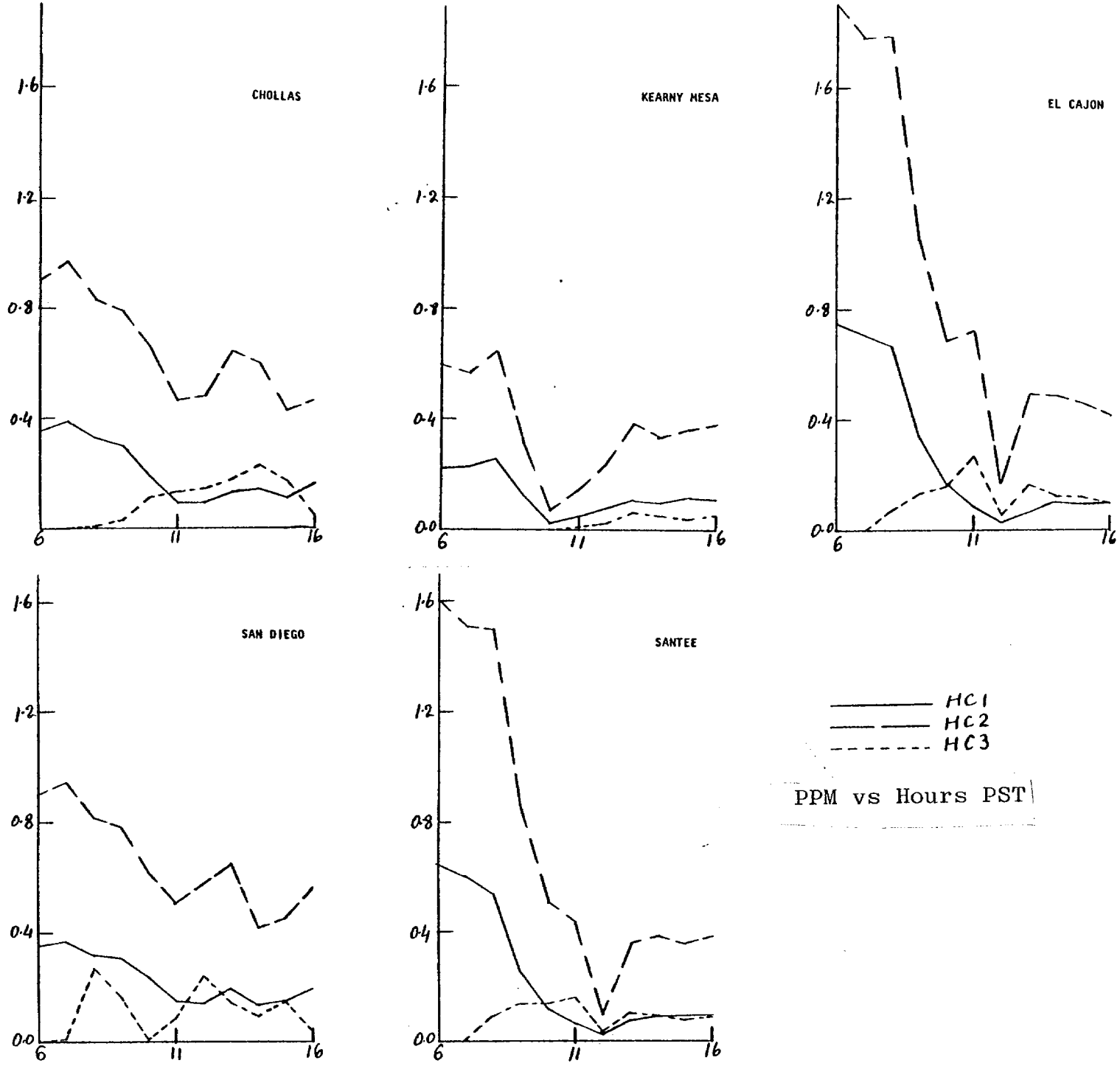

Figure 3.26 HC1, HC2, HC3, Temporal Profiles, MADCAP 20 x 10 x 5, 10/3/75 Run

3.5 SIMULATION 37 x 51 x 5 MADCAP RUN ON 10/16/75

Another large regional simulation (37 x 51 x 5) was performed for the date 10/16/75 in the San Diego Air Basin. There were a total of 21 stations providing meaningful wind data (whereas on 10/3/75, there were 26 stations generating wind data). In comparison with 10/3/75, 10/16/75 is a slightly cooler day with about 10% higher wind speed than the wind observed on 10/3/75. It was a sunny day with cloud cover less than 20% except at 1400 PST at the Imperial Beach station. The simulation results are very much similar to the 10/3/75 simulation. Figure 3.27 and 3.28 plot the simulation results and observations of CO and O_3 concentrations, respectively, at many different stations. Again, the general trends agree well, especially the ozone concentration. Unfortunately, due to a small debugging error, (this error is related to the incapability of processing more than two UV station records in PREMET and has been corrected), the solar insolation values were calculated erroneously by the numerical interpolation scheme, hence the ozone predictions after 1400 PST are incorrect and not shown in Figure 3.28. The comparison of CO concentration indicates that there might be some difficulties in the transport treatment. Some of the transport effects are discussed in the sensitivity study (Chapter 4). In general, the simulation of CO shows the correct trend with a two to three hour shift in comparison with the measurements. There are some local maximums observed in CO concentration at San Marcos and Poway stations. Much like the simulation on 10/3/75, the MADCAP model does not predict these local maximums. CO predictions at Kearny Mesa on 10/16/75 behave similarly to the simulation on 10/3/75, which predicts high concentration of CO. However, the measurements show a consistantly low level of CO concentration. It is felt that this discrepancy might be due to the location and/or instrument difficulties at the Kearny Mesa station. The ozone predictions show remarkable agreement with the observed data, except at El Cajon. The similar ozone trend which was observed on 10/3/75 is also shown in this simulation.

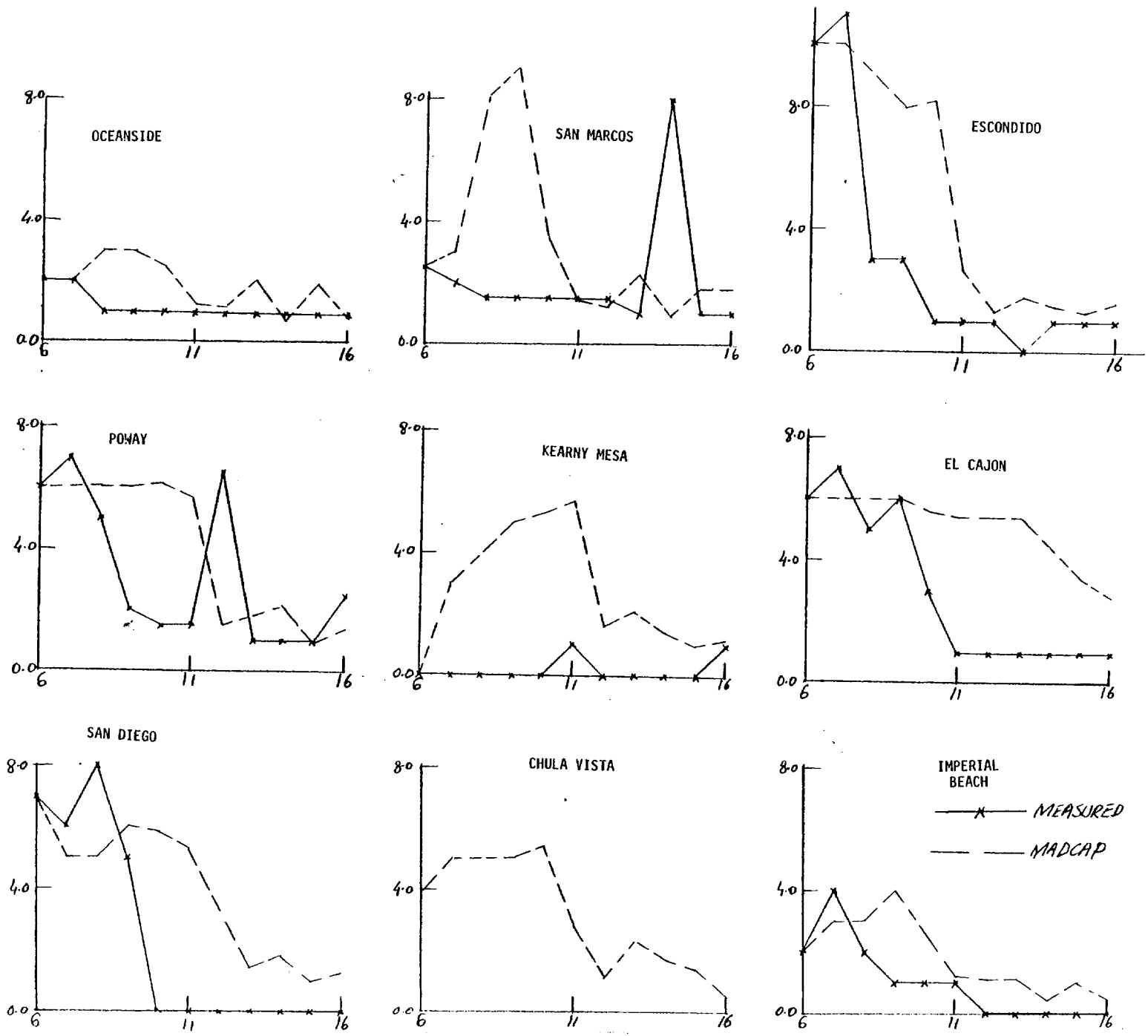

PPM of CO vs Hours PST

Figure 3.27 CO Temporal Profiles, MADCAP 37 x 51 x 5, 10/16/75 Run

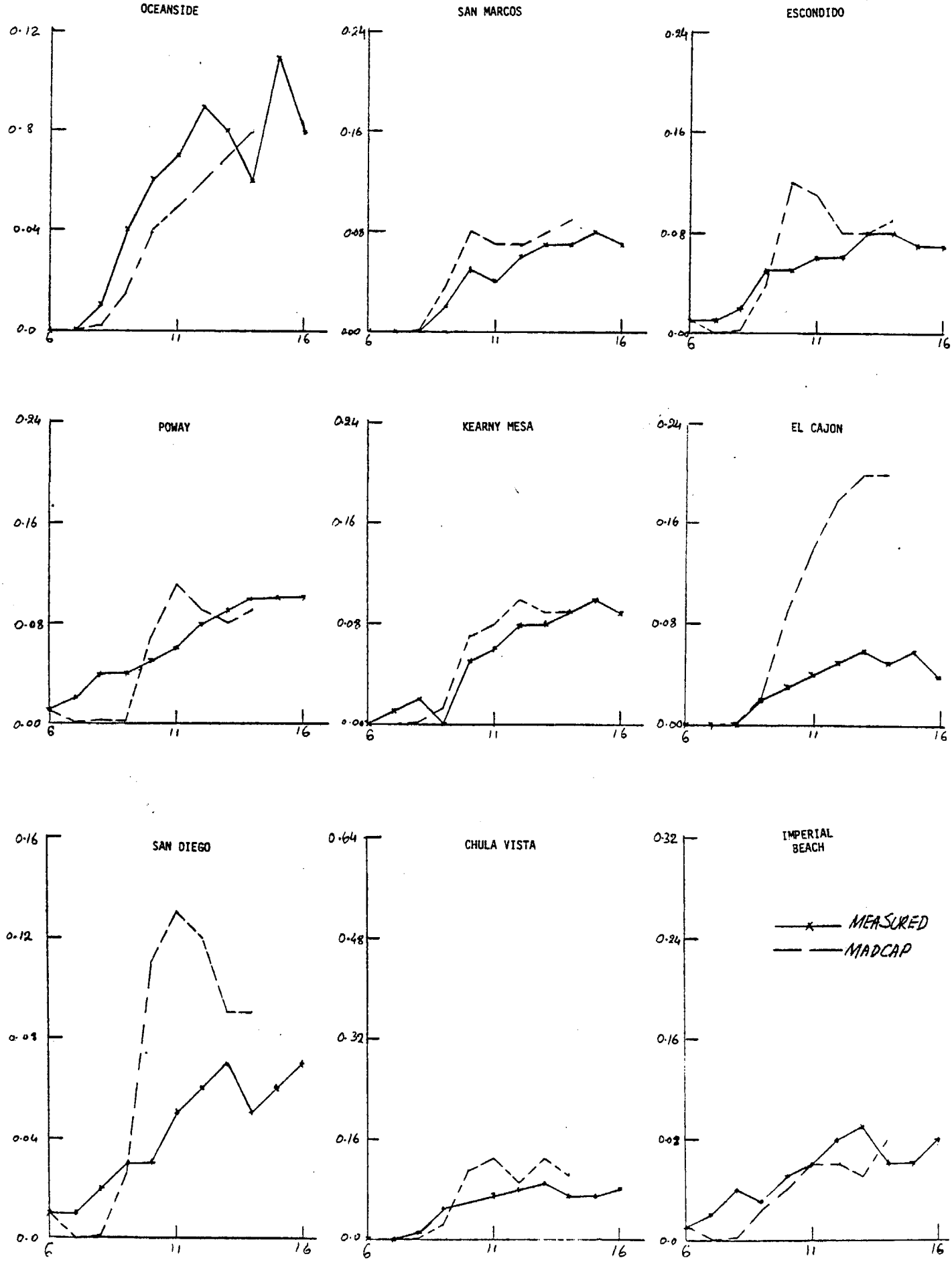

Figure 3.28 O_3 Temporal Profiles, MADCAP 37 x 51 x 5, 10/15/75 Run

It is shown here that the MADCAP simulation consistently predicts correct photochemistry trends and compares well with the observed trends. The discrepancies could be due to the ineffective diffusion scheme (see the discussion in Chapter 4) and some local effects which the regional models are not capable of predicting.

4. SENSITIVITY ANALYSIS ON MADCAP

The purpose of this sensitivity analysis is to evaluate the response of the model to the variation of some selected inputs. Thus, a baseline run of the model is required to serve as the standard of comparison. In principle, any reasonable set of input values can be established as the standard. In this report, the October 3, 1975 San Diego run is established as the baseline. In order to minimize the computation time, a small grid size (20 x 10 x 5) is chosen instead of the large grid size (37 x 50 x 5).

The grid selected for analysis was chosen in a region of high air quality interest encompassing five recording stations - San Diego, Chollas, El Cajon, Santee, and Kearny Mesa. This region is depicted in Figure 4.1 and includes the position of the coastline consistent with the 2 Km resolution. The five sites in Figure 4.1 are at their true geographical locations. Figure 4.2 shows the same region with the imposition of the 2 Km x 2 Km gridding and the relocation of sites to the nearest cell-center. The basic aerometric data for the application of MADCAP to San Diego is relative to a master 50 cell by 60 cell grid, and so for convenience Figure 4.2 includes a reference to coordinates of the basic 50 x 60 grid. Unless explicitly noted otherwise all further reference in this chapter is to the 20 x 10 grid.

Eleven consecutive hours from October 3, 1975 (0600 to 1600 PST) were selected to form the sensitivity baseline. This time period permits morning sources to enter the simulation and carries the calculation past the time of expected ozone maxima.

In this report, three different sensitivity analyses are performed. The first sensitivity study is devoted to understanding the evolution of inert pollutants due to the wind and diffusion influences and the numerical effects. The second sensitivity

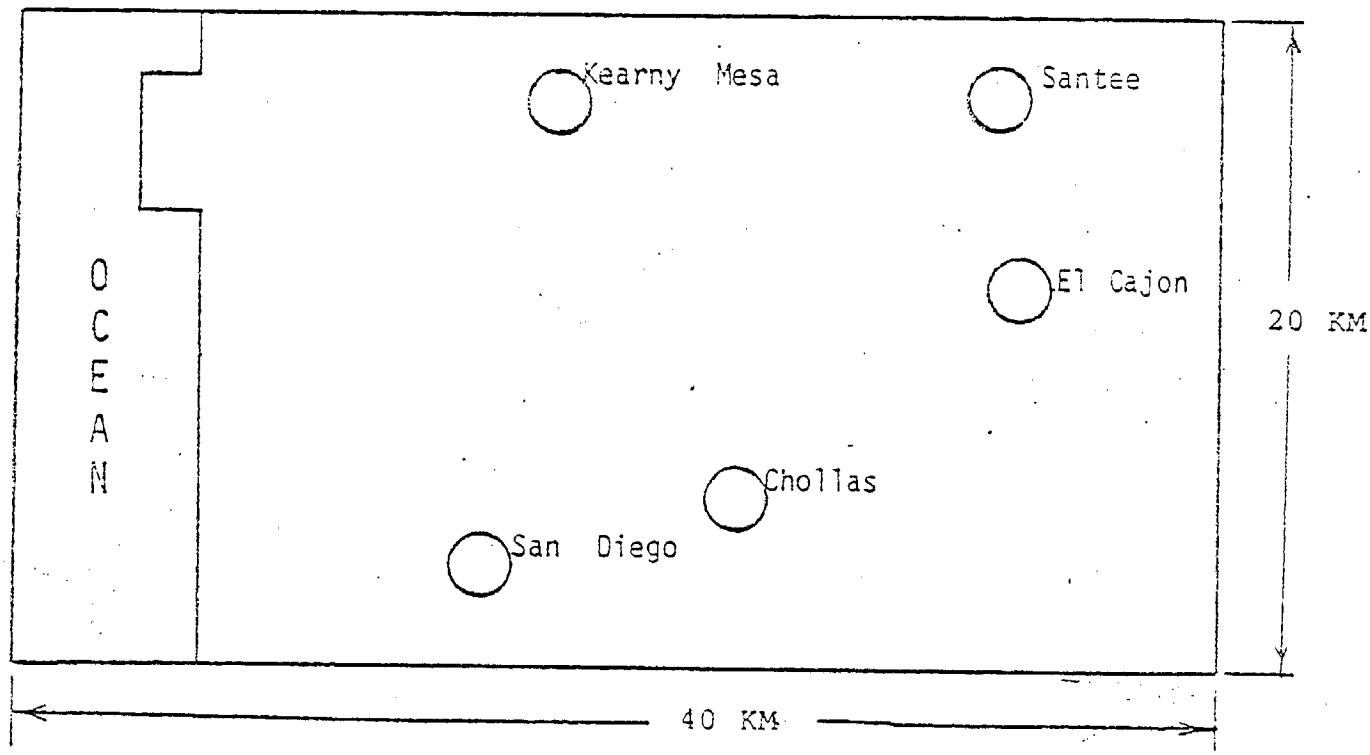

Figure 4.1 Sensitivity Region

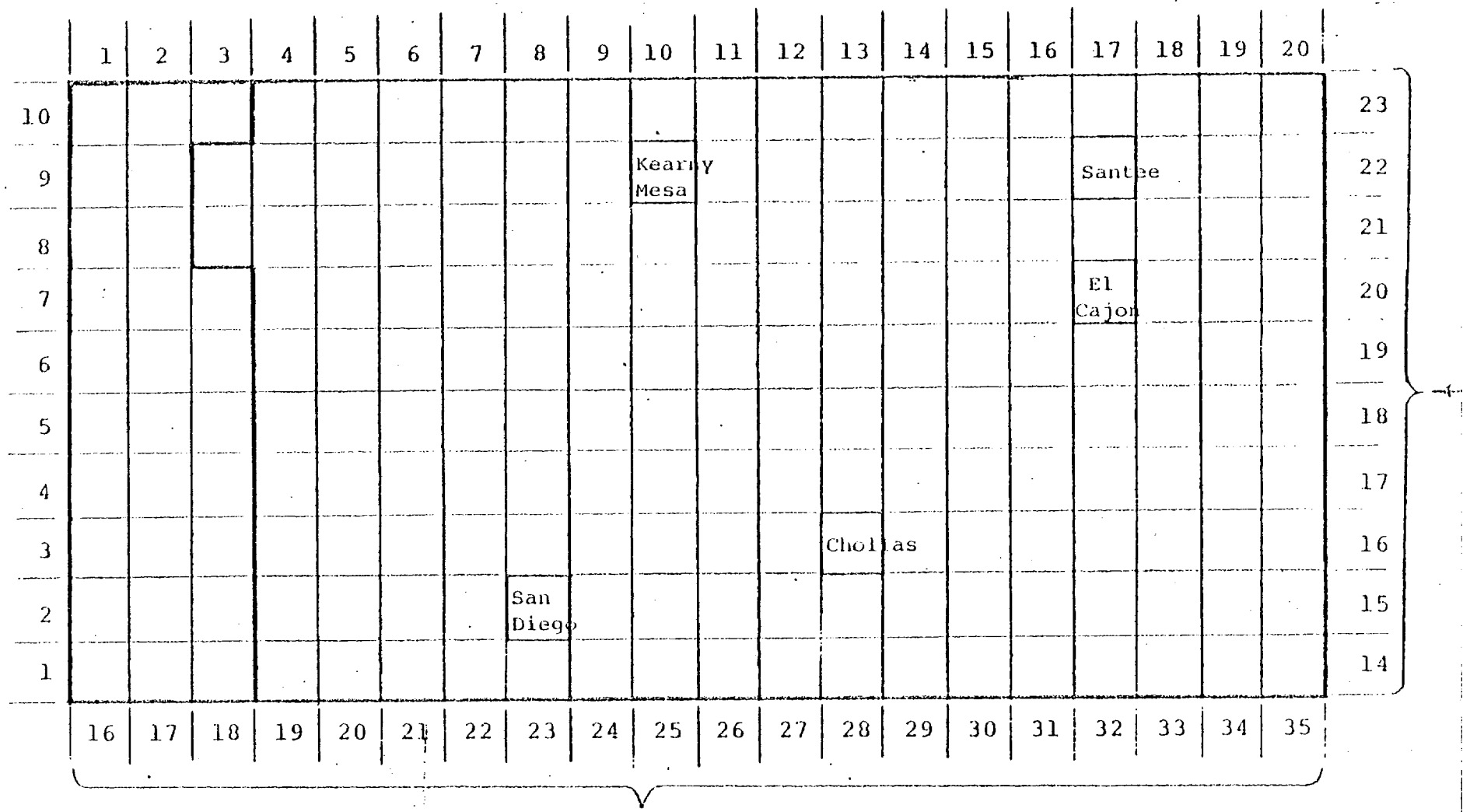

I - coordinate relative to large 50 x 60 outer grid

DX=DY=2KM

J - coordinate relative to 50 x 60 grid

Figure 4.2 The 20 x 10 Grid

analysis is performed on the photochemical model along within a given stream tube to provide some understanding of the photochemistry model. Finally, the full algorithm of MADCAP with advection, diffusion and photochemistry is studied. In this chapter, first the sensitivity parameters are defined. Then the results of three different sensitivity studies are presented, i.e. the inert pollutants analysis, the photochemistry analysis and the full dispersion and photochemistry analysis.

4.1 SENSITIVITY PARAMETERS

Table 4.1 summarizes all parameters studied in the above mentioned three different types of sensitivity analysis. All parameters can be separated into the following seven categories. The first two categories are studied in the inert pollutant analysis to assess the accuracy of numerical method and to establish the sensitivity of the dispersion effects on the model. The last five categories are related to the photochemistry model. Therefore, these parameters (in the last five categories) are studied in both the photochemistry analysis and the dispersion and photochemistry analysis. There are a few exceptions and these exceptions are described in the appropriate categories. The seven categories of sensitivity parameters are

A. Resolution: Both spacial and temporal resolution are studied. The variations are;

- Vertical Direction - change of vertical resolution from 5 level to 3 level
- Horizontal Direction - decrease horizontal resolution by transforming from a 2 Km grid spacing to 4 Km grid spacing
- Time Step - change the number of time steps from 10 to 5 per hour

Table 4.1 Sensitivity Parameters

		Inert Pollutants Analysis	Photochemistry Analysis	Dispersion and Photochemistry Analysis
Resolution	Vertical	3 level		
	Horizontal	4 Km grid		
	Time Step	5/hour		
Dispersion	Mixing Height	± 1 cell		
	Diffusivity	x 5. x 0.2		
	Diff. Algorithm	Post diffusion		
Air Quality	Initial Condition		x 2, x 0.5	x 2
	Boundary Condition			x 2
Emission	HC		x 2, x 0.5	x 2, x 0.5
	NO_x		x 2, x 0.5	x 2, x 0.5
	HC and NO_x		x 2, x 0.5	
HC Splits	HC1 = HC		x	x
	HC2 = HC		x	x
	HC3 = HC		x	x
NO_x Splits	NO = NO_x		x	
	NO_2 = NO_x		x	
Insolation			x 2, x 0.5	

B. Dispersion: Dispersion effects on the model are studied in the following three cases;

- Mixing Height - lowering or raising mixing height by one cell height
- Diffusivity - variation by factors of 5 and 0.2
- Diffusivity Algorithm - change of diffusion algorithm to permit post-diffusion

C. Air Quality: Sensitivity of air quality data is studied through both the initial and boundary conditions.

- Initial Conditions - variation by factors of 2 and 0.5
- Boundary Conditions - variation by factor of two, only studied in the dispersion and photochemistry analysis.

D. Emissions: In order to establish the model sensitivity on the emission data, the following variations on hydrocarbon species and nitrogen oxides are studied.

- HC - variation by factors of 2 and 0.5
- NO_x - variation by factors of 2 and 0.5
- HC and NO_x - variation jointly by factors of 2 and .5, only studied in photochemistry analysis.

E. Hydrocarbon Splits: The reactive hydrocarbons are separated into three aggregate species. Since the exact splitting factors of these three species are not known, it is of interest to study the sensitivity of each species. In this category, three cases are studied;

- HC1 = HC, HC2 = O, HC3 = O
- HC1 = O, HC2 = HC, HC3 = O
- HC1 = O, HC2 = O, HC3 = HC

F. Nitrogen Oxide Splits: Similarly, the sensitivity of nitrogen oxides are also studied in the following two cases;

- $NO = NO_x$, $NO_2 = 0$
- $NO = 0$, $NO_2 = NO_x$

Due to the fact that nitrogen oxides of the source emissions consist mostly of NO and the splitting factor between NO and NO_2 can be accurately measured, the splitting effects are not studied in the dispersion and photochemistry analysis.

G. Insolation: The amount of insolation incident on the ground will affect the photochemical rates used in the chemistry module. Therefore, insolation is varied by factors of 2 and 0.5 in the photochemistry analysis to determine the solar intensity effects on oxidant generation.

4.2 INERT POLLUTANTS ANALYSIS (SENSITIVITY STUDY WITHOUT PHOTOCHEMISTRY)

This sensitivity study is devoted to understanding the accuracy of the numerical method used in the model and the sensitivity to the dispersion effect. Of the major pollutants, only CO is not substantially affected by reactive processes and it therefore is used as the point of discussion for the sensitivity runs. With this analysis, a baseline calculation without photochemistry is performed first. The actual data from 10/3/75 in the San Diego basin are used as the input data. Of the five grid stations shown on Figure 4.2, three recorded valid CO for the eleven hour period - Kearny Mesa, El Cajon and San Diego. In the following presentation the measured data are also included for discussion.

4.2.1 Sensitivity to Vertical Resolution

To test the sensitivity to vertical resolution the 1000 meter simulation height was divided into three layers instead of five layers as used in the baseline. The five baseline layer thicknesses are 50, 75, 125, 250, and 500 meters while the three sensitivity grid layers were set to 125, 375, and 500 meters. The relationship of the new vertical resolution to that of the baseline is graphically shown in Figure 4.3.

Figure 4.4 displays the ground level results of the sensitivity run, comparing them to both the baseline and the measured values.

As would be expected, upon more than doubling the volume of the ground cells the new calculated ground level concentrations are generally one-half of the baseline. Smaller changes between the two simulations correspond to instances of very high diffusion when the vertical distribution of concentrations is almost uniform anyway (See Section 4.2.5). An interesting feature of the sensitivity run is the disappearance of the calculated morning CO peak. This is probably related to higher diffusivities corresponding to cell centers being higher above local ground level. Another contributing factor to this effect is the higher wind speed assigned to the ground level as a result of averaging the input of the first two levels.

From Figure 4.4 it can also be noted that in addition to calculating lower concentrations than the baseline, the sensitivity run generally underpredicts relative to measured values.

4.2.2 Sensitivity to Horizontal Resolution

Of prime importance in the application of grid models is a knowledge of the applicable range of horizontal resolution. Data for the San Diego County grid is based on 2 Km by 2 Km cells. The

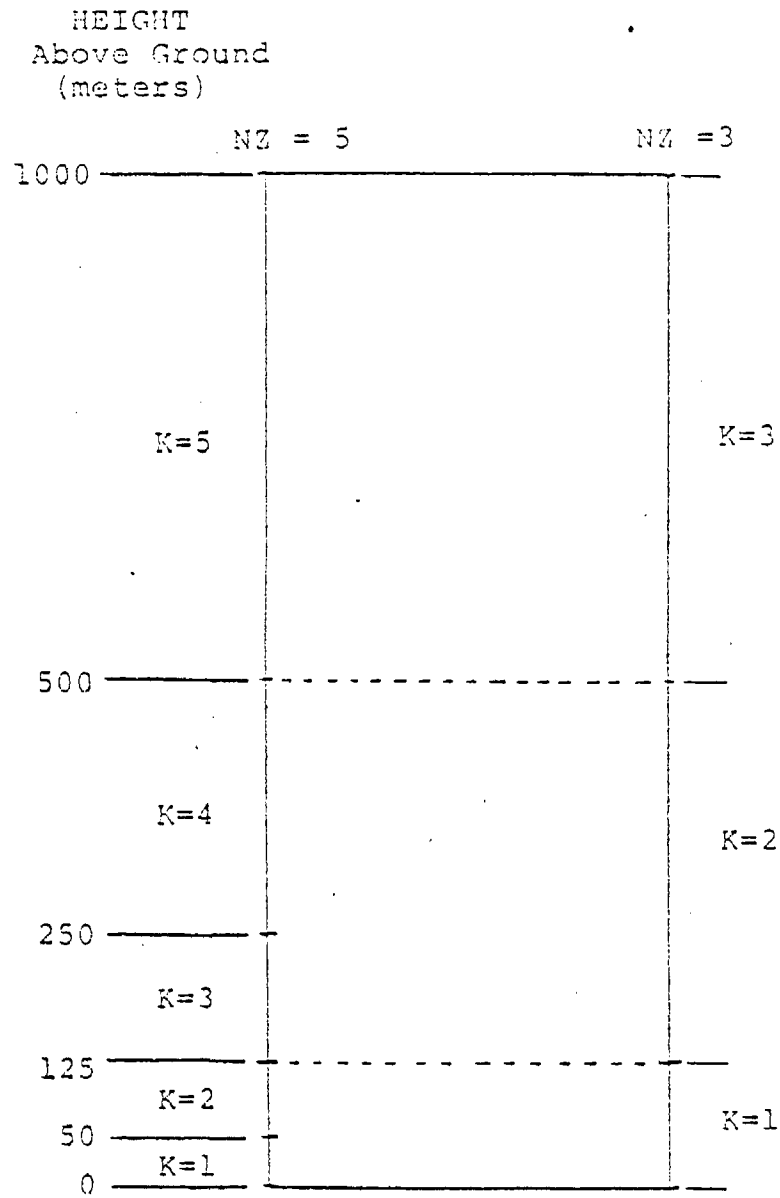

Figure 4.3 Relationship of the NZ = 3 Grid
The Baseline NZ = 5 Grid

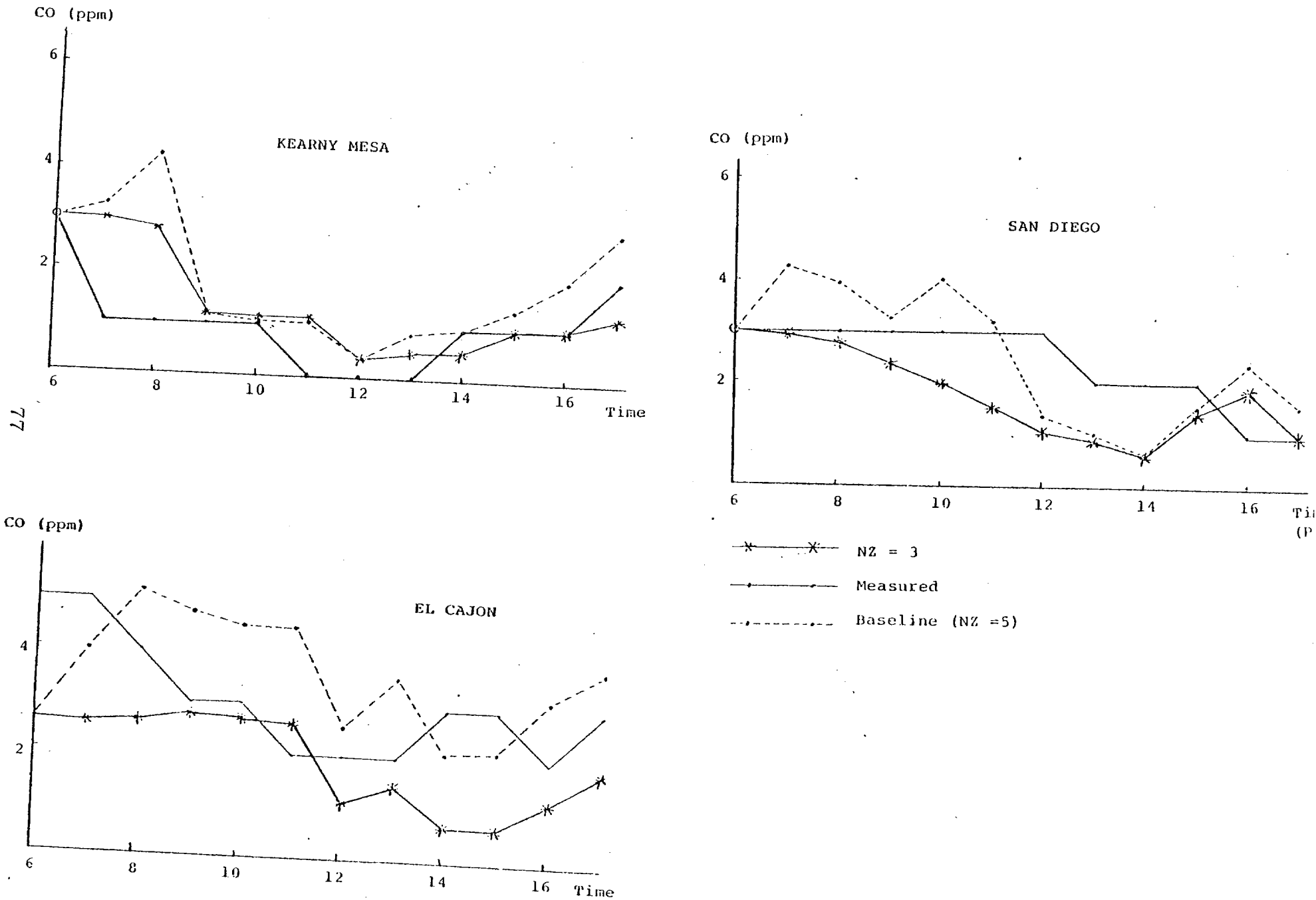

Figure 4.4 Dispersion Sensitivity to Vertical Resolution

sensitivity run discussed in this section used 4 Km by 4 Km cells. A sensitivity run on a 1 Km by 1 Km grid was not made and would not be meaningful since the input source resolution is limited to 2 Km. The effect of a run on a 1 Km by 1 Km grid under these conditions would be very similar to the results of merely increasing the number of steps per hour from 10 to 20 and, as will be shown in Section 4.2.3, this would result in very little change from the baseline.

To obtain 4 Km x 4 Km input for MADCAP, initial concentrations, diffusivities, winds and sources were each averaged over 4 cells. Resulting input arrays were then based on a 10 cell by 5 cell grid. Figure 4.5 present the results of this run at each of three CO stations, including for comparison, baseline and measured values.

As can be seen from Figure 4.5, the 4 Km results, as expected, are lower than the baseline. The difference is not great and is always less than 20%. The reasons for this small difference are three-fold; a 4 Km grid corresponds to just under 2-1/2 miles and is not an excessively large cell for regional simulations; the source array is relatively uniform, i.e., it is not dominated by large localized plumes; the small sensitivity grid size causes MADCAP calculations to tend to reflect boundary values.

It is interesting to note that the morning CO peak still appears - a fact which is consistent with morning CO emissions being regional in character.

4.2.3 Sensitivity to Time Step

As explained in the opening section, MADCAP calculates one hour average pollutant concentrations by accumulating grid sources at a finite number of points along a one-hour path delineated by the wind field. The purpose of these runs was to determine how the calculated results change with differing choices

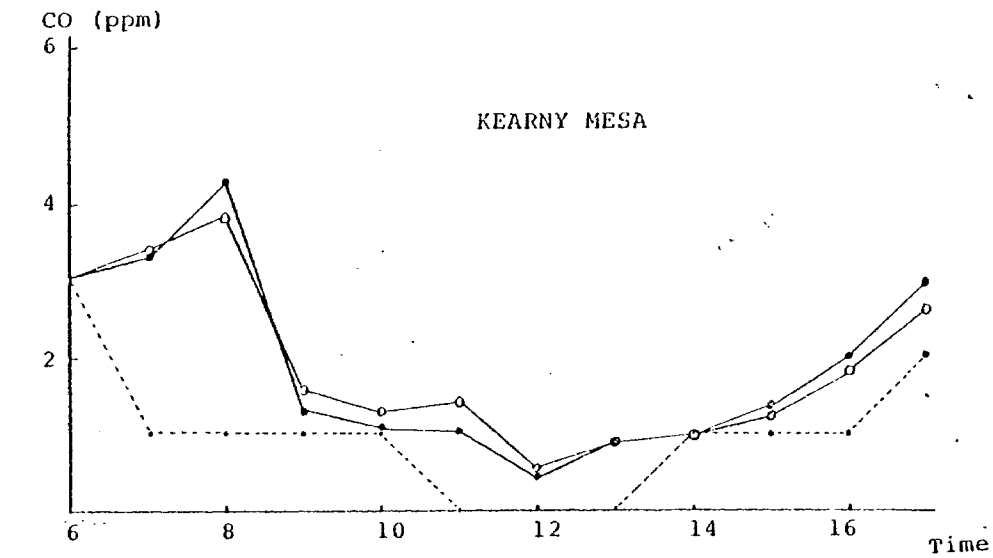

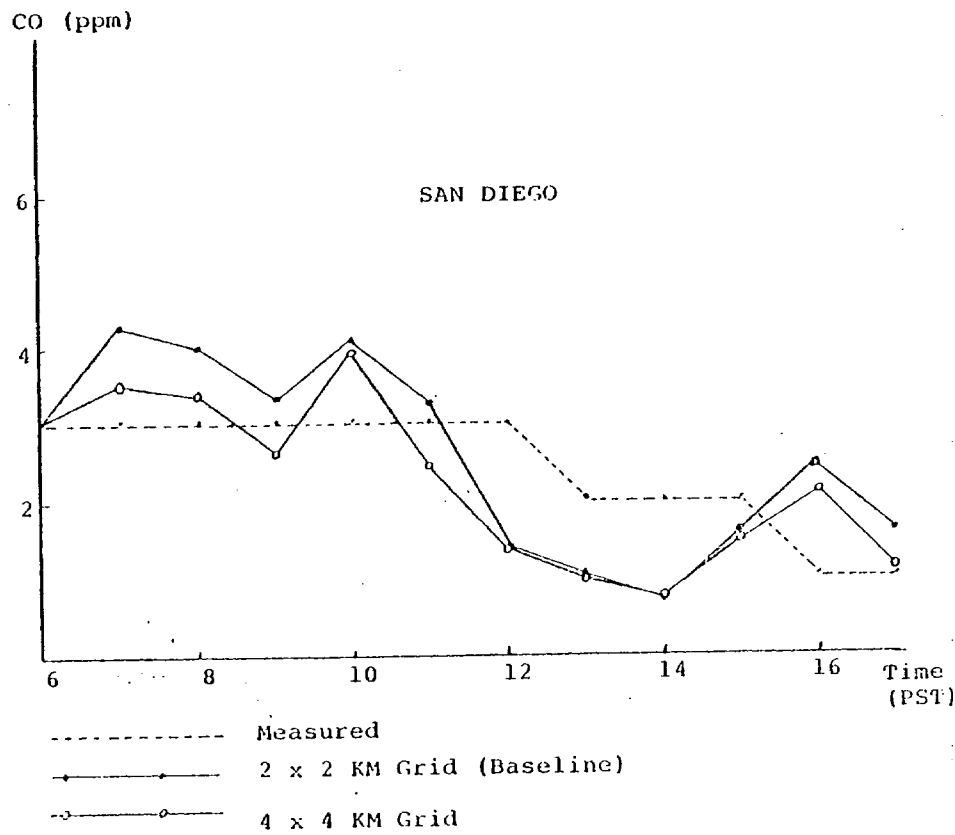

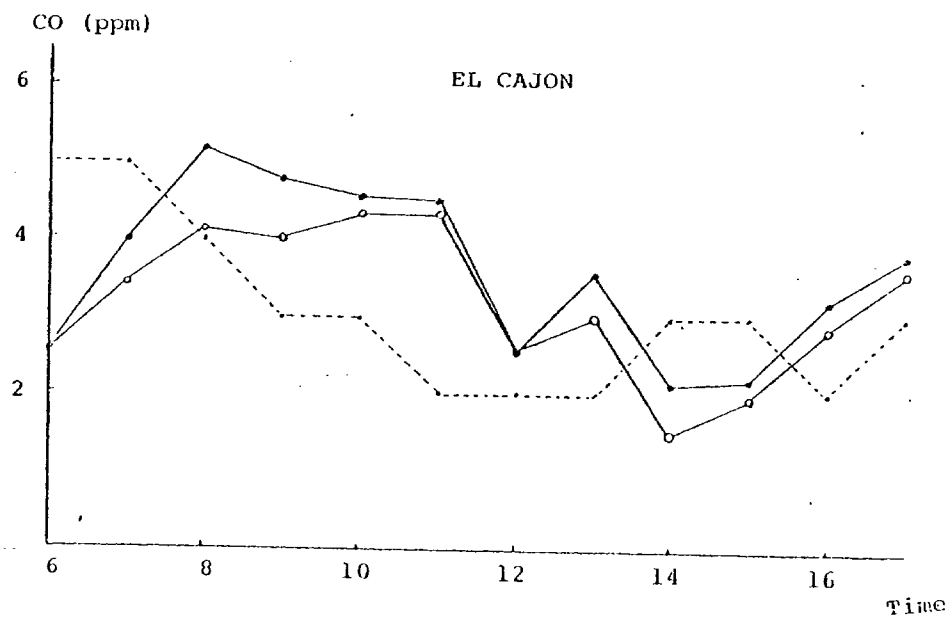

Figure 4.5 Dispersion Sensitivity to Horizontal Resolution

of time step. The baseline utilized 10 steps per hour and the sensitivity run 5 steps per hour. The eleven simulation hours with the wide range of wind speeds represents a good test of how few steps are possible without degrading the results. The fear in using too few steps per hour is that significant sources may not be properly sampled every hour.

The results of the sensitivity run surprisingly showed very little change from the baseline. Figure 4.6 is an illustration of this for Kearny Mesa. Increasing the number of steps per hour above 10 would show even less change. Thus it can be concluded that, at least for the San Diego region, 10 steps per hour appears more than adequate.

4.2.4 Sensitivity to Mixing Height

To effect a lowered mixing height MADCAP was modified by simply assigning the baseline diffusivities one cell lower. That is to say the sensitivity diffusivities for Level 1 were taken as the diffusivities from Level 2 of the baseline. Similarly, sensitivity Level 2 diffusivities came from those of Level 3, 3 from 4, 4 from 5 and 5 remained as 5. This is illustrated in Figure 4.7.

While this procedure of moving diffusivity values down one cell does correspond to a lowering of mixing heights, the actual sensitivity run surprisingly produced concentrations differing from baseline by less than 1%.

An explanation for this is to be had by consulting Figure 4.8 which is a plot of inversion base vs time of day. This data came from the raw input tape to PREMET (note that hours 13 and 16 had multiple data entries). For all simulation hours on October 3, 1975 the bottom two layers were generally characterized by neutral or unstable atmospheric conditions. Accordingly, for all hours the diffusivity algorithm in PREMET always produced high diffusivity values for layers 1 and 2 relative to layers immediately above which lay in

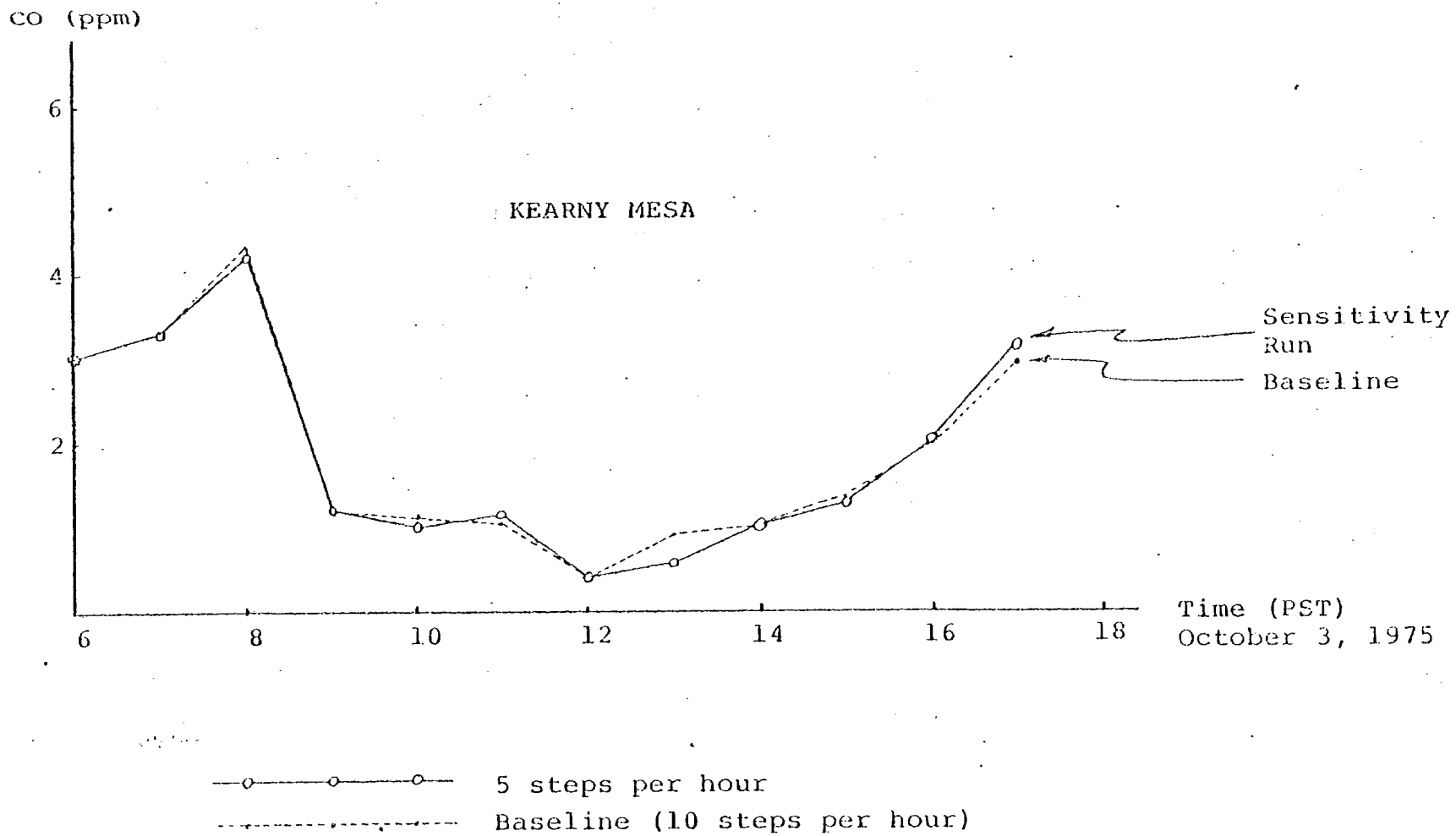

Figure 4.6 Dispersion Sensitivity to Number of Steps Per Hour

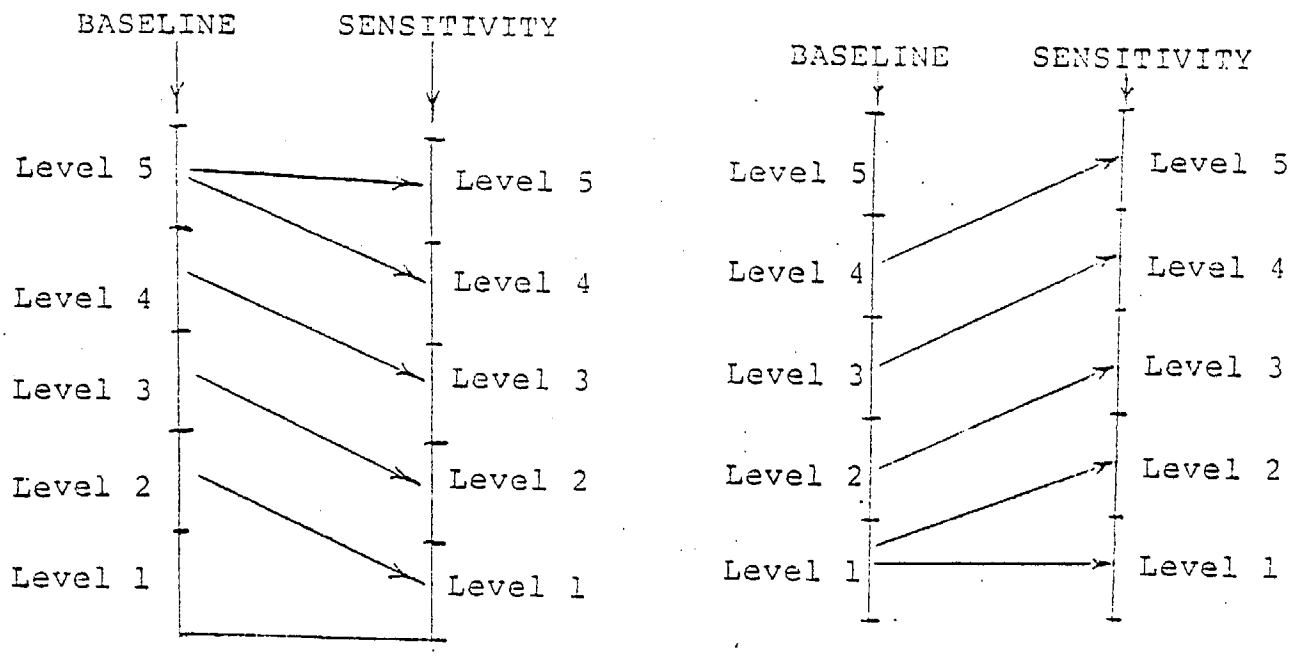

A. Lowering Mixing Height

B. Raising Mixing Height

Figure 4.7 Relation of Sensitivity Diffusivities to Baseline Diffusivities

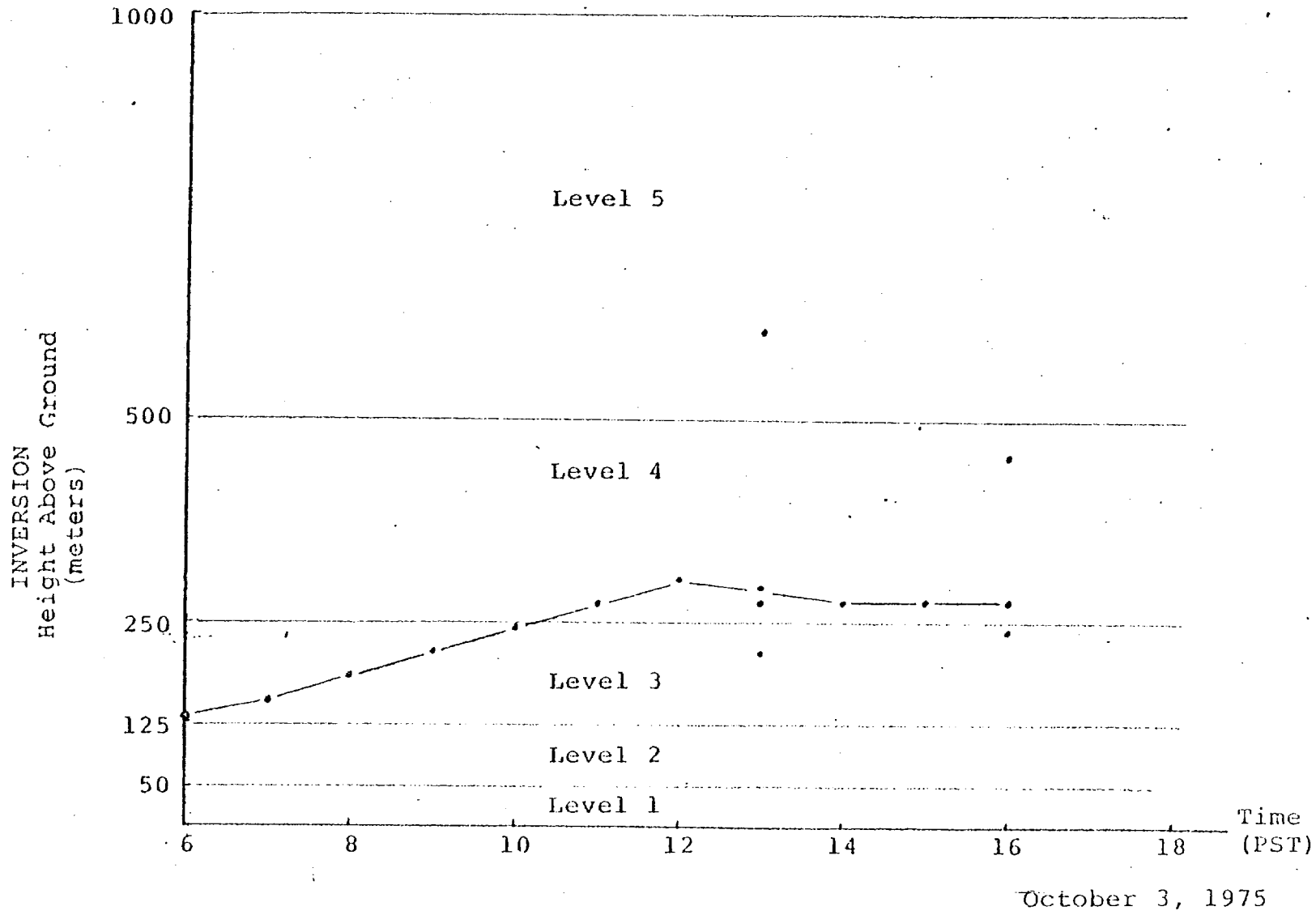

Figure 4.8 Variation of Inversion Base Height in San Diego County

the inversion. This was also true for Levels 1, 2 and 3 for several hours. Lowering diffusivities by one level caused Level 1 to have neutral to unstable diffusivity values calculated for Level 2 of the baseline. Thus ground level diffusivities for the sensitivity run were as large, or larger, than those of the baseline run. Since MADCAP diffuses pollutants out of the ground level using ground level diffusion values, there resulted little difference between the two runs due to diffusion profile changes. A major cause of invariance of ground level concentrations is the cycle of diffusing, source injection and printing that is used in the MADCAP baseline code. This process is independent of diffusivity values and is discussed in Section 4.2.5.

To generate the required conditions to simulate a raised mixing height the opposite process of lowering mixing height was followed (Figure 4.7). As with the case of lowered mixing height, changes from baseline values were always less than 1%.

As mentioned, the baseline has neutral to unstable diffusivity values in the bottom two (or more) layers for all hours and so further raising of the mixing lid did little to change them. Calculated ground level concentrations were thus primarily determined, as in the baseline and previous case, by the fact that the MADCAP code injects sources <u>after</u> diffusion is completed. This is the reason why almost all the diffusivity sensitivities are identical to the baseline.

4.2.5. Sensitivity to Diffusion

A sensitivity run was made to assess the effect of increasing vertical diffusion above baseline values which generally are on the order of 1 to 5 m^2/sec for the two lower levels. The increase was achieved by simply multiplying all elements of the three-dimensional vertical diffusion array by a factor of 5. The sensitivity run was made, and resulting output at most points was identical to the baseline, differing only occassionally, and then by less than 1%.

The explanation is that the MADCAP baseline code calculates diffusion for each cell in one stroke at the beginning of every hour. After the diffusion calculation is completed, an hour of accumulated sources are injected into the cell, and the result is printed as the hour average. Diffusion rates on the order of 1 to 3 m^2/sec imply that in one hour pollutants in the 50 m ground level cells will be completely mixed upward. This tends to produce a uniform vertical distribution of concentrations. Injection of sources then results in ground level concentrations being equal to the sum of sources diluted by the ground cell volume plus the uniform vertical distribution. From the above discussion it is clear that increasing diffusion by a factor of 5 will tend only to make the vertical distribution uniform - which it already is - and have no affect whatsoever on sources injected after the diffusion calculation. Thus little difference results between the baseline and sensitivity runs.

A sensitivity run was executed in which all vertical diffusivities were decreased by a factor of 5. The resulting output was once again almost identical to the baseline. For most sites and hours the difference was zero or less than 1%. Few points showed a 10% increase over baseline values. The explanation for this involves an understanding of the MADCAP baseline diffusion treatment as presented in the previous section. For the present case it is sufficient to note that ground layer baseline diffusivities on the order of 2 m^2/sec imply a diffusion velocity of .04 m/sec. In one hour this results in a diffusion transport of about 145 meters. Since the ground layer is only 50 meters thick, considerable vertical mixing still occurs, and the ground level concentrations are generally controlled by simple volume dilution of sources, just as in the previous sensitivity run.

The results of these diffusion sensitivity runs led to re-examination of the diffusion scheme employed in MADCAP resulting in a reformulation of the algorithms and new sensitivity runs which are presented in the next section.

4.2.6 Sensitivity to Diffusion Scheme

The MADCAP baseline formulation essentially runs through successive cycles of doing hourly diffusion, adding hourly sources and printing the resultant concentrations. This procedure, coupled with the magnitude of actual diffusivities causes ground level concentrations to be high and produces a uniform concentration profile above. This section presents results of a simple remedy to the situation - namely to do 1/2 hour of diffusion before source injection plus 1/2 hour of diffusion after source injection and then to print concentration values. A summary of these 1/2 hour post-diffusion runs is presented in Figure 4.9 which shows vertical CO profiles at three monitoring sites for 900 PST, 1200 PST and 1600 PST and include for comparison the baseline results as well as ground level measurements. In all cases the calculated (and measured) values are plotted at cell center heights. From these figures the previously discussed baseline behavior can clearly be seen, i.e., ground level concentrations are high due to the treatment of source injection while upper levels are almost uniform due to strong upward diffusion and lack of significant elevated sources. These figures also show that the post-diffusion sensitivity run resulted in almost totally uniform concentrations, Level 1 through Level 5, for each station and hour. It is to be noted that the baseline and post-diffusion runs are in agreement for the upper levels indicating that, at least for the upper levels, the calculated values are <u>not</u> controlled by the diffusion scheme but simply determined by the actual diffusion values themselves. Figure 4.10 indicates that the post-diffusion run tends to underpredict the ground level relative to measurements. This inference can be examined more closely by plotting ground level concentrations for all hours and is presented in Figure 4.10. From these figures it is apparent that while the baseline overpredicts, that indeed post-diffusion underpredicts

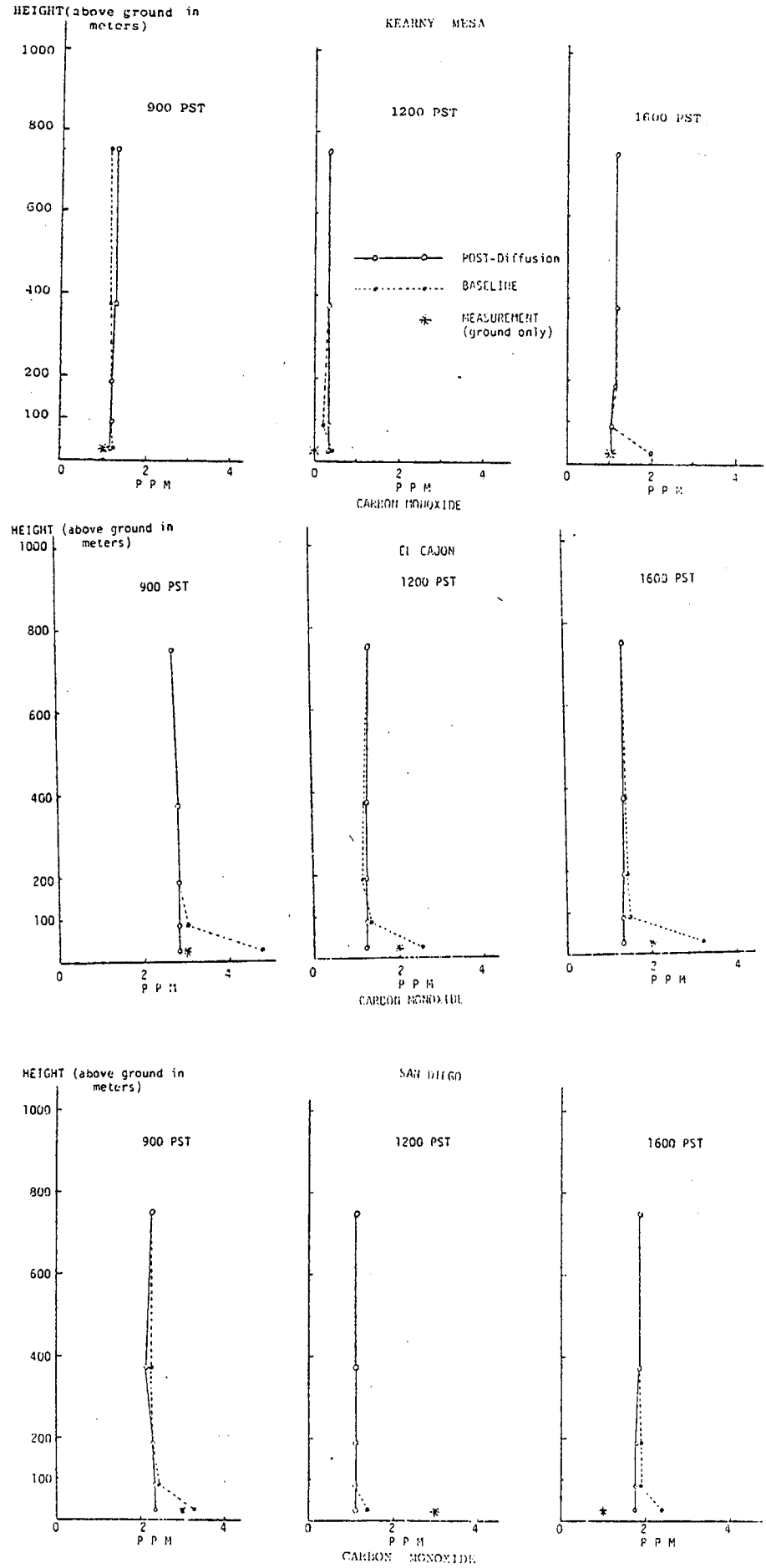

Figure 4.9 Vertical Dispersion Sensitivity to Diffusion Scheme

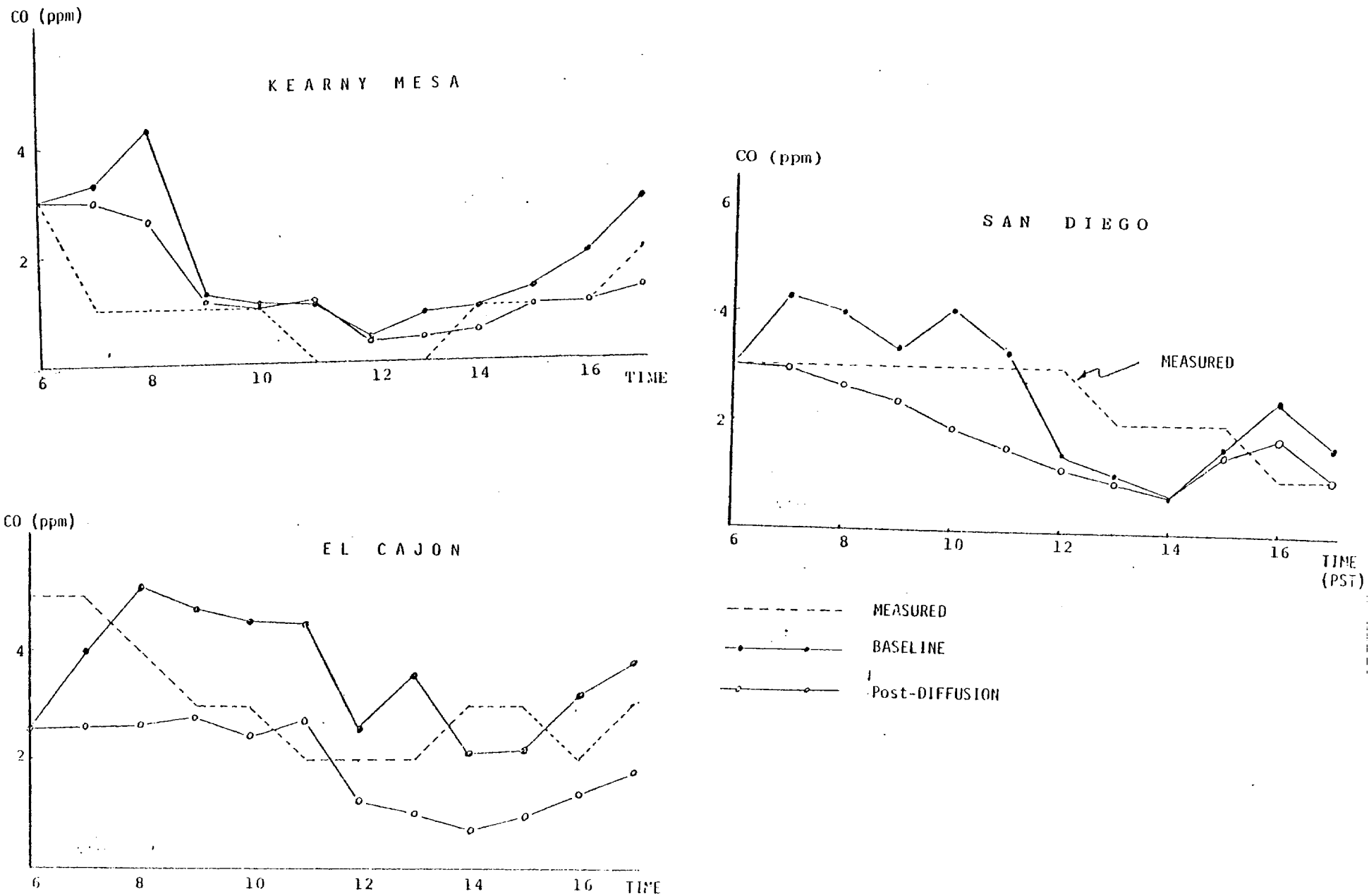

Figure 4.10 Ground-Level Dispersion Sensitivity to Diffusion Scheme

relative to measurements. It is recommended here that for San Diego County, 45 minutes of diffusion prior to source injection coupled with 15 minutes of diffusion after source injection would yield best agreement with measured data. Hence in all the results presented in this report, a 15 minute post diffussion is used.

4.3 PHOTOCHEMICAL ANALYSIS

The chemical kinetics module incorporated into MADCAP for these calculations is called CHEMC, which is based on an exponential predictor-corrector solution of the updated LIRAQ-2 photochemical mechanism as reported in Reference 3. The mechanism uses three hydrocarbon species and gaseous sulfur dioxide/sulfate reactions for a total 59 reactions and 19 dynamic species. In CHEMC, four of the species are treated in quasi-equilibrium and two as non-accumulating, leaving 13 active species for storage and transport in MADCAP.

Photochemical kinetics itself is a very active research field. This updated LIRAQ-2 photochemical model is one of many photochemical models available today. As the authors of this model described in their paper[3], it is wholly their intent to analyze photochemical mechanisms according to classic scientific methodology of hypothesizing, testing, validating and feeding back results to renewed hypotheses, etc. It is clear that the state of the art of photochemistry modeling is still in the hypothesizing, testing and validating stage. In this report, we are testing and validating this updated LIRAQ-2 photochemical model. One way to test and validate this model is through a sensitivity study. In this section a stream tube model is used to analyze this chemical model. The other method to gain understanding of the model is through a sensitivity study of the full model which includes both dispersion and chemical effects.

The results reported in this section are keyed to a "stream tube", a parcel of air that transverses the San Diego regional grid. The calculations simulate the effects of chemical reactions within the parcel as well as approximate the emission, dispersion and changing insolation. The stream tube for these calculations was to provide a long transport and include the ozone maximum timing. Thus, the stream tube begins early in the morning near the coast and proceeds to mid-afternoon in the inland mountains. Matching the stream tube to pass near monitoring stations was not possible since the data for too many of the stations was missing. The chemistry is stressed in these calculations on a "single cell", and diffusion can only be approximated. For simplicity, diffusion was assumed to account for a 20% dillution each hour in the baseline run. The baseline had an ozone maximum of .18 ppm at 1300 as shown in Table 4.2. The sensitivities with respect to this baseline are summarized by the timing and magnitude of the ozone maximum, and are also reported in Table 4.2.

Through these sensitivity analyses, the photochemical module exhibits the following variations:

- ozone peaks soon after noon
- peak ozone magnitude varies with respect to HC
- peak ozone magnitude next varies inversly with NO_x
- hydrocarbon 3 produces the most ozone
- more ozone would be produced if NO_x emissions were NO_2
- ozone production is very sensitive to and follows the insolation behavior

In addition, the chemistry module was tested with 13 and 15 active species, and since less than a 5% variation was observed the 13 species module was accepted.

Table 4.2

Photochemistry Sensitivity Analysis

Variable	Change By A Factor Of:	Response: Ozone Maximum Time	Response: Ozone Maximum Magnitude (ppm)
Baseline	-	1300	.18
Emissions: HC	2.0	1300	.21
HC	0.5	1300	.11
NO_x	2.0	1300	.10
NO_x	0.5	1200	.20
HC & NO_x	2.0	1300	.21
HC & NO_x	0.5	12-1300	.15
Initial Conditions	None	1300	.14
	2.0	12-1300	.20
	0.5	12-1300	.16
HC Splitting	HC1=THC	1200	.26
	HC2=THC	1300	.003
	HC3=THC	1200	.42
NO_x Splitting	$NO=NO_x$	1300	.18
	$NO_2=NO_x$	1200	.21
Insolation	2.0	1200	.37
	0.5	1300	.05

4.4 DISPERSION AND PHOTOCHEMISTRY ANALYSIS

Before we discuss the results of this sensitivity study, some important differences between the sensitivity studies performed in this section and the previous section should be reviewed. In Section 4.3, a single Lagrangian fluid element is selected. A trajectory of this Lagrangian cell is calculated according to the wind speed and direction. Along the trajectory, the proper source emissions are injected into this stream tube. An artificial 20% dilution is assumed for the diffusion effect. There is neither spatial nor temporal interaction between any other stream tubes in the entire study region. This stream tube model can be envisioned as if it is a smog chamber simulation. In this section, a fully interactive dispersion and photochemical model is used, where at any given station, many stream tubes pass at different times. Therefore, in the previous section the results show the sensitivity of the photochemistry module in an isolated situation. In this isolated condition, one should see the expected photochemical phenomena normally observed in a smog chamber experiment. Indeed the results in the previous section show the expected sensitivities to different species, which demonstrates the validity of the photochemistry module. With this conclusion, we have embarked on the following sensitivity study.

4.4.1 Sensitivity to NO_x Emission

In this study, the emission source rate has been halved and doubled in order to understand the sensitivity of the total air quality to NO_x. Figure 4.11 shows the comparison of the ozone predictions at different stations between the base case and the studied cases, i.e., the 0.5 x NO_x case and the 2 x NO_x case. Whenever the predictions of the two studied cases are different from the base case by 5%, the differences are shown in the plots. It is clear that except at San Diego where high emission rates from

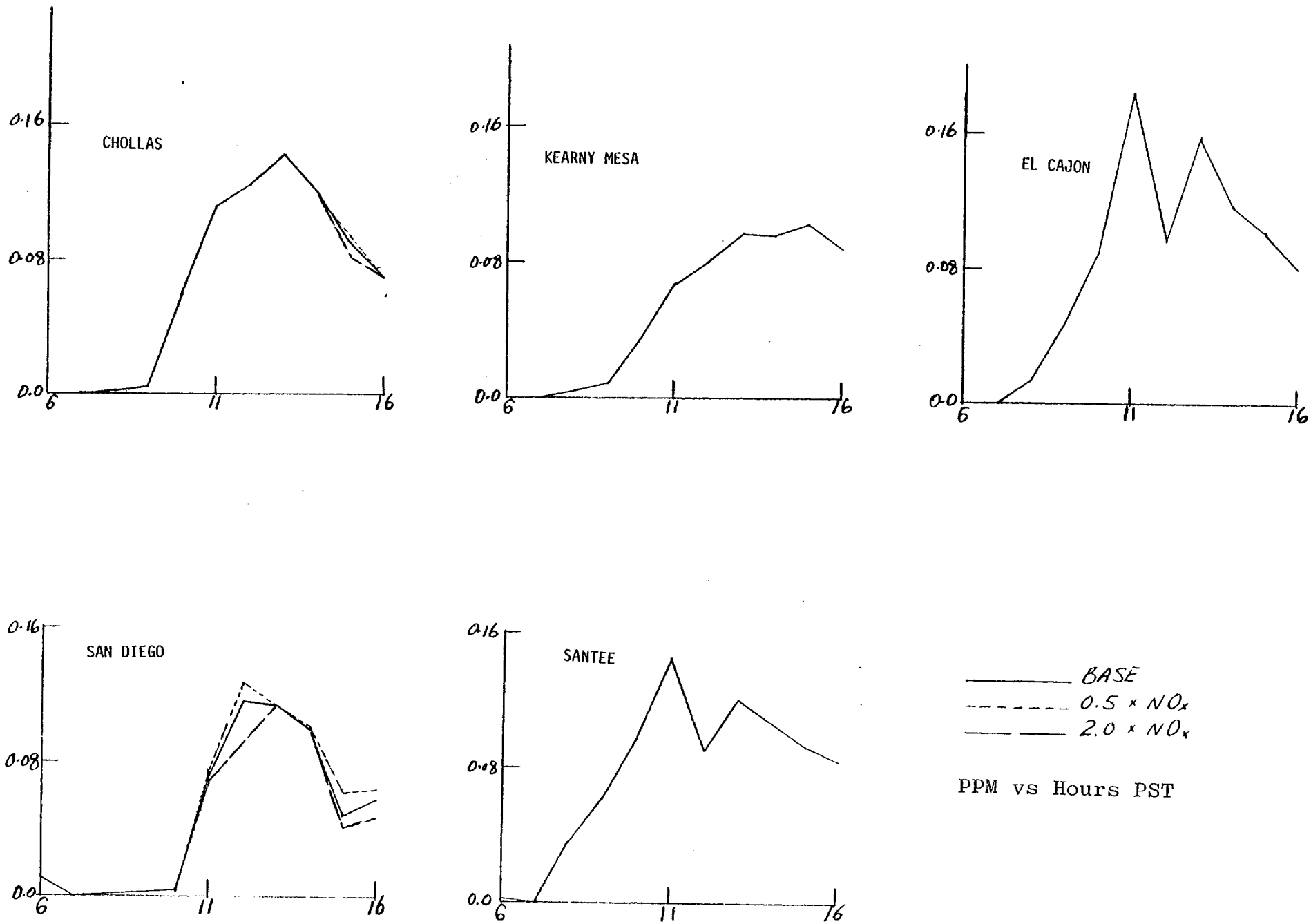

Figure 4.11 MADCAP Sensitivity of Ozone to NO_x Emissions

airplanes affect the ozone prediction, there is no significant change in the ozone level by either doubling or halving the NO_x emission rate. This small sensitivity to NO_x is not surprising, since total source volume emitted over a day is small relative to the total holding volume of the species in the San Diego Air Basin. Integration of the ground level NO_x emission rate over 10 hours within this small regional simulation gives an average of 60 ppm within a 40 Km^3 volume (40 Km x 20 Km x 0.05 Km). Since most emissions are on the ground level, it is estimated that the total source emitted within the simulation volume (40 Km x 20 Km x 1 Km) is on the order of 100 ppm. On the other hand, the total background (as reflected in the initial and boundary conditions) NO_x is about 400 ppm within the simulation volume. The average wind speed is about 10 Km/hr. It is estimated that the hourly accumulated source emission volume is equivalent to a mere 20 ppm within the total simulation volume. Therefore it is clear that the sensitivity to ozone is insignificant. In San Diego, where some difference is observed, the sensitivity to NO_x shows the correct trend. Increasing NO_x supresses the ozone level, and decreasing NO_x promotes ozone growth.

4.4.2 Sensitivity To Hydrocarbon Emissions

Two cases were studied for the sensitivity to hydrocarbon emissions. The first case, where hydrocarbon source emissions are reduced to one half of the base case, was run successfully and the results are shown in Figure 4.12. The second case, where the emission source is doubled, was only simulated in the early hours due to a system error. However, examining the available results for the 2xTHC case shows insignificant differences from the base case. Hence the 2XTHC has not been re-simulated and only the 0.5xTHC case is reported here. As shown in Figure 4.12, there are very small changes in ozone concentration when the total hydrocarbon was reduced by a factor of two. It is found that the total hydrocarbon emission over a day within the simulation volume is

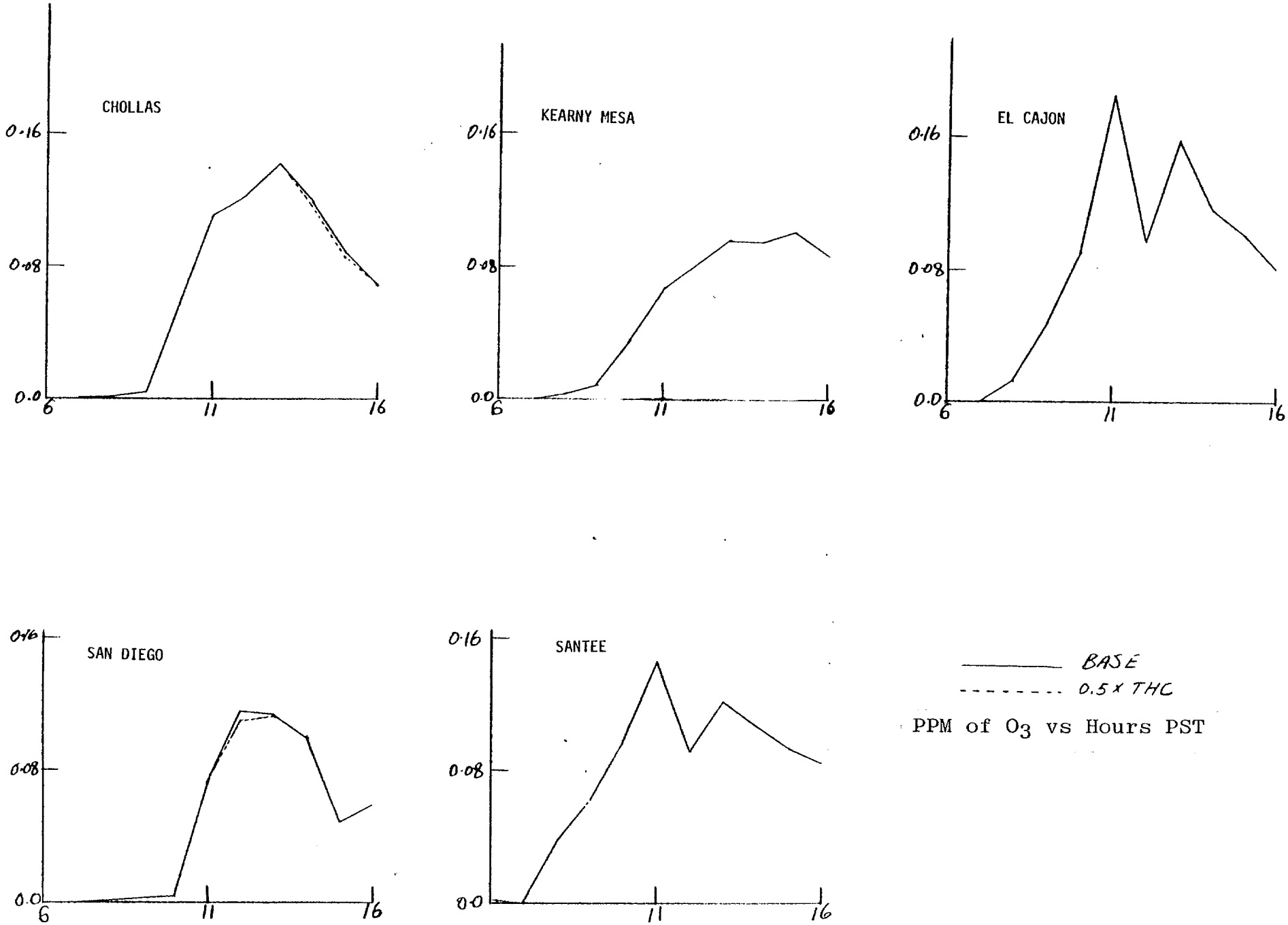

Figure 4.12 MADCAP Sensitivity of Ozone to THC Emissions

only about 6% of the total holding volume of hydrocarbon concentration in the same simulation region. Therefore, changing the total hydrocarbon emission by a factor of two does not show any significant impact on the model. However, at the San Diego station, decreasing total hydrocarbon does reduce the ozone concentration as shown in Figure 4.12. This agrees well with the stream tube sensitivity study results and shows the correct trend of this photochemical model.

4.4.3 Sensitivity To Hydrocarbon Split

In this photochemical model, the hydrocarbon species are separated into three species; HC1 (olefins), HC2 (alkanes) and HC3 (oxygenates), according to their reactivity with O, OH and O_3. Therefore, it is interesting to study the sensitivity to hydrocarbon splitting. Unfortunately, for the same reason as described in the previous section (the low pollution level in San Diego Air Basin), very small sensitivity is shown in this hydrocarbon splitting study. Figure 4.13 shows the results of this simulation. In general there are insignificant changes from case to case, except in the early morning for the case HC3 = THC. Due to the reactive nature of HC3 it is assumed that no HC3 exists overnight, i.e., HC3 = 0 at 0600 PST. By assigning all hydrocarbon emissions as HC3, an effective reactive precursor of ozone is provided and therefore, in the first hour (where background HC3 is zero) of simulation, high ozone concentration is predicted.

4.4.4 Sensitivity to Air Quality (Initial and Boundary Conditions)

Figure 4.14 shows the sensitivity of the MADCAP simulation to the initial and boundary conditions. In contrast to all the above sensitivity studies, the results show great sensitivity to both initial and boundary conditions. These results are expected, since the initial and boundary conditions are representative of and

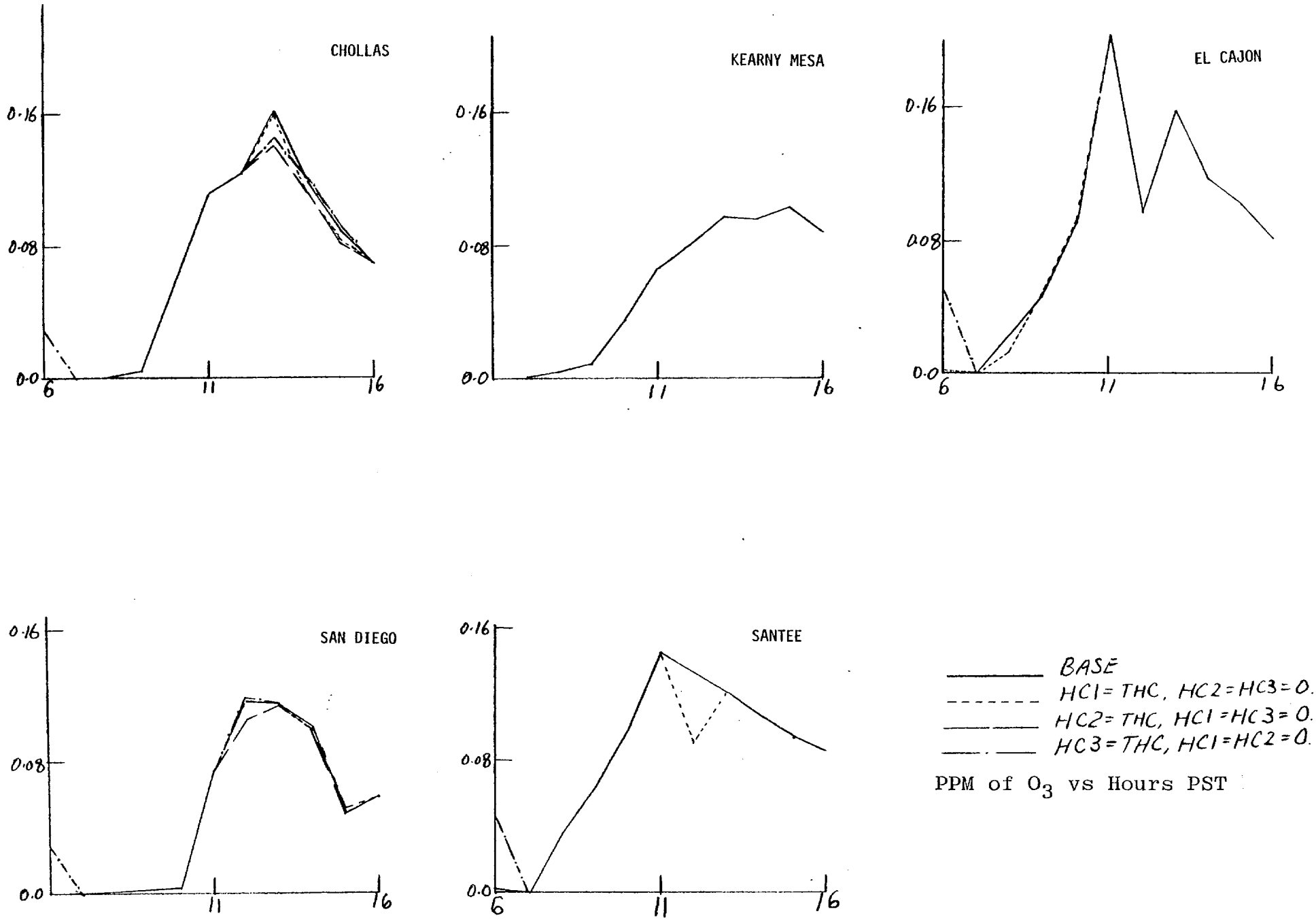

Figure 4.13 MADCAP Sensitivity of Ozone to THC Splitting

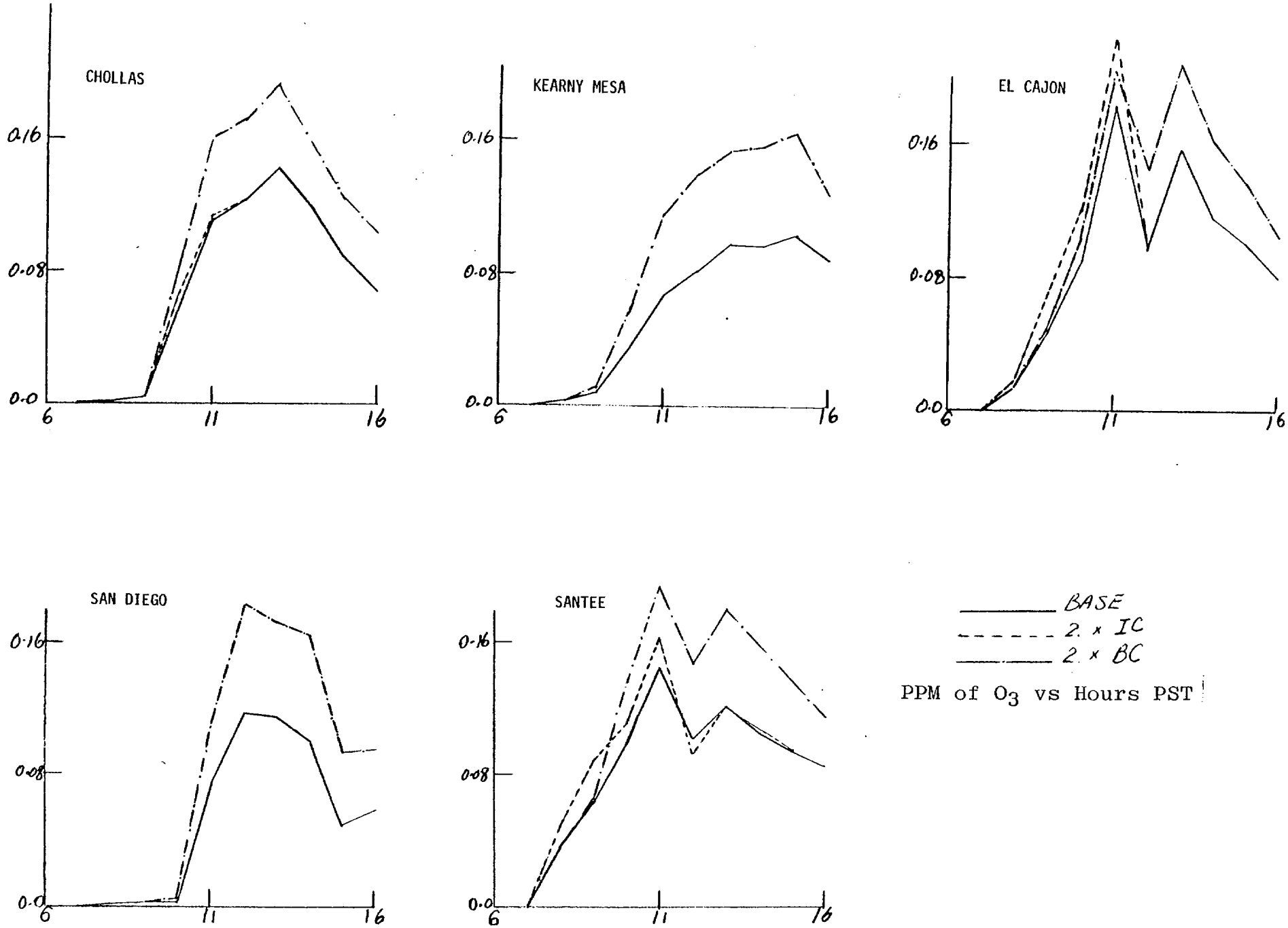

Figure 4.14 Sensitivity of Ozone to Initial Boundary Conditions

commensurate with the pollution within the total atmosphere in all levels. It is shown that doubling the initial concentrations influences the photochemical simulation in the first few hours. As time progresses, the effects of changing the initial conditions become progressively less pronounced. On the other hand, doubling the pollutant concentrations on the boundary increases the ozone concentration by approximately a factor of 1.5 over the base case simulation.

In all the above regional sensitivity studies it is shown that because of the low level of pollution in San Diego Air Basin, there is a very small sensitivity to the source emissions. However, if the source volume were increased by a factor of five or higher, significant changes in the photochemical predictions are expected.